A detailed field and geochemical investigation of the volcanic sequence in the Grimelid-area: The Solund-Stavfjord Ophiolite Complex

Thesis for Master degree in Geochemistry

Sunniva Alsaker

December

2021

supervised by Harald Furnes

Department of Earth Science

University of Bergen

2021

Abstract

This master thesis focuses on the volcanic sequence of the Solund-Stavfjord Ophiolite Complex (SSOC) in Grimelia, in order to provide more detailed information and a better understanding of the development. The SSOC (443 Ma, $\pm$ 3 Ma) is located within the western parts of the Norwegian Caledonides, between Solund and Bremanger, and represents a remnant of the Iapetus oceanic lithosphere evolved in the Caledonian marginal basin.

As a result of detailed fieldwork and thorough mapping of the sequence, a Master profile of Grimelia is constructed with a division into two parts. The first 500 m of the sequence is represented by the first part, which is furthermore divided in two parts (Part 1A and 1B), due to major differences within short distances. Part 1B is located near by the Grimelia mines and is therefore composed of varying degree of VMS deposits. It is, however, important to highlight that this will not be the focus of the thesis but considered with general knowledge about mineralization at spreading ridges. A proposed model for the Grimelia deposits is hence presented, which will suggest the controlling factor for the formation of VMS deposits in Grimelia.

The volcanic sequence, represented by the Master profile, is composed of three main components, 1) massive sheet flows, 2) pillow lavas, and 3) volcanic breccias. By measuring the vertical and horizontal axis of the different pillows, as well as other factors further discussed, it will be possible to calculate and predict the degree of deformation in the area, and hence, reconstruct the volcanic sequence to an estimated new thickness. Before reconstruction, the Master profile is measured to be 1205 m, excluding the metasedimentary cover of metagraywacke and phyllite. However, various calculations propose an estimated original thickness of 1430 m, which makes this, yet the longest registered volcanic sequence of the SSOC.

Last, but not least, several samples of metabasalts are collected from the study area, leading to a geochemical investigation for parts of the SSOC. Previously studies from the SSOC suggests that the metabasalts are formed from magmas that were produced in a trench-distal suprasubduction-zone setting, sufficiently far from the subducting slab with only minor influence of slab-derived fluids. The various presented diagrams of this study compliment the numerous studies of the SSOC, reflecting minor subduction influence for some of the presented components, yet a dominance of a subduction-unrelated character.

Acknowledgement

First, and most important of all, I would like to greatly thank my supervisor Professor Emeritus Harald Furnes for super guidance during part of the fieldwork, and a special gratitude for valuable comments and feedback during the writing of my thesis. I also utterly appreciate the time and effort you have made to have physical meetings at the University, especially considering the difficulty and problems regarding Covid-19 seasons. Furthermore, I greatly thank my father and co-worker Einar Alsaker for guidance during part of the fieldwork, and a special gratitude for giving me the opportunity to work with this project. I am also delighted to my co-supervisor Professor Rolf Birger Pedersen for making this a possibility.

Furthermore, I would like to thank my good friend and co-student Amalie Skreden Erga for one unforgettable field season and assistance during that time. And also, an appreciated thanks to my fiancé for splendid assistance during some of the sampling in Grimelia. Further, I cannot stress how much I appreciate my mom and (future) mother-in-law, for babysitting our kids during both field seasons, and during the sample preparations, in order to make this work. I truly could not have done this without your help.

I am very grateful to Ida Marie Gabrielsen and Lubna Sami Jawad Al-Saadi for teaching me how to use the different instruments in the crushing-labs at the University, prior to the sample preparations. A special thanks to Hildegunn Amelid for ICP-OES analysis, Siv Hjort Dundas for LA-ICP-MS analysis, and Yuval Ronen for help with some of the sample preparations. Furthermore, I am grateful for Andreas Viken for preparing the glass beads prior to the analysis and the thin sections from some of the collected samples.

I also want to thank my fellow students and good friends for these unforgettable years at the University of Bergen, and for making them considerably memorable. It would not have been the same without you guys.

Last, but not least, an extra grateful and appreciated thanks to my fiancé, family, and friends for always supporting me, being patient, helpful and showing interest in my work during this period.

Bergen, 08.12.2021

Sunniva Alsaker

Sunniva Alsaker

Table of contents

Chapter 1 – Introduction

Within the Scandinavian Caledonides several ophiolites and/or arc-related complexes occur. Dunning and Pedersen (1988) U/Pb-dated four ophiolite complexes (Karmøy, Gulfjellet, Leka, and Solund-Stavfjord) in the Norwegian Caledonides, and thus documented the presence of a lower Ordovician (489-497 Ma) generation, and an Upper Ordovician/Lower Silurian generation. The latter-mentioned, the Solund- Stavfjord Ophiolite Complex (SSOC) is dated to 443 $\pm$ 3 Ma and has, since the 1970s, been thoroughly mapped and studied (e.g., Furnes et al 1979; Furnes et al., 1985; 2003, 2006, 2012; Dunning and Pedersen, 1988; Pedersen et al., 1988). The first petrographic and tectonostratigraphic studies of the Solund-Stavfjord area were conducted by Kolderup (1921; 1928), and further by Skjerlie (1969, 1974), Furnes (1972, 1973, 1974), Furnes et al. (1976) and Gale (1975). Furnes et al. (1985) categorized the Scandinavian Caledonides in two groups of ophiolites, representing marginal basins of different age. Later, Brekke and Solberg (1987) summarized an extensive review of the general geology in the Solund- Stavfjord area, which led to the tectonostratigraphy divided into lower-, middle- and upper tectonic units (Fig. 2.1) (Furnes et al., 1990).

SSOC is located between Solund and Bremanger (Fig. 1.1), in the south-western parts of Norway. The lithology of the ophiolite is mainly dominated by sheeted dikes and volcanic rocks (e.g., Andersen et al., 1990; Furnes et al., 1990, 2003, 2012.). The relevant data for this study is collected in the Grimelid area in the Stavenes Peninsula (Fig. 1.1), also with some focus on elementary mineralization within the volcanic sequence (the VMS deposits at Grimelia).

Most studies regarding ophiolites, have focused on the tectonic evolution of sheeted dike complexes and plutonic units and/or on melt migration channels in the mantle rocks on ophiolites. However, little attention has been devoted to the detailed volcanic stratigraphy in ophiolites (Furnes et al., 2001). This study focuses on getting a better understanding of the volcanic evolution, formation, and the construction of the upper part of the SSOC, as well as mineralization in the sequence related to the Grimelia Mines. The hypotheses are that the mineral-enrichments are potentially to be found in areas with detectable hydrothermal activity, related to hydrothermal activity at the oceanic stage.

In order to achieve a better understanding of the volcanic, magmatic, and tectonic evolution of the SSOC, a detailed mapping of a limited geographical area near by the Grimelid mines

were conducted. As a result of this, a constructed Master profile throughout the study area is presented, with two different versions of the lowermost section.

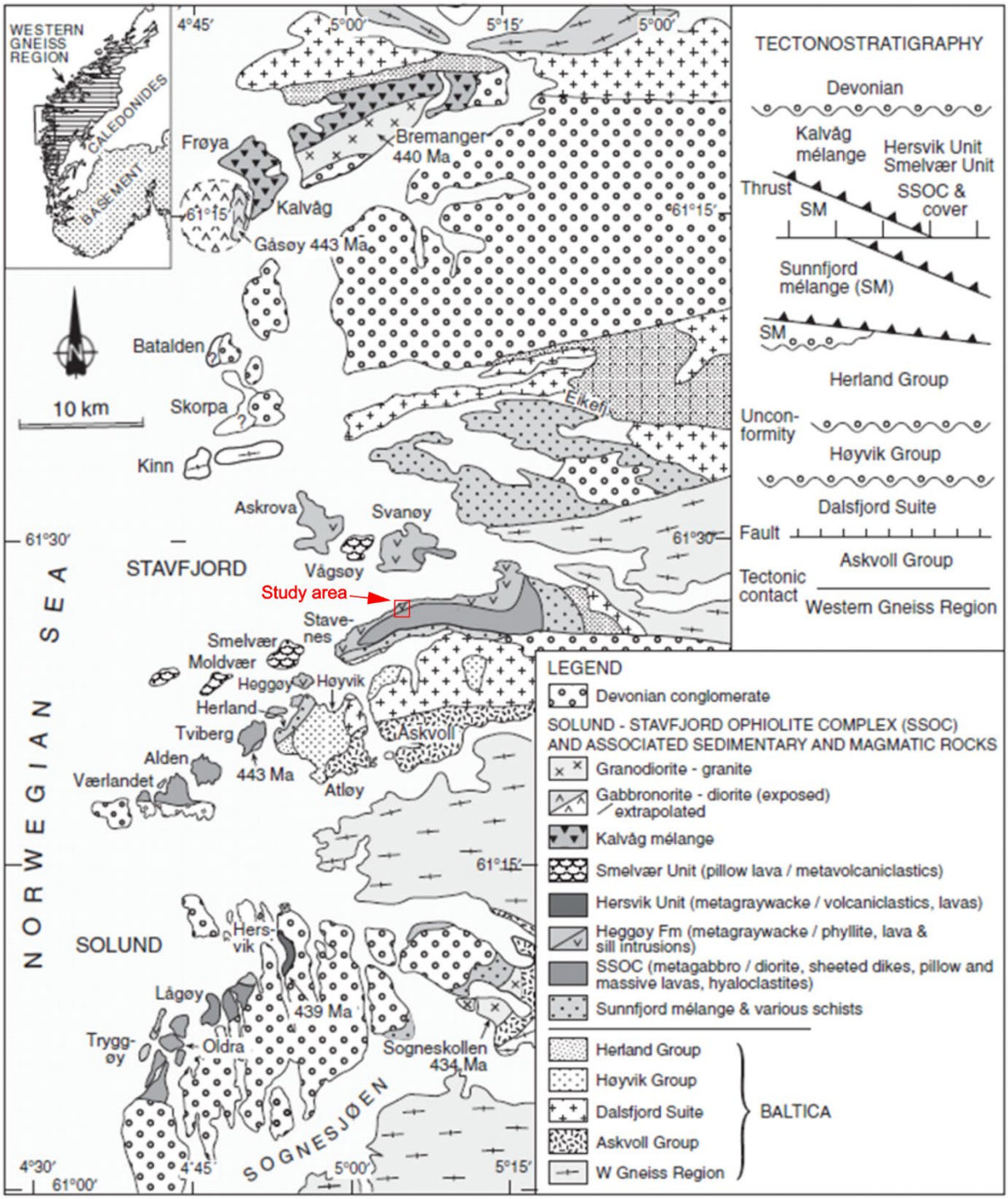

Fig.1.1: Geological map of the Solund- Bremanger area in Sunnfjord, showing the stratigraphy and tectonostratigraphic units of various rock complexes. From Furnes et al. (2012) (modified from Furnes et al., 1990).

Chapter 2 – Geological setting

2.1 The Scandinavian Caledonides

2.1.1 Evolution and tectonostratigraphy of the Caledonides

The Caledonian Mountain range extends from western and north-western parts of Europe through Ireland, Scotland, and Scandinavia to Svalbard in the north, and evolved through Cambrian, Ordovician, Silurian and Lower Devonian times (Fossen et al., 2013). The Caledonian evolution was initiated in the end of Neoproterozoic when Baltica rifted from Laurentia, as well as the formation of the Iapetus Ocean, ending with the eventual collision of the two blocks (Corfu et al., 2007), involving subduction of the margin of Baltica beneath Laurentia (Roberts, 2003). During this collision, nappes of different origin were evolved and emplaced onto the Precambrian Fennoscandian Shield (Roberts and Gee, 1985; Stubseid, 2017).

The tectonostratigraphy of the Scandinavian Caledonides defines different ages and units (Fig.2.1). The Autochthon-Parautochthon consists of the basement of the Fennoscandian Shield and the cover of late Proterozoic and early Paleozoic age (Andersen and Andresen, 1994), and is dominated by many Sveconorwegian plutonic rock complexes (Fossen and Hurich, 2005). The Lower Allochthon comprises manly of low-grade sedimentary sequences of late Proterozoic to early Paleozoic age, where the basement lithologies of the Fennoscandian Shield are involved in the uppermost parts. The Middle Allochthon contains Precambrian gneiss complexes and thick psammitic sequences and is overlain by Paleozoic metasediments, whereas The Upper Allochthon is dominated by early Paleozoic outboard terranes, as well as ophiolites and island-arc complexes. The Uppermost Allochthon consists of a heterogenous complex of nappes, dominated by schists, marbles, granitoids and gneisses, and is only present in the regions of Nordland and Troms (Andersen and Andresen, 1994). In the three first units, including the lowermost part of unit four, the Baltic crust miogeocline and transitional continental/oceanic crust, respectively, are represented (Andersen and Andresen, 1994; Roberts, 1988; Stephens and Gee, 1989). The uppermost parts of unit four is considered to form the remnants of the Iapetus Ocean, whereas unit five is composed of oceanic and continental terrane, with a very uncertain definite evolutionary history and origin. However, a Laurentian origin is suggested for the uppermost Allochthon (Sturt et al., 1984; Dallmeyer and Gee, 1986; Stephens and Gee, 1989; Andersen and Andresen, 1994).

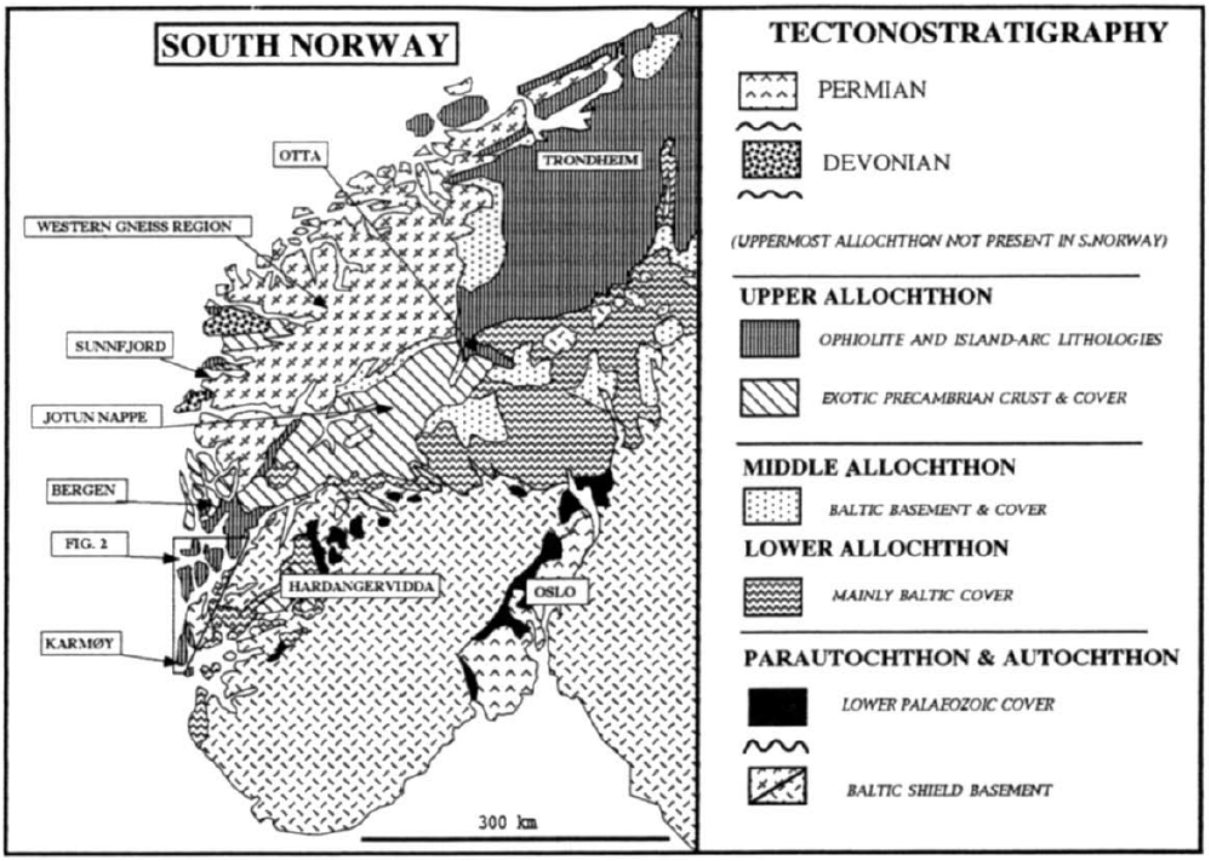

Fig.2.1: Tectonostratigraphic map of southern Norway representing the different nappes evolved during the Caledonian collision, emplaced onto the Precambrian Fennoscandian Shield. From Andersen and Andresen (1994).

2.1.2 The Caledonian extension

As a result of the extensional collapse of the Scandinavian Caledonides, rapid tectonic denudation of the orogen occurred, as well as exhumation of high- and ultra-high-pressure metamorphic rocks during the Late Paleozoic. The extensional deformation led to vertically variations in the crustal section, as well as horizontal variations from east to west across the orogen, where both structures are represented by eclogite to amphibolite facies, and amphibolite to greenschist-facies. While the contraction of the Scandinavian Caledonides is characterized with nappe transport and southeast-directed structures, the extension is mainly associated with west and northwesterly directed structures which is thinning the stack of the nappes (Andersen, 1998). The Caledonian collapse also led to reworking and decompression of the high-pressure metamorphic rocks, creation of massive extensional detachments faults, as well as the Devonian detachment basins (Andersen et al., 1994; Osmundsen, 1996; Osmundsen et al., 1998).

The role of extensional tectonics in the Scandinavian Caledonides of south Norway was studied by Fossen (1992), and two modes of extension were recognized and presented. In the

first mode (Mode 1) back movement of the Caledonian nappes dominated, whereas the second mode (Mode 2) was characterized by extension of the Baltic Shield during the development of major oblique Shear Zones (Fossen, 1992). The Hardangerfjord Shear Zone (HSZ) is considered as one such Shear Zone, as well as the Nordfjord-Sogn Detachment (NSD), nearby the study area. Fig. 2.2 displays Mode 2 extension where HSZ and NSD runs parallel to the Caledonian orogenic belt, with NW-SE trending ductile structures (Fossen and Hurich, 2005). The NSD is defined as a classic detachment combining four basins with sediments of Devonian age. These sedimentary deposits are known as the Hornelen-, Håsteinen-, Kvamshesten- and Solund basins, and are each bounded to the east by major fault zones (Norton, 1987).

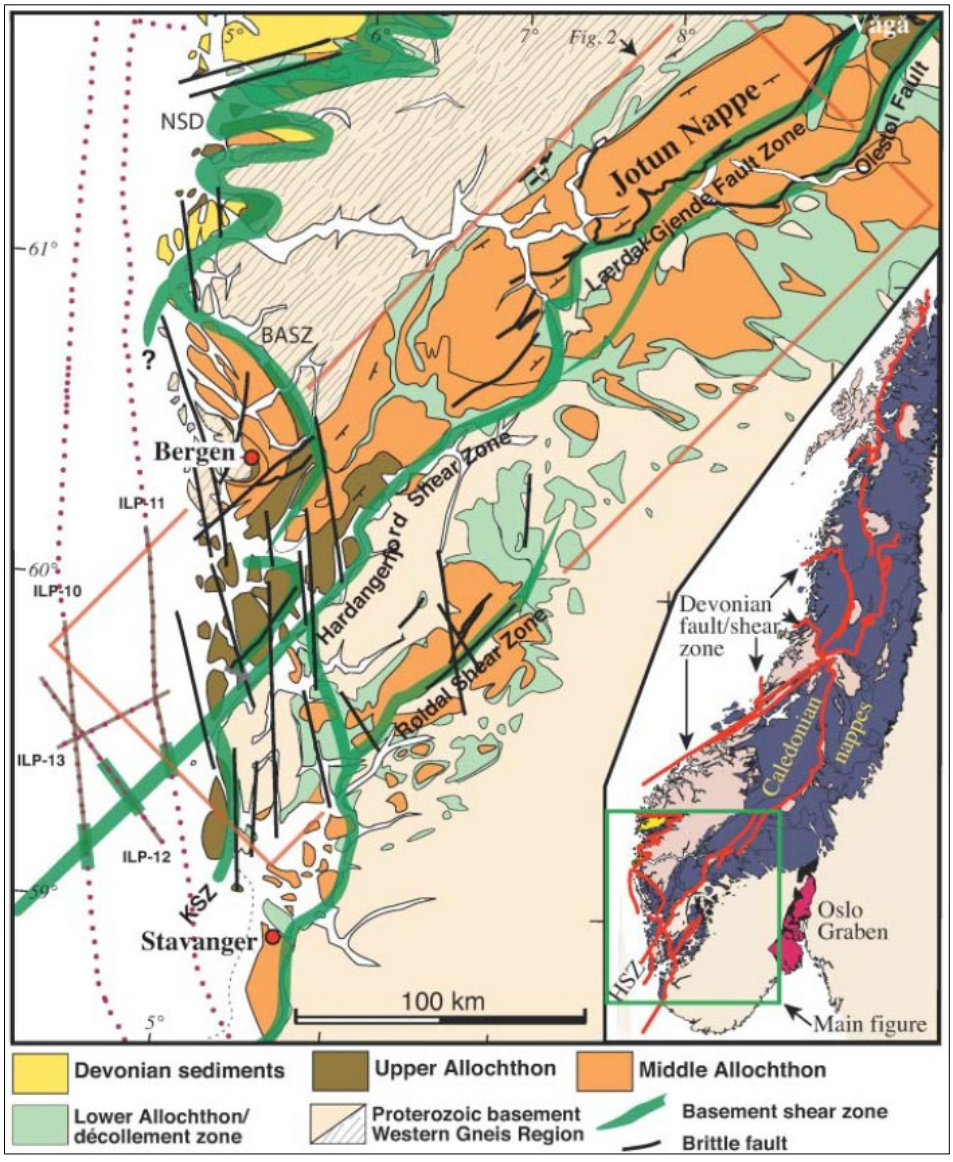

Fig.2.2: Geological map of southwest Norway, representing the Hardangerfjord Shear Zone and how it has affected other structures in the region. The thick green line represents Mode 2 extension and has formed the Nordfjord- Sogn Detachment (NSD) and Bergen Arc Shear Zone (BASZ). From Fossen and Hurich (2005).

2.2 Magmatic and tectonic evolution of the island arcs and ophiolites in SW-Norway

According to Pedersen and Dunning (1997) the new ages of the ophiolitic terrane in SW-Norway proves that the complexes are related in time and space with typically island arc complexes. Based on U/Pb ages, together with their field relations and geochemistry, they suggest a magmatic evolution for the SW-Norwegian ophiolitic terranes which can be summarized in three main stages. The first stage is characterized by crust forming event with tholeiitic magma developing ophiolitic axis sequences. The second stage is characterized by boninitic magmas with subordinate tholeiitic magmas, which intruded the newly formed tholeiitic crust. And finally, the third stage is dominated by calc-alkaline and alkaline magmatism, which in interrelation with highly alkaline formed shoshonitic magmas, led to eruption of a thick sequence of oceanic island basalts (OIB) (Pedersen and Hertogen, 1990; Pedersen and Dunning, 1997).

According to Pedersen et al. (1992) there is a marked change around the Cambro-Ordovician boundary, changing from a spreading-dominated to a subduction-dominated situation resulting in island-arcs and ophiolite complexes. An important and crucial question was still whether these magmatic sequences (ophiolites and arcs) developed adjacent to Baltica or Laurentia. New geochemical data of the magmatic rocks, combined with provenance, including existing faunal information, strongly suggested that parts of the Upper Allochthon, developed on or adjacent to the Laurentian margin (Pedersen et al., 1992). Further, they developed an evolutionary model for the early Ordovician ophiolite and island arc sequences and rift-related sequences of late Ordovician to early Silurian age (Fig. 4, Pedersen et al., 1992). The model is divided into six steps, where the two first steps represent subduction and the development of immature island arc systems. The third step is dominated by mature island arcs, which is colonized by shallow marine, Toquima-Table Head faunas, whereas the fourth step is characterized by accretion of the island arc system to the Laurentian continental margin. The two last steps represent the rifting stage of the continental margin and the formation of a marginal basin of late Ordovician-early Silurian age, initiated by Hirnantian and Holorhynchus faunas (Pedersen et al., 1992).

2.3 Ophiolitic Terrane related to the Solund-Stavfjord Ophiolite Complex

The ophiolitic terrane of south-western Norway has been thoroughly mapped and studied (e.g., Furnes et al., 1979; Furnes et al., 1985; Dunning and Pedersen, 1988; Pedersen et al., 1988). In the Scandinavian Caledonides two groups of ophiolites are recognized, representing marginal basins of different age. Group 1 comprises major ocean or mature marginal basins, whereas group 2 defines small and younger marginal basins. (Furnes et al., 1985). The main crust-building period was between approx. 500-470 Ma giving the formation of several major ophiolite complexes, whereas the second period was a short-lived event during approx. 445-435 Ma (Dunning and Pedersen, 1988; Pedersen et al., 1991; Dilek et al., 1997; Furnes et al., 2012; Furnes et al., 2014). The oldest generation of spreading events is represented by Lyngen, Leka, Trondheim area, Gulfjell and Karmøy ophiolites, whereas the youngest generation is represented by the Sulitjelma and the Solund-Stavfjord ophiolites (Furnes et al., 2014). Similar ages of large mafic intrusive complexes occur in Newfoundland (Pedersen et al., 1991).

2.3.1 The Sulitjelma Gabbro

In Northern Norway, the Sulitjelma Gabbro has been dated with U/Pb zircon/sphene method to 437 $\pm$ 2Ma. Trace element geochemistry, Nd and Sr- isotopic composition and geological relationship indicates that the gabbro, associated dike swarms and pillow lavas formed during initial stages of backarc spreading, like the Solund-Stavfjord Ophiolite. The Sulitjelma Gabbro can be correlated with the Solund-Stavfjord Ophiolite due to the similarities in age and spreading-related magmatism and marginal-basin development, which confirms that the gabbro formed along the margin of Iapetus in late Ordovician-early Silurian times (Pedersen et al., 1991).

2.4 Geology of the study area in the Solund-Stavfjord region

2.4.1 Tectonostratigraphy in the Solund-Stavfjord region

In the Sunnfjord area the Nordfjord-Sogn detachment zone (NSDZ) is a dominant structural element, which equates a series of allochthonous units against the Western Gneiss Region basement (Corfu and Andersen, 2002). The composition of the allochthonous units were in 1990 divided into three tectonic units by Furnes et al. (1990) after detailed mapping of the Solund-Stavfjord area (Furnes et al., 1990) (Fig. 1.1).

The lower tectonic unit consists of the Vevring Complex of eclogite-bearing gneisses which belongs to the Western Gneiss Region of Precambrian age. The unit also comprises the Askvoll Group, consisting of low- to medium grade sedimentary, volcanic, and plutonic rocks (Furnes et al., 1990). The middle tectonic unit is dominated by the Dalsfjord Suite, Høyvik Group and Herland Group. By the extensional Kvamshesten fault, the middle unit is separated from the lower tectonic unit (Fig. 1.1) (Furnes et al., 1990). According to Kolderup (1921), the Dalsfjord Suite is composed of syenitic to charnockitic orthogneisses, granites and gabbros, where a monzonite sample yields a zircon age of 1.634 $\pm$ 3 Ma (Corfu and Andersen, 2002). The Høyvik group is locally resting with a primary depositional contact on the Dalsfjord Suite, and has a pre-Silurian age, whereas the Herland Group has a Silurian age (Furnes et al., 1990).

Between the middle- and the upper tectonic units, the Sunnfjord Mélange (Andersen et al., 1990) is located and stratigraphically overlies the Herland Group with a depositional contact. As a result of this, the mélange provides a terrane link between the SSOC and the continental margin (Furnes et al., 1990). The upper tectonic unit is dominated by the SSOC, as well as a cover of metasediments and metavolcanites. Devonian sedimentary rocks of the Kvamshesten Group are the uppermost unit in this area and was developed during the post-collisional extension of the Caledonian orogen (Osmundsen et al., 2000; Corfu and Andersen, 2002). Other Devonian basins in the area is the Hornelen basin, Håsteinen basin, and the Solund basin, all developed during the extensional faulting in the upper crust (Andersen et al., 1994). The four Devonian basins are all bounded to the east by major fault zones, such as the Nordfjord-Sogn Detachment Zone (Norton, 1987).

2.4.2 Solund-Stavfjord Ophiolite Complex

The Solund-Stavfjord Ophiolite Complex (443 $\pm$ 3 Ma) and its cover is localized in the area between Solund and Bremanger (Fig. 1.1), and contains sheeted dikes and volcanic rocks, as well as high- level isotropic gabbro and diorite in some places, i.e., mainly on the Island of Tviberg, and Lågøy in Solund (Furnes et al., 1990). The ophiolite represents a remnant of the Iapetus oceanic lithosphere evolved in a Caledonian marginal basin (Dilek et al., 1997), and in the western Norwegian Caledonides this complex is representing the youngest phase of oceanic crust formation (Furnes et al., 1990; 2012). In the upper-crustal unit of the SSOC, the geochemical features indicates that the melt evolutions only involved minor or no subduction-derived components. The evolution of the SSOC oceanic crust occurred in a short-lived (~10-20 m.y.), trench-distal, continent-proximal back arc basin, close to the eastern margin of Laurentia, during the closure of Iapetus (Furnes et al., 2012).

SSOC contains three structural domains generated during two episodes of seafloor spreading, and each unit has its own geological characterization and different types of crustal architecture (Dilek et al., 1997). Domain 1 comprises pillow lavas, massive sheet flows, hyaloclastites, NE- trending sheeted dikes, and high-level gabbros. Domain 2 represents the oldest preserved oceanic crust in the ophiolite and is dominated by pillow lavas, W-NW-trending sheeted dikes and underlying isotropic gabbros, whereas Domain 3 is represented by shear zones of dike swarms, plutonic rocks, serpentinite breccias, and fault-bounded serpentinite slivers in deformed isotropic to flaser gabbros (Furnes et al., 2000; 2012). The presence of broad shear zones on the Island of Tviberg, where serpentinite bodies were emplaced contemporaneously with and prior to the last phases of magmatic activity, is an important tectonic feature of the SSOC. This tectonic zone is considered to have originated at the oceanic stage as part of a transform fault (Skjerlie and Furnes, 1990), which subsequently became the site where obduction initiated, i.e., formation of the Sunnfjord Mélange (e.g., Furnes et al., 1990).

The Stavenes Group

The SSOC is conformably overlain by an assemblage of sedimentary and volcanic rocks, called the Stavenes Group (e.g., Furnes et al., 1990). The Stavenes group is a sedimentary and a volcanic sequence, divided into the Heggøy Formation and the Hersvik and Smelvær Units (Fig.1.1) (Furnes et al., 1990). Of all tectonostratigraphic assemblages constituting the Upper

Tectonic Unit in the western Norwegian Caledonides, Sunnfjord Mélange and the Heggøy Formation are the only rock-formations to have exposed contact with the SSOC (Furnes et al., 2012). Furnes et al. (2012) concluded that (1) the Sunnfjord Mélange is structurally the lowest tectonostratigraphic unit, (2) the Heggøy Formation rest with a primary stratigraphic contact on the SSOC, (3) the Hersvik Unit is representing an island-arc complex which is coeval or younger than the SSOC, (4) the Smelvær Unit comprises off-axis mafic volcanic and intrusive rocks that has evolved on and across the SSOC oceanic crust, and final (5) the Kalvåg Mélange (Ravnås and Furnes, 1995), dominated by material derived from both Hersvik and Smelvær Units, is representing the youngest tectonostratigraphic in the region (Furnes et al., 2012).

Sunnfjord Mélange

The southern and eastern parts of the Stavenes Peninsula is the type locality for the Sunnfjord Mélange (Andersen et al., 1990), where the sheeted dike complex of the SSOC rests tectonically on the sub-ophiolitic mélange (Furnes et al., 2012). Sunnfjord Mélange is a sub-ophiolitic mélange that is a strongly tectonized sedimentary assemblage, comprising fine-grained quartz bearing chlorite-muscovite schists and metagraywacke rocks, as well as bocks of metabasalt, serpentinites, marble, and meta-arkose (Fig. 1.1) (Alsaker and Furnes, 1994; Furnes et al., 2012).

Heggøy Formation

The Heggøy Formation constitutes the sedimentary cover of the SSOC (Fig. 1.1), locally hosting mafic, minor intrusions (Furnes et al., 2012). Geochemical characters from the Heggøy Formation can be correlated to those of the SSOC and basic metavolcaniclastites of island arc tholeiite (IAT) composition, which indicates that both SSOC and the Heggøy Formation developed in a marginal basin between a continental margin and an active subduction system (Furnes et al., 1990).

Hervik Unit

The Hersvik Unit has a different geochemical composition throughout the sequence and is only exposed in the Solund region. In this region the unit is unconformably overlain by the Devonian conglomerate (Furnes et al., 2012). Previously, the Hersvik Unit were divided into three minor groups based on the lithological developments (Furnes, 1974), a subdivision that subsequently was repealed (Furnes et al., 1990). Now the whole sequence is considered as

one unit, where about 50% of the unit is composed of mafic lavas of plagioclase-phyric basalt intercalated with sedimentary and volcaniclastic rocks (Fig. 1.1) (Furnes et al., 2012).

Smelvær Unit

The exact stratigraphic position for the Smelvær Unit is uncertain due to the lack of exposed contacts to the above-described components (Furnes et al., 2012). On the Island of Smelvær the unit comprises non-vesicular pillow lavas, minor massive lavas and green volcaniclastic rocks interbedded with black chert and graphite-bearing black schists (Fig. 1.1). On the Island of Vågsøy (Fig. 1.1), the sequence is dominated by green volcaniclastic rocks and minor flaser-gabbro (Furnes et al., 2012).

Kalvåg Mélange

In the area of Kalvåg-Bremanger, the Kalvåg Mélange is located and is represented by an olistostromal mélange with olistolith blocks of variable size (Fig. 1.1). According to Ravnås and Furnes (1995), the geological characterization can be defined by a compositional range of mafic volcanic rocks of tholeiitic, boninitic, and calc-alkaline to alkaline affinities. Hence, it was suggested that this mélange originated from sources having different tectonomagmatic settings (Furnes et al., 2012).

Ore deposits

Ophiolites represent an important source for Cu, and to some extent for Zn and Pb, as well as Ag and Au in the recorded human history (Dilek and Furnes, 2014), and these elements are in general spatially and temporally associated with volcanogenic massive sulfide deposits (VMS). In the SSOC, mining for Cu and Zn has been conducted in the Grimelia area. During the periods of 1759-1782, 1851-1906, and 1914-1919 the mines in Grimelid were operational, with a production of 300-1100 tons ore a year and a Cu average of 3.5-4.5% (Stensrud, 1976; Korneliussen and Often, 1980). The mining has been conducted on minerals such as magnetic pyrite, iron pyrite, copper pyrite and zinc blende or sphalerite. Mineralization is linked to pillow lavas and meta-hyaloclastic breccias, and the thickness of the mineralized zones range from a few mm to several meters. The sulfide content and composition of the ore mineralization varies greatly, and are commonly found as solid iron pyrite ore, solid iron pyrite-magnetic, pyrite-copper, and pyrite-zinc blende ore, as well as small pyrite strips, veins, and impregnations (Korneliussen and Often, 1980).

Chapter 3 – Fieldwork and field-description

The investigated area for the study of this master thesis is located on the southwest coast of Norway, in the area between the mines in Grimelia, and Stavfjorden (Fig. 3.1). The area of interest extends from Merkesheia in the south to Revebergtåna in the north, with a total extent of approximately 1.2 km. As a result of thorough fieldwork and field-mapping, a Master profile is constructed through the area of interest, showing the pseudostratigraphy from bottom to top (Fig. 3.1), including the cover sediments from Staurholmen in the North (H. Furnes, personal information, 2021). The constructed Master profile provides two versions from part 1 of the profile (A and B), as the lithologies in this section varies a lot. Further, the profile contains 13 smaller detail profiles, to show the in-situ variations within the sequences (Fig.3.2).

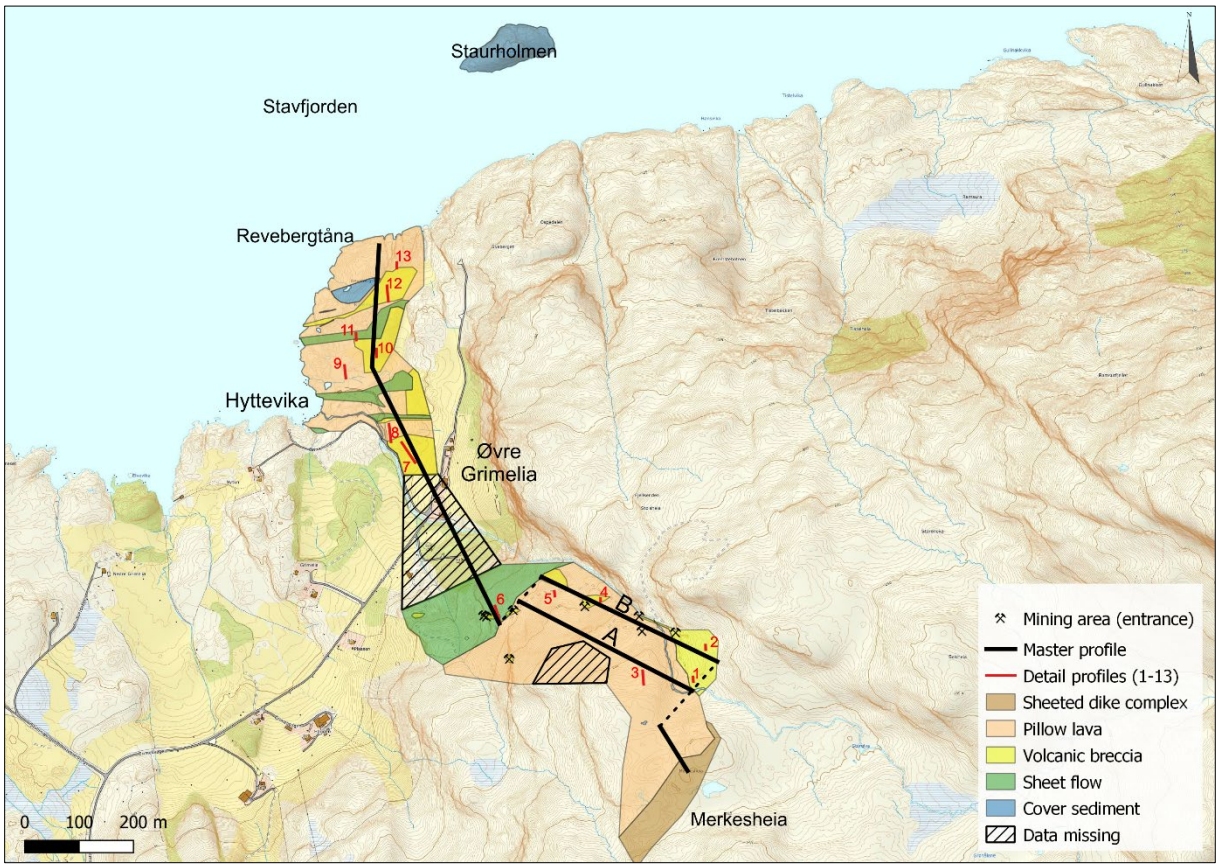

Fig.3.1: Geological map of the investigated area of Solund-Stavfjord Ophiolite Complex, showing the pseudostratigraphy from bottom (Merkesheia) to top (Revebergtåna), including the cover sediments from Staurholmen in the north. The Master profile includes both version A and B from part 1 of the profile, where A represents only a pillow lava section from the sheeted dike complex, and B includes the volcanic breccias with ore deposits (see Fig. 3.2), as well as pillow lavas.

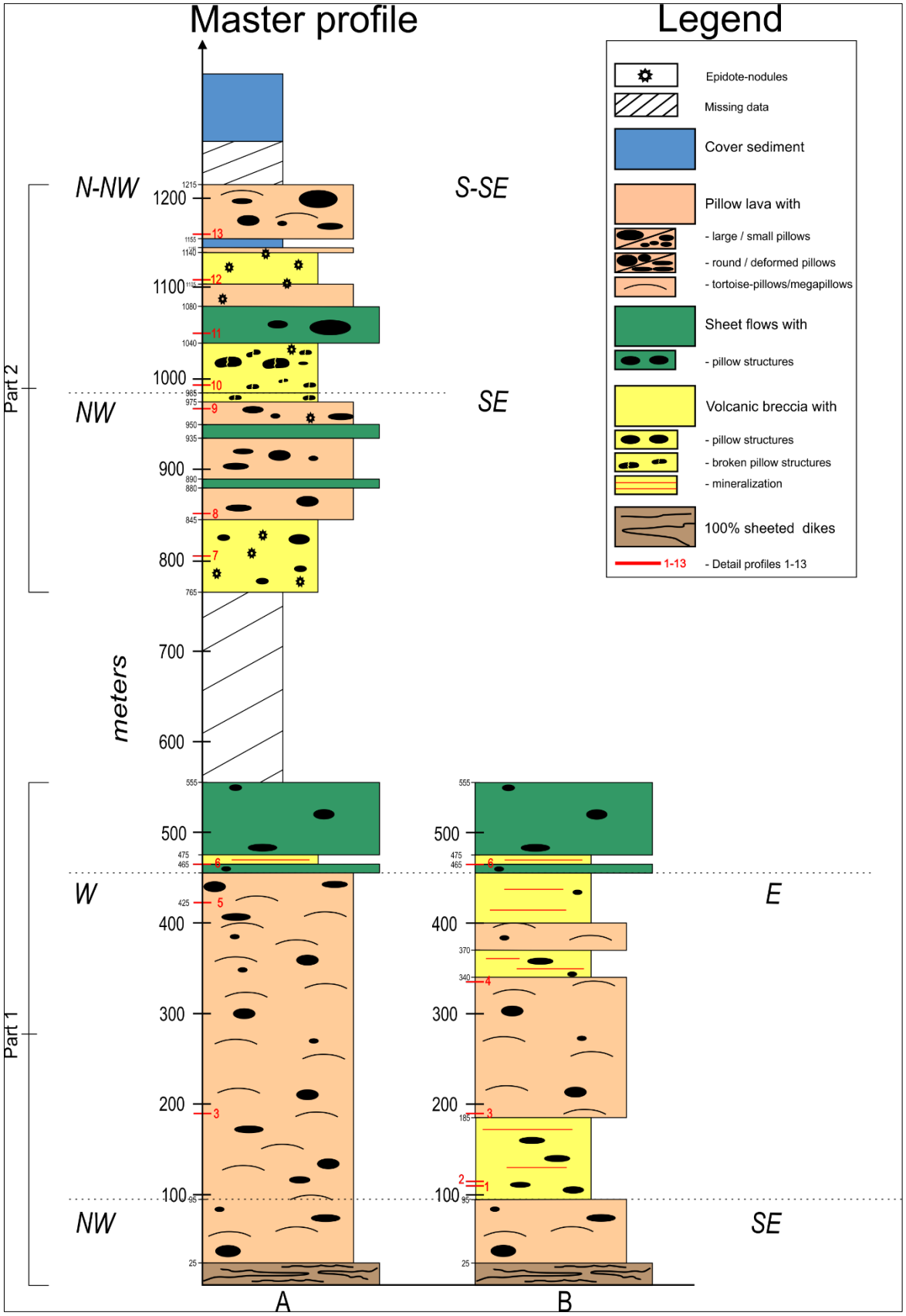

Fig.3.2: Master profile consisting of sheeted dike complex at the bottom and a variation of pillow lavas, sheet flows and volcanic breccias towards the top, as well as cover sediments at the top (Staurholmen). The profile is further divided into two parts. Part 1 represents the lowermost part of the profile, starting at Merkesheia in the south, including detail profiles 1-6. This part is further divided into an A- and B- section. Part 2 constitutes the uppermost part of the profile, ending at Revebergtåna, including detail profiles 7-13.

3.1 Master profile – Part 1

Part 1 of the Master profile represents the first 550 m of the stratigraphy above the sheeted dike complex furthest south. This part includes both profile A and B, due to major lithological differences. The sheeted dike complex is only registered and not further discussed.

3.1.1 Detail profile 1

This profile is located near 110 m stratigraphically (not adjusted) above the starting point of the Master profile (B), at the boundary between the sheeted dike complex and the volcanic sequence (Figs. 3.1 and 3.2), and approx. 50 m west of the Master profile. The rock-material within this sequence is mainly dominated by volcanic breccias with large lateral differences, for instance, areas with and without mineralization, as well as inconsistent presence of pillow lava. Typical structures within this sequence are also pillow fragments covered in mineralized zones (Fig.3.3). Within this exact profile, pillow lava-structures of different sizes occurs, as well as smaller areas with mineralization (Fig. 3.4). The rock-material is predominantly fine-grained with a gray color, whereas areas dominated with mineralization is rust colored with the same fine-grained quality. Measured pillows in the area range from 15x3 cm to 45x10 cm, which gives them an elongated effect (Appendix 1).

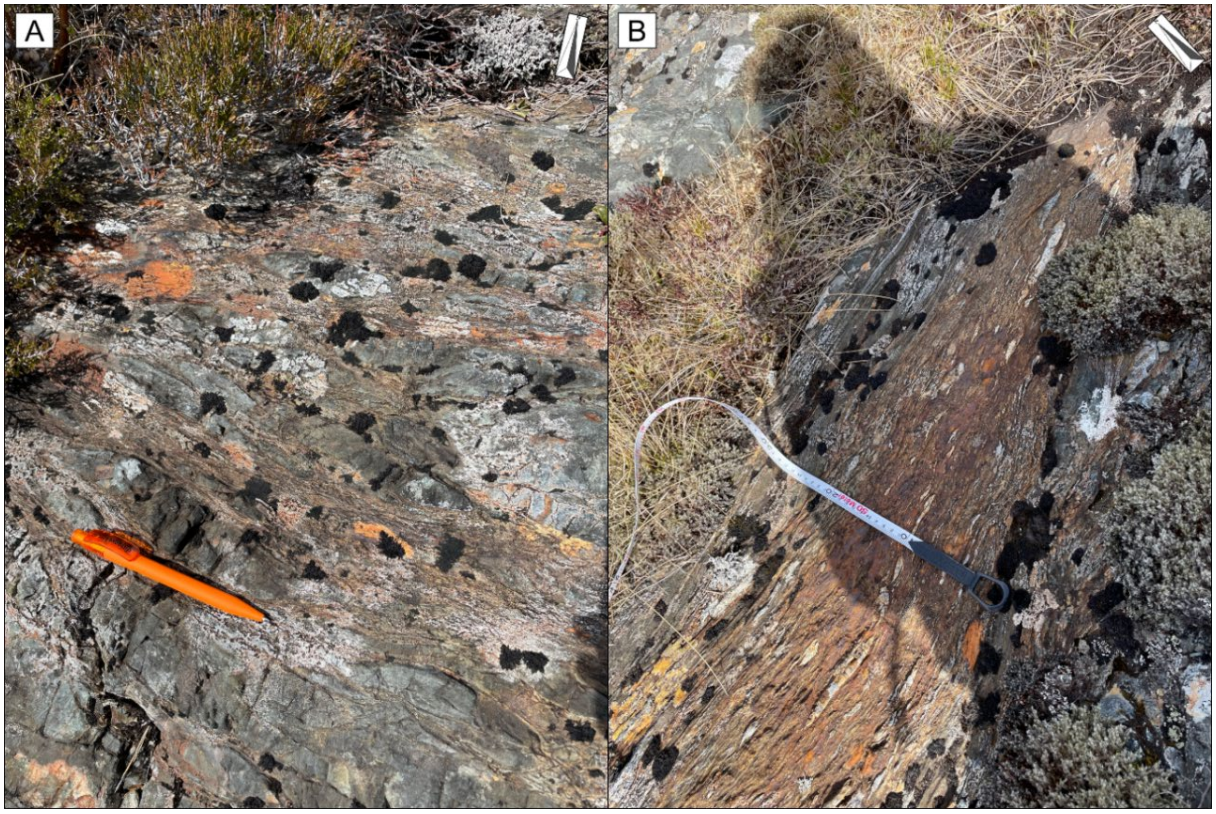

Fig.3.3: Pictures showing rock-material appearing within the sequence of volcanic breccias. Both pictures appear with strongly deformed zones consisting of varying degree of mineralization, and with whole rock-fragment (hyaloclastites/pillows) of different size. A: taken randomly within the volcanic breccia sequence. Pen size: 13.5 cm. B: taken at top of detail profile 2.

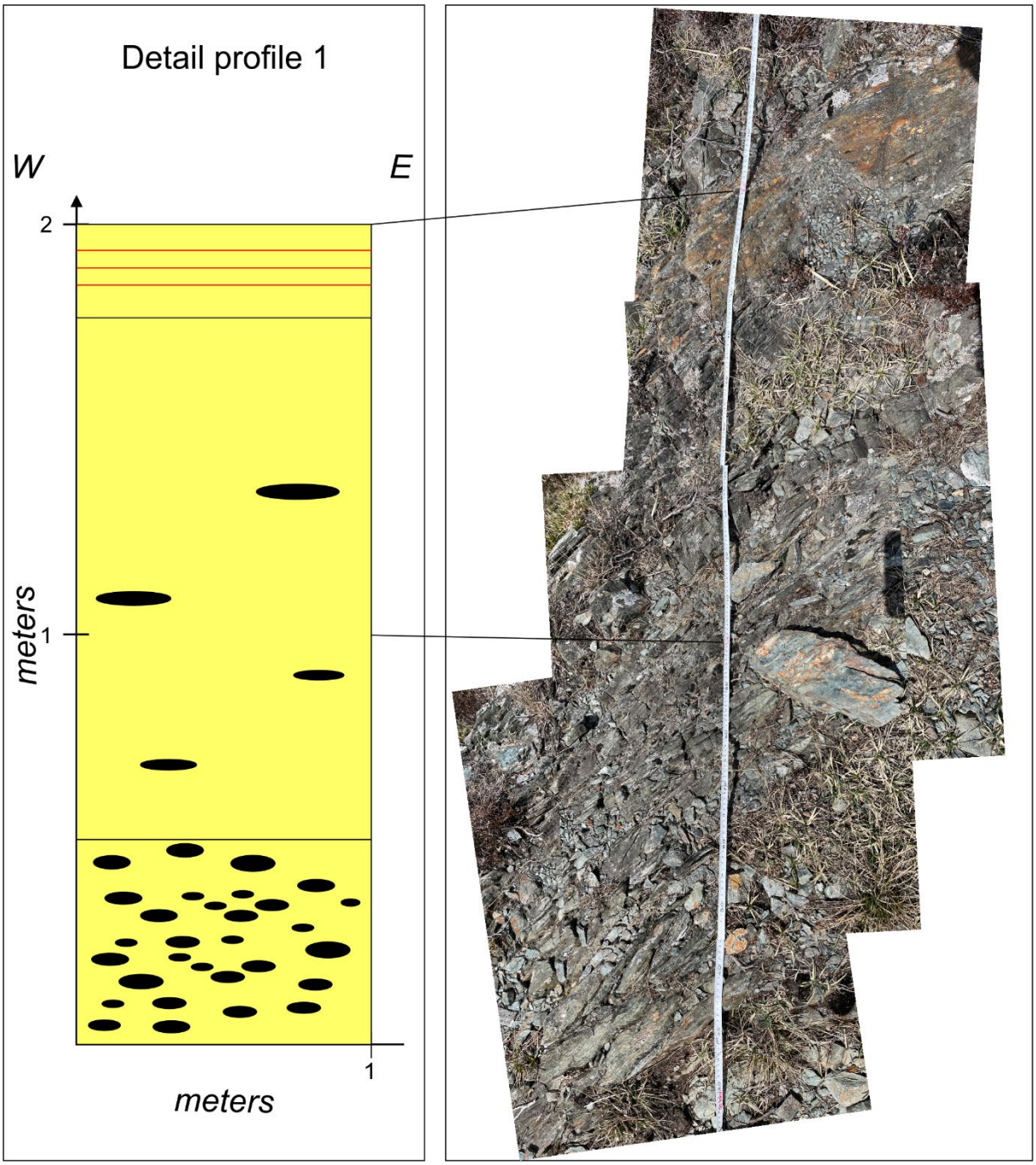

Fig.3.4: Sketch of detail profile 1 as well as live photos representing the different stages within the profile. The horizontal scale is not accurate for pillow measurements. The profile exhibits volcanic breccia with some pillow fragments at the bottom, and a few throughout the profile. Towards the end of the profile some mineralization occurs.

3.1.2 Detail profile 2

Detail profile 2 is located within the same sequence as the previous profile, approx. 10 m stratigraphically above and with a lateral difference of 70 m towards the northeast (Figs. 3.1 and 3.2). The reason why the profiles, 1 and 2, are so close is to reveal the big lateral differences within the sequence at the same stratigraphic level (volcanic breccia). The rock of this profile consists of marked zones of volcanic breccias, both with and without mineralization

(Fig.3.5). The area without mineralization has a grey color and a wavier surface due to occurring pillow fragments. These areas are represented by a mixture of volcanic breccias and pillow lavas, the latter is sometimes difficult to distinguish. In areas dominated by mineralization (rusty color), the rock-material is strongly deformed with clear hyaloclastites and pillow fragments in between. The color of the fragments is predominantly dark gray to black, but in this case, there are also a lot of white-colored fragments (Fig. 3.3B). Similar to detail profile 1, the pillows in this area appear elongated (Appendix 1).

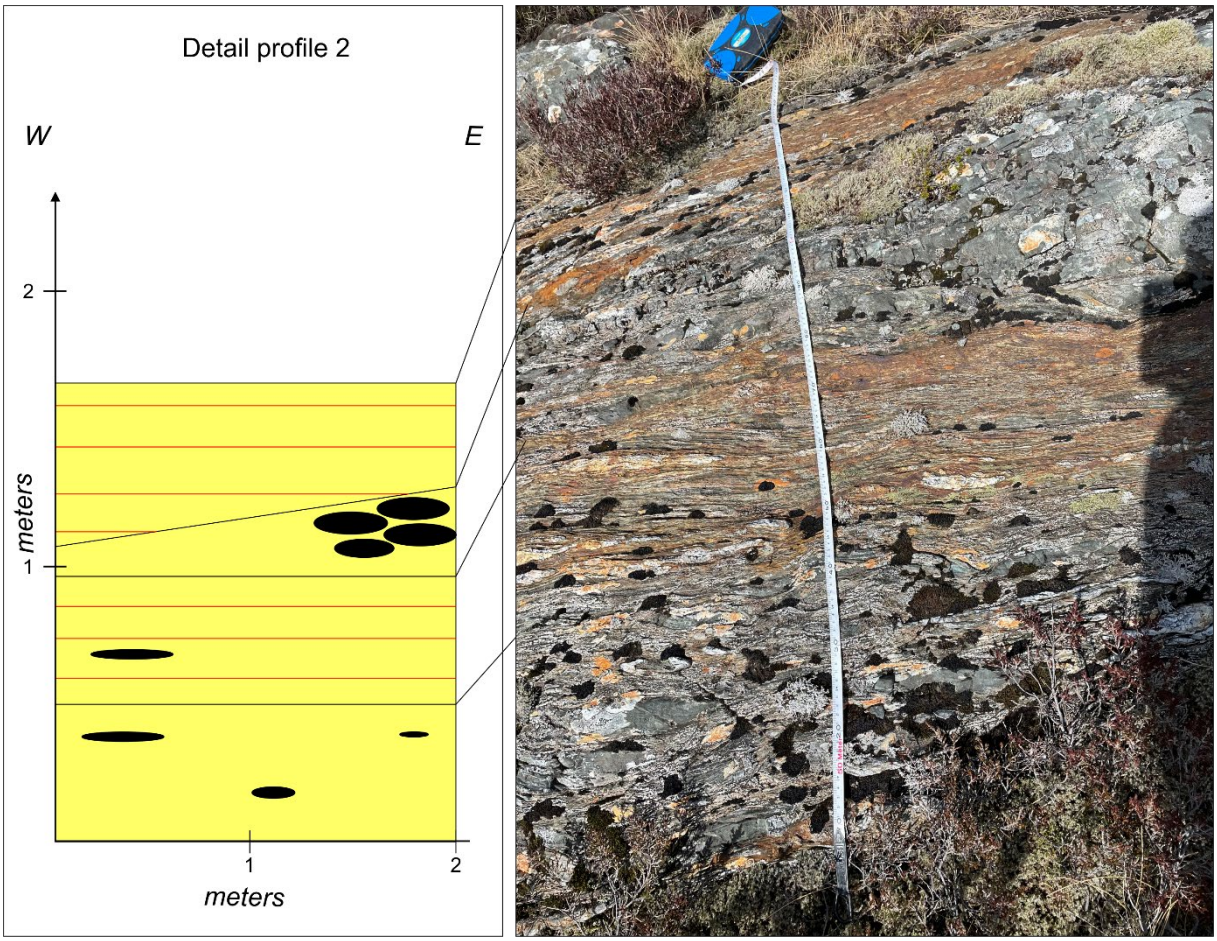

Fig.3.5: Sketch of detail profile 2 as well as live photos representing the different steps within the profile. More detailed picture of mineralized zones with fragments presented in Fig.3.3B. The horizontal scale is not accurate for pillow measurements. The profile indicates a section of volcanic breccias dominated by mineralized veins. Pillow fragments appear throughout the profile.

3.1.3 Detail profile 3

Detail profile 3 is located 190 m stratigraphically (not adjusted) above the sheeted dike complex and is predominantly consisting of pillow lavas with minor brecciated areas (Fig. 3.7). This profile represents the pillow section of part 1A of the master profile (Figs. 3.1 and 3.2). The rock-material in this area does not differ from the other areas, but in contrast it contains mostly pillow lavas of different shapes and sizes (Fig. 3.6) (Appendix 1). The predominant

feature of the pillow in this sequence, where detail profile 3 is located, is shown in Fig. 3.6A-B. Lobe-shaped, tortoise-like pillows is dominant throughout the sequence, and can easily be misinterpreted or taken as massive sheet flows in some cases. Minor pillows, shown in Fig. 3.6C, occurs within the sequence, but to a less extent.

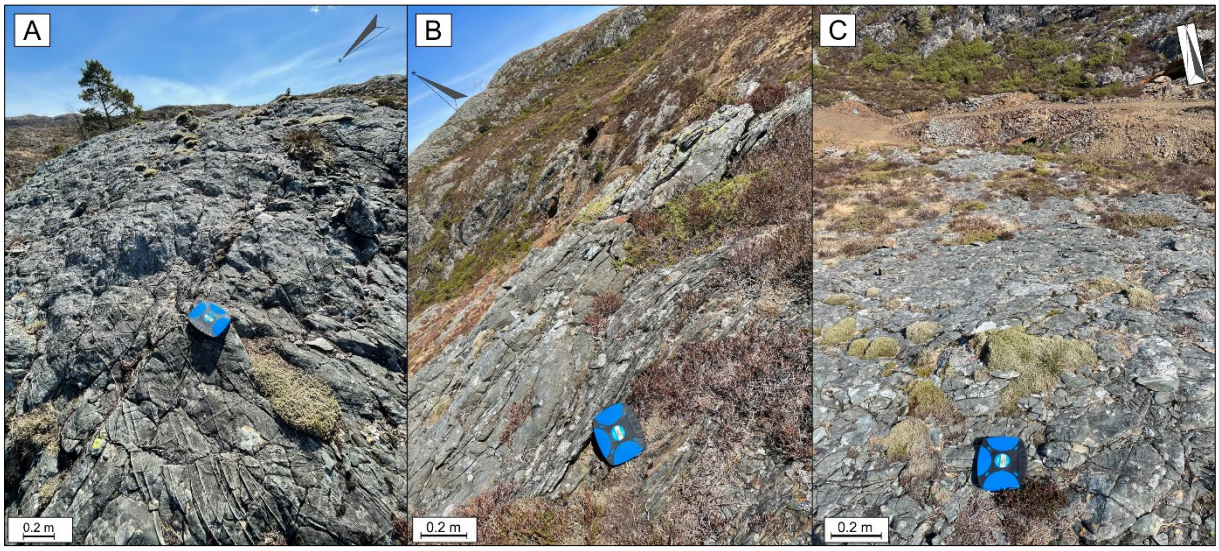

Fig.3.6: A: Picture showing the typically wavy surface of massive pillows within the sequence. Picture taken approx. 250-300m above the sheeted dike complex in part 1A. B: Picture showing a more detailed picture of detail profile 3, where the large pillows at the top of the profile is presented. Also, the brecciated zone is more present at this picture. C: minor pillows approx. 10 m above detail profile 3. The pillows in this area appear more rounded than in the profile.

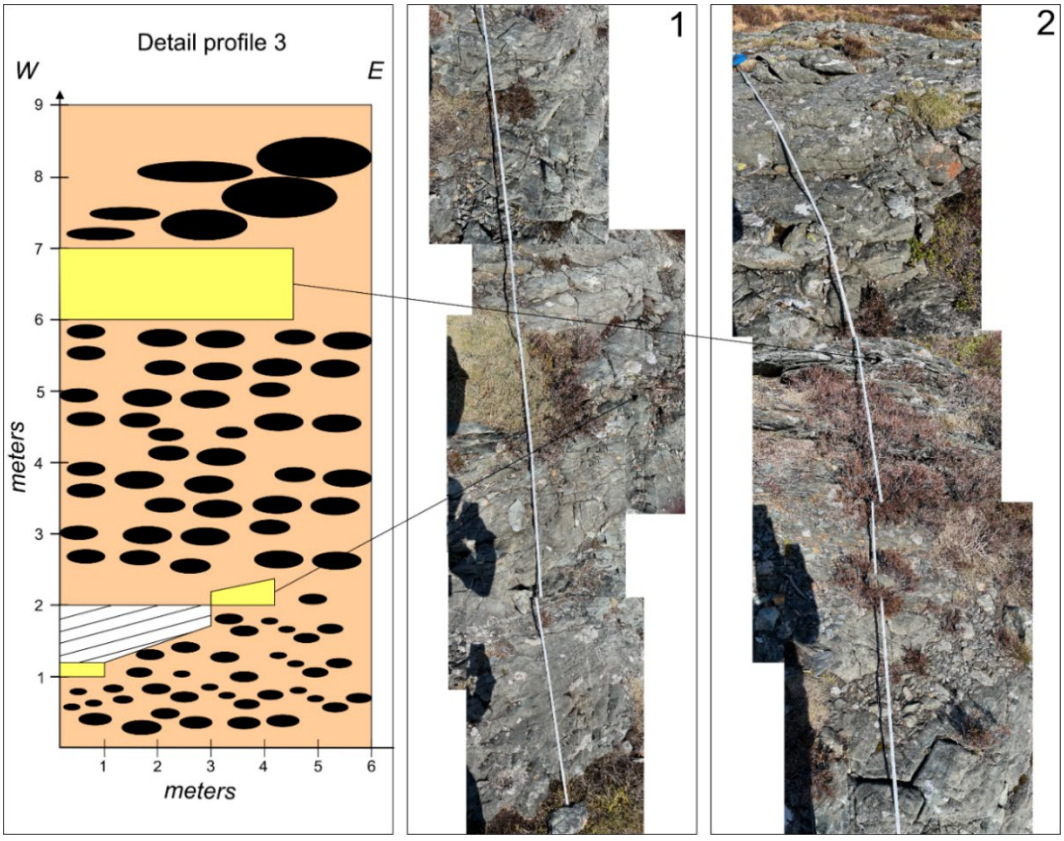

Fig.3.7: Sketch of detail profile 3 as well as live photos representing the different stages within the profile. The horizontal scale is not accurate for pillow measurements. The profile is dominated by pillow lavas, representing different pillow sizes and shapes. Within the profile a few zones of volcanic breccia occur.

3.1.4 Detail profile 4

Detail profile 4 is located 335 m stratigraphically (not adjusted) above the sheeted dike complex, within the transition between a pillow-dominated and volcanic breccia dominated sequence of the Master profile (Figs. 3.2 and 3.8). Again, this detail profile is intended to depict that there are lithological differences within one defined sequence. The bottom of the profile is represented by mineralized volcanic breccia. The mineralization is constrained to the brecciated areas, leaving most of the preserved pillows unaffected. Further, the area is again pillow-dominated without any mineralization. The pillows in this area are more abundant and easily recognizable, and similar to other pillows within the sequence (Appendix 1). Eventually, the area is represented by mineralized breccias again, as well as a massive sheet flows at top.

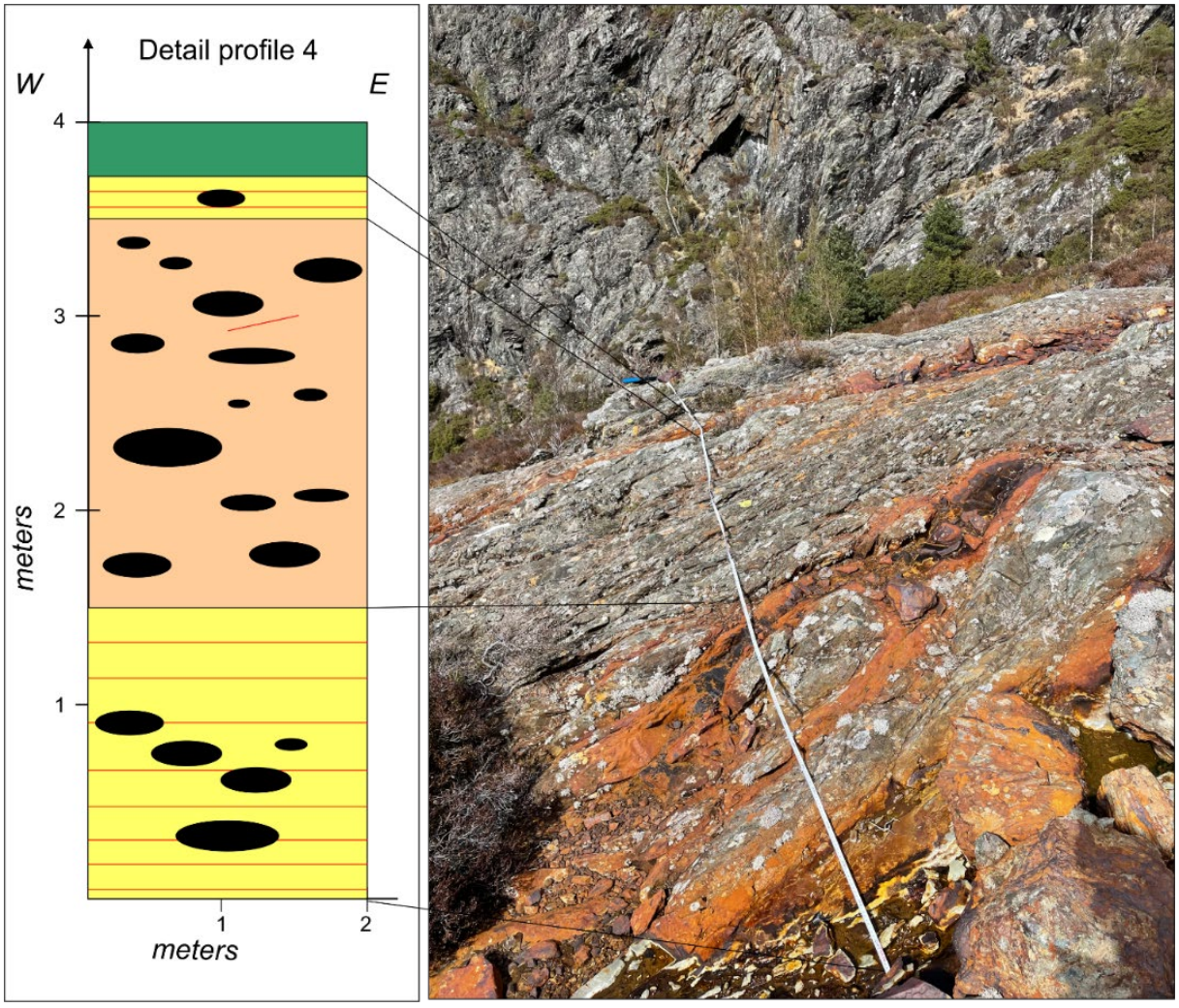

Fig.3.8: Sketch of detail profile 4 as well as live photos representing the different steps within the profile. The horizontal scale is not accurate for pillow measurements. This profile exhibits zones of volcanic breccia with mineralization, abundant pillow lava and a massive sheet flow at the top.

3.1.5 Detail profile 5

Detail profile 5 is located 425 m stratigraphically (not adjusted) above the sheeted dike complex (Figs. 3.1 and 3.2), and is dominated by massive sheet flows containing large pillow lavas between the flows (Fig. 3.9). The pillows in the area are generally massive and big, with smaller pillow in between. There are poorly defined brecciated areas, both with and without mineralization. Measured pillows range from 30x20 cm to 80x18cm, giving them an elongated surface (Appendix 1).

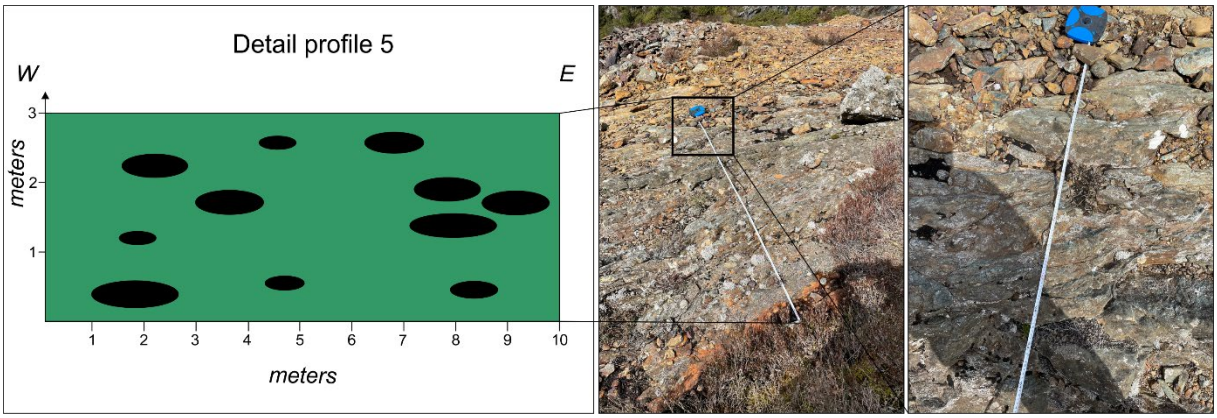

Fig.3.9: Sketch of detail profile 5 as well as live photos representing the different stages within the profile. The horizontal scale is not accurate for pillow measurements. This profile is dominated by massive sheet flows, with some measurable pillow lavas in between.

3.1.6 Detail profile 6

Detail profile 6 is located approximately 465 m stratigraphically (not adjusted) above the sheeted dike complex (Figs. 3.1 and 3.2), and is represented by massive sheet flows as well as volcanic breccias with mineralization (Fig. 3.11). The bottom four meters predominantly consists of massive sheet flows with clear brecciated zones, with a thickness of 10-20 cm. The next 8 meters represents volcanic breccia zones, which are strongly deformed and carries abundant mineralization (from 5-13m), which is placed right above one of the mines in the area (Fig.3.10). The massive sheet flows within the profile can easily be misinterpreted or taken as mega-pillows when they appear in smaller occurrences, such as at 1-1.4 m height. The rock-material in this profile varies between volcanic breccia and sheet flows, with fine grained material ranging from gray to rusty color, depending on the material. Pillow lavas occur within the profile as well as hyaloclastites (Appendix 1).

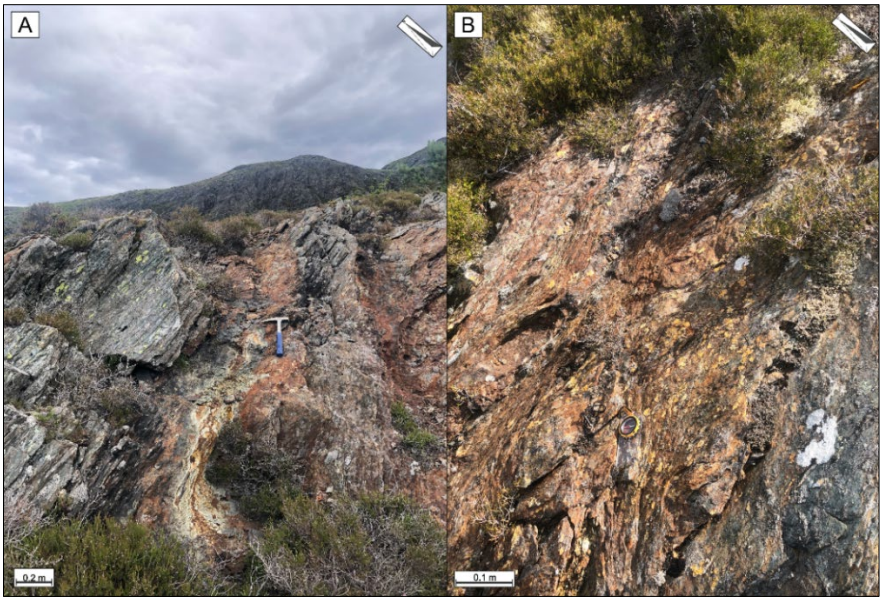

Fig.3.10: Showing more detailed pictures of the brecciated areas from detail profile 6, from 5-13 m. A: towards the top of the profile ending in massive sheet flows. B: from the middle of the profile, right above one of the mines in the area.

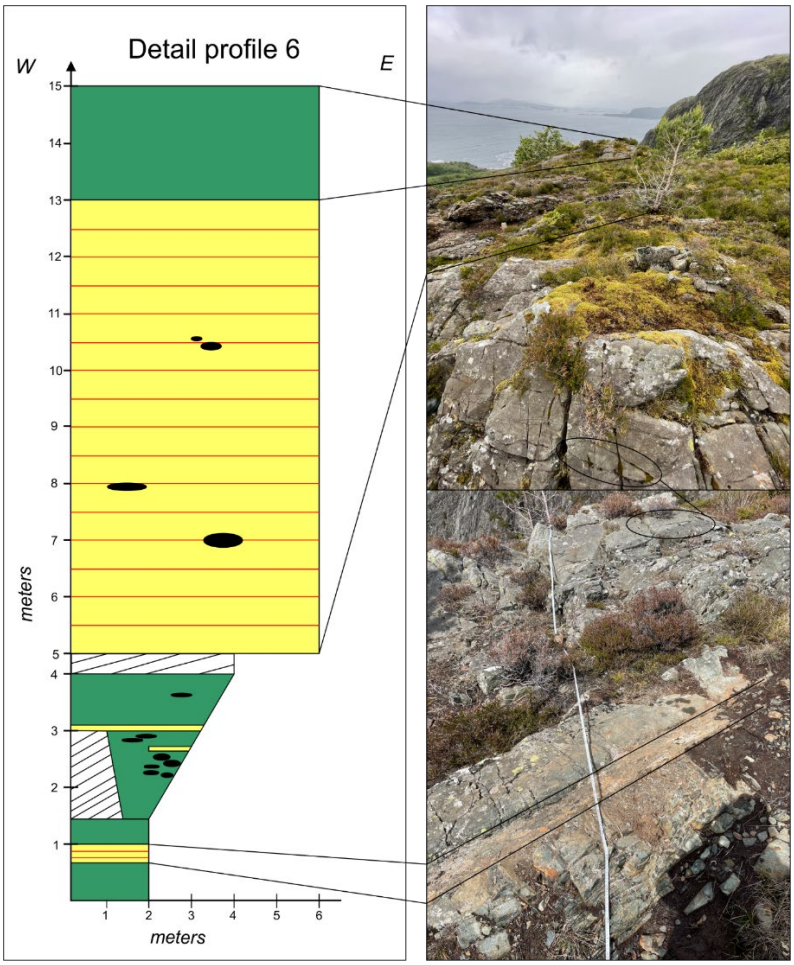

Fig.3.11: Sketch of detail profile 6 as well as live photos representing the different steps within the profile. The horizontal scale is not accurate for pillow measurements. The first four meters is dominated by massive sheet flows with zones of volcanic breccia. From 5-13 m the profile is represented by volcanic breccia affected by mineralization. Eventually the profile ends with massive sheet flows.

3.2 Master profile – Part 2

Part 2 of the Master profile represents 450 m of the volcanic stratigraphy, excluding the areas with missing data. The missing data section is due to vegetation and the lack of block-exposure within a small area.

3.2.1 Detail profile 7

Detail profile 7 is located 810 m stratigraphically (not adjusted) above the sheeted dike complex (Figs. 3.1 and 3.2). It is a strongly deformed sequence interpreted to consist of volcaniclastic rocks composed of different volcanic rock fragments (Fig. 3.13). Within this area, several epidote-nodules of varying size occur, as well as other volcanic rock fragments (Fig.3.12, Appendix 1). The rock-material in this sequence is much finer grained than earlier observed, plus with a bit darker shade (black). This may be interpreted as black chert (Fig. 3.12B). There is no sign of mineralization in this area, compared to part 1 of the Master profile.

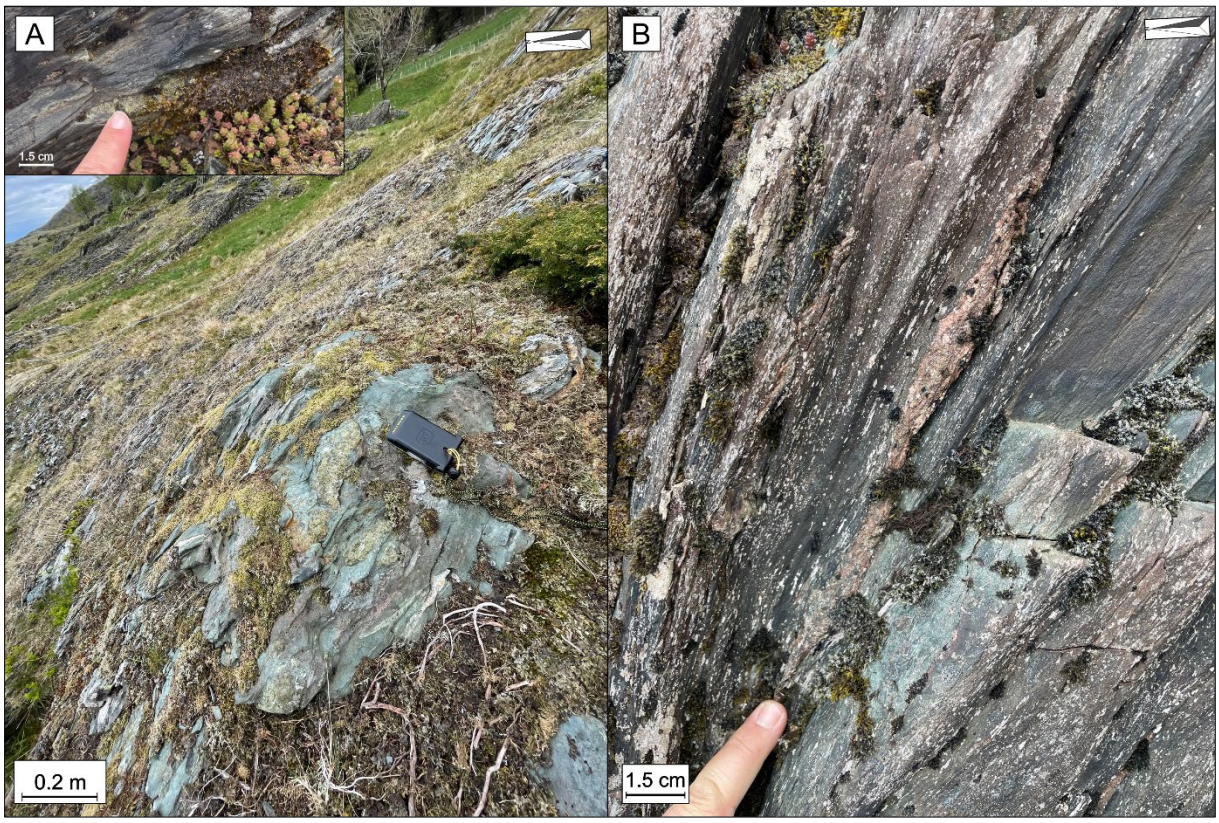

Fig.3.12: A: showing two different epidote nodules in the same area, one measured to be 3x1.5 cm, and the other 0.8x0.4 m. The largest one is a drained pillow filled with epidote. B: typical structure of the volcaniclastic rocks, appearing strongly deformed with structures of different volcanic rock fragments. The finest-grained material of black color may be interpreted as black chert.

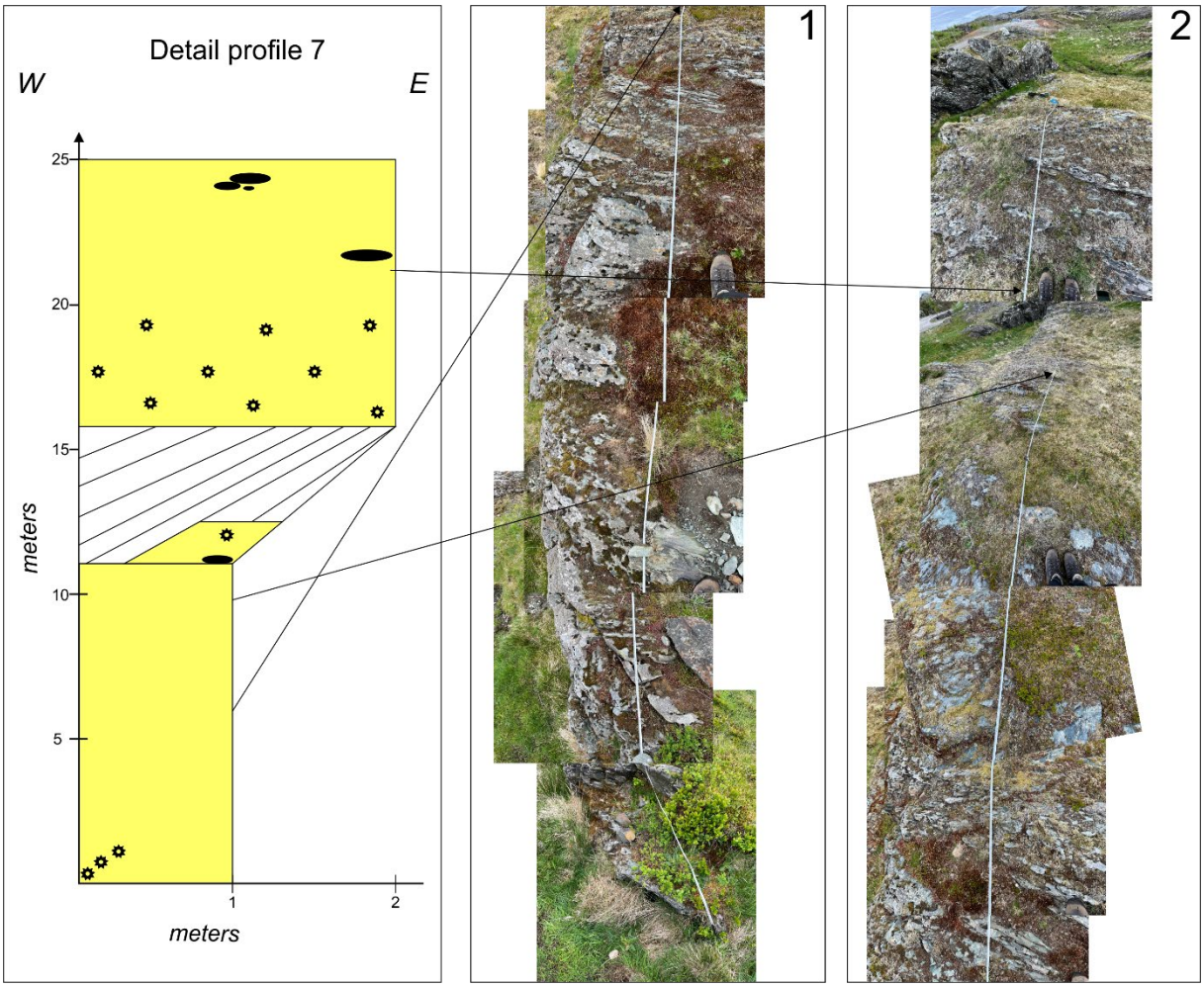

Fig.3.13: Sketch of detail profile 7 as well as live photos representing the different steps within the profile. Picture 1 and 2 depicts a strongly deformed volcanic breccia, defined as volcaniclastic rocks. The horizontal scale is not accurate for pillow and epidote measurements. The profile exhibits volcaniclastic rocks with epidote nodules, as well as some pillow fragments.

3.2.2 Detail profile 8

Detail profile 8 is located 850 m stratigraphically (not adjusted) above the sheeted dike complex (Figs. 3.1 and 3.2), and is predominantly consisting of pillow lava (Fig. 3.14). However, it is difficult to clearly distinguish pillows and to separate them from each other due to the strong deformation in this area. Measured pillows of detail profile 8 range from 11x3 cm to 84x24 cm (Appendix 1). Small amounts of non-mineralized volcanic breccia occur within this sequence. No sign of epidote-nodules at this point.

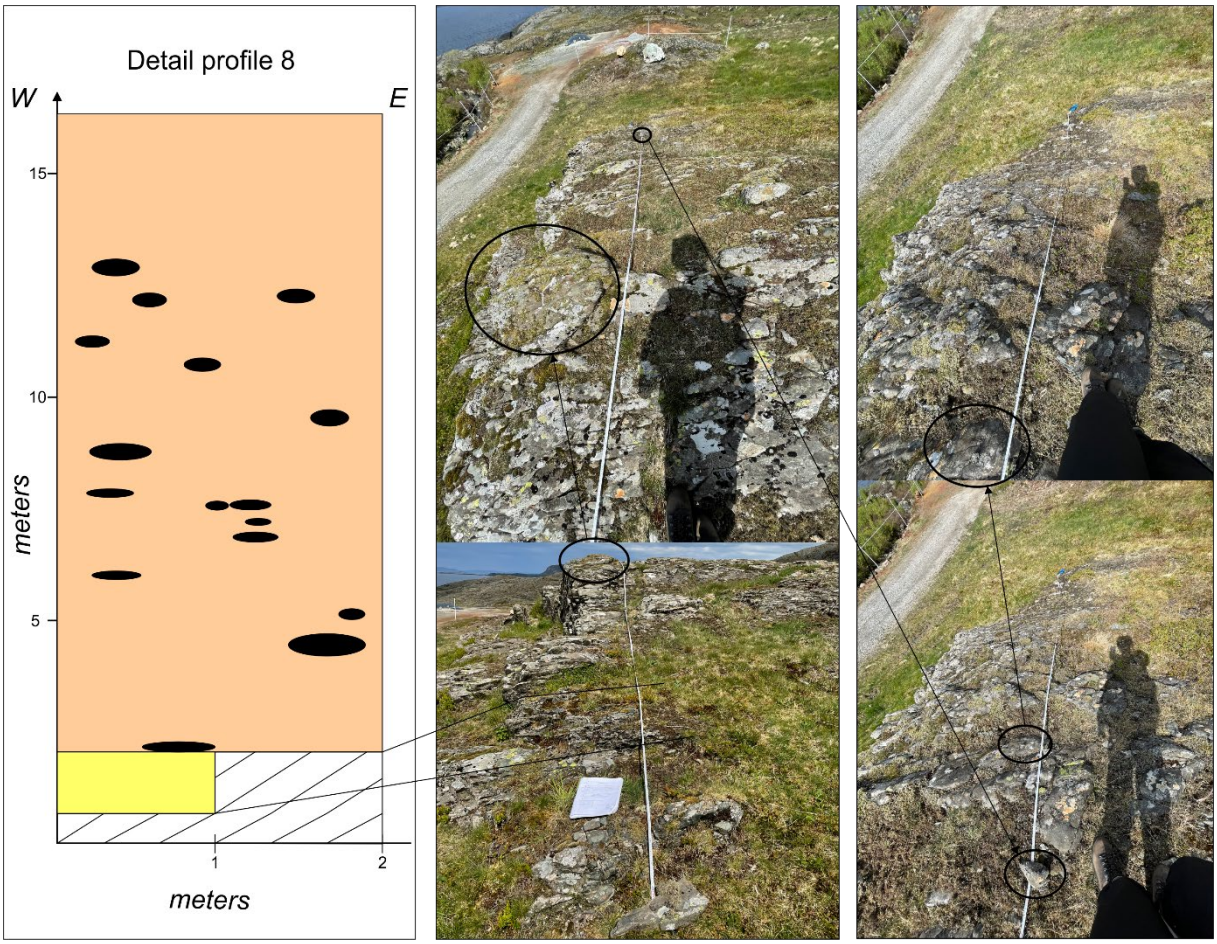

Fig.3.14: Sketch of detail profile 8 as well as live photos representing the different stages within the profile. The horizontal scale is not accurate for pillow measurements. This profile indicates that the area is dominated by pillow lava. Due to high deformation in the area, it is difficult to distinguish pillows and separate them from each other.

3.2.3 Detail profile 9

Detail profile 9 is located 970 m stratigraphically (not adjusted) above the sheeted dike complex (Figs. 3.1 and 3.2), and is composed of pillow lavas defining varying shapes and sizes (Fig. 3.15). The area is characterized by large pillows with smaller pillows in between. Volcanic breccia is insignificant in this area (Appendix 1). The rock-material in the area is fine grained with a gray to dark gray color, whereas the surface is more uneven and spiked than the surfaces of pillow lavas in other areas within the Master profile.

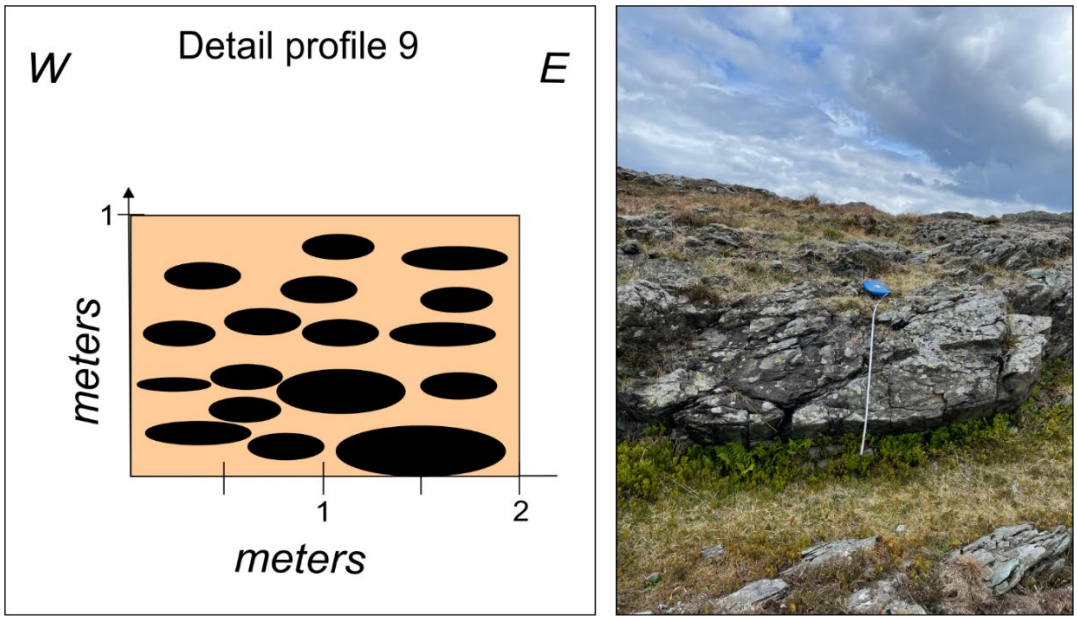

Fig.3.15: Sketch of detail profile 9 as well as live photos representing the different steps within the profile. The horizontal scale is not accurate for pillow measurements. The profile indicates that the area is dominated by pillow lavas of different size.

3.2.4 Detail profile 10

Detail profile 10 is located 990 m stratigraphically (not adjusted) above the sheeted dike complex (Figs.3.1 and 3.2), and is the only area comprising broken pillow breccia (Fig.3.17). The area is composed of a mixture of broken and whole pillows, as well as hyaloclastites and pillow-fragments within the breccia (Appendix 1). The sequence can be characterized by elongated pillows, both whole and broken pillow, within a brecciated groundmass with minor mineralization (Fig.3.16). The rock-material is a gray colored, for both the volcanic breccia and the broken pillows, as well as fine grained.

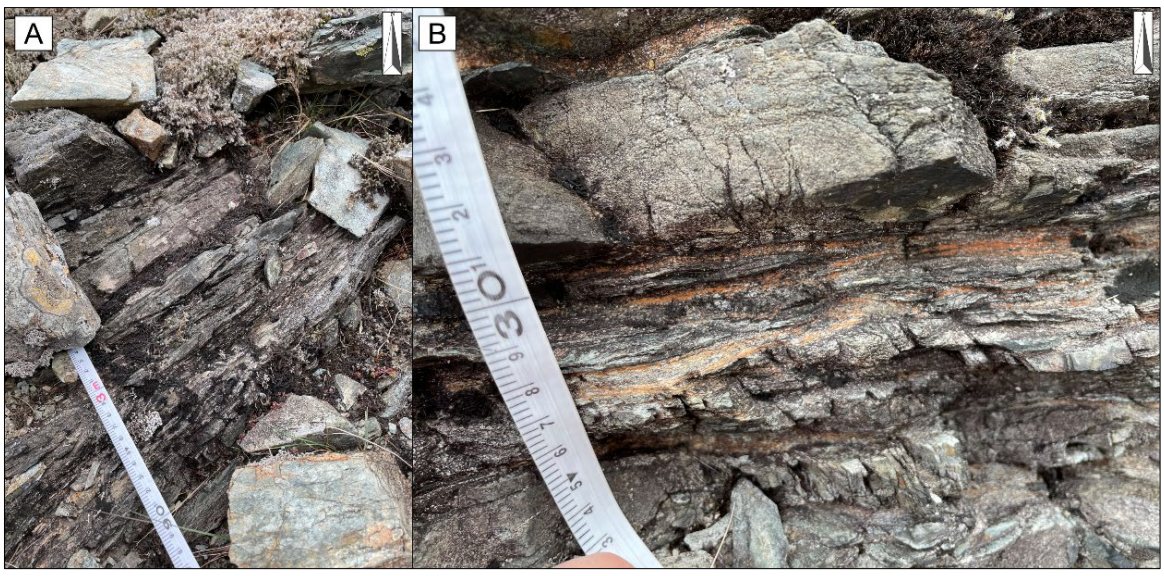

Fig.3.16: A more detailed picture of the volcanic breccia comprising hyaloclastite and pillow fragments. A: towards the top of the profile. B: volcanic breccia at the bottom of the profile showing a bit mineralization.

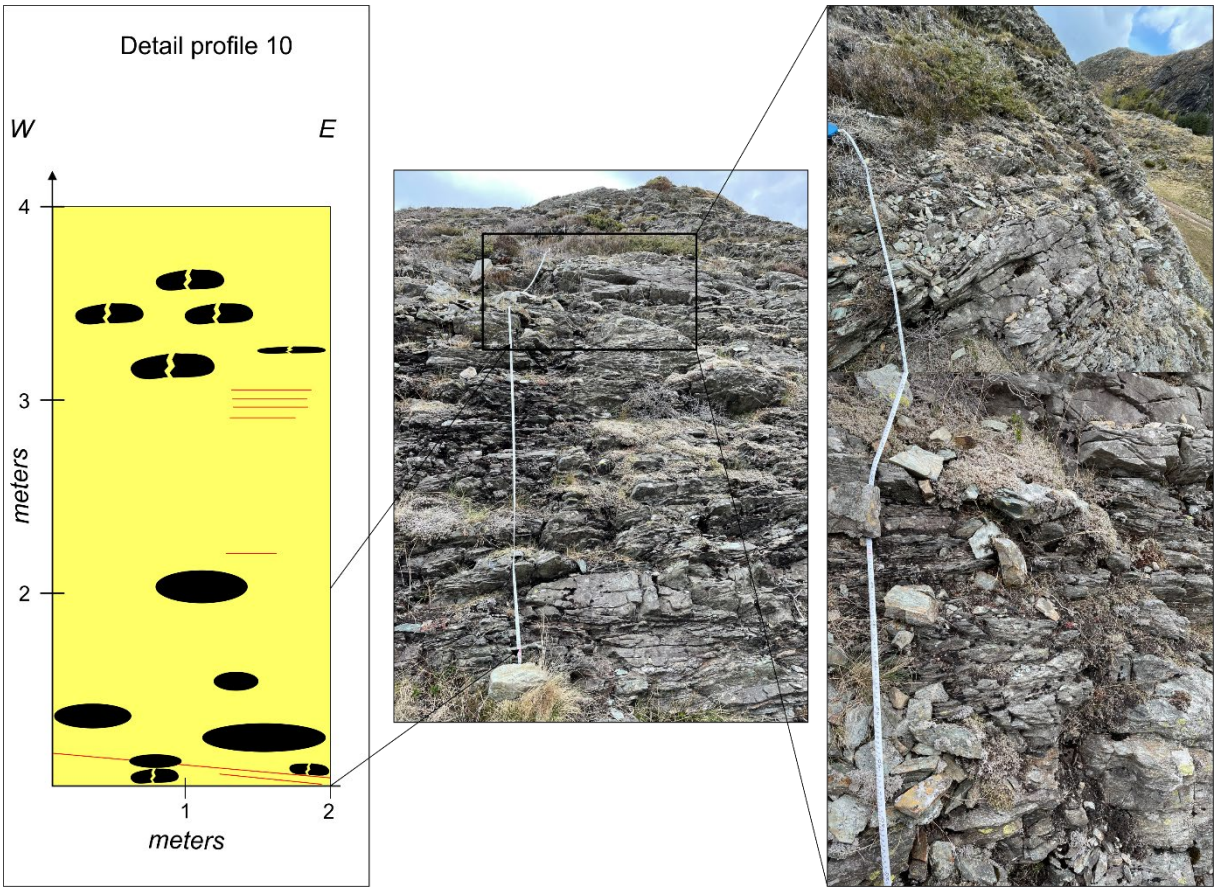

Fig.3.17: Sketch of detail profile 10 as well as live photos representing the different steps within the profile. The horizontal scale is not accurate for pillow measurements. The profile exhibits broken pillow breccia, composed of a variation between broken pillows, pillow fragments and hyaloclastite. Minor mineralization occurs in some areas, defined by red lines in the profile.

3.2.5 Detail profile 11

Detail profile 11 is located 1050 m stratigraphically (not adjusted) above the sheeted dike complex (Figs. 3.1 and 3.2), and consists of both massive sheet flow and pillow lavas, as well as a minor layer of mineralized volcanic breccia (Fig. 3.18). Within the massive sheet flow layer, there is no clear structure, except for a few pillow structures measured to approx. 50x10 cm (Appendix 1). The layer consisting of volcanic breccia carries minor mineralization zones and a few measurable layers of hyaloclastites. Towards the top, the pillows are stacked on top of each other with smaller pillows in between. The rock- material is, like in the other sequences, fine-grained with dark gray colors.

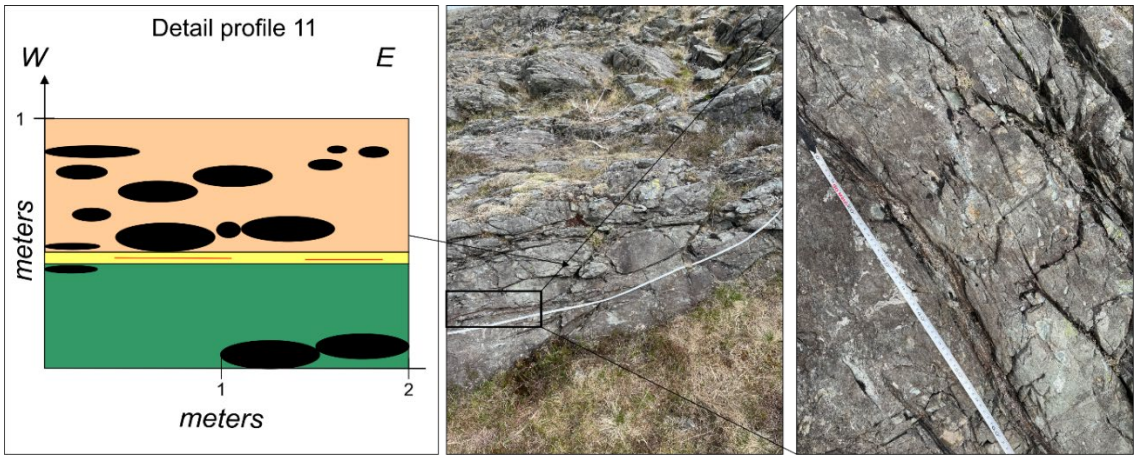

Fig.3.18: Sketch of detail profile 11 as well as live photos representing the different sages within the profile. The horizontal scale is not accurate for pillow measurements. In the profile massive sheet flows appears at the bottom as well as a minor zones of volcanic breccia. The rest of the profile is dominated by pillow lava.

3.2.6 Detail profile 12

Detail profile 12 is located 1110 m stratigraphically (not adjusted) above the sheeted dike complex (Figs. 3.1 and 3.2), and is predominantly composed of volcanic breccia with some epidote-nodules showing pillowy structures (Fig. 3.20). The volcanic breccia appears as a coherent unit without distinct structures, except some drained pillows with epidote-filled cavities, giving drain-out floors in the pillow lavas (Fig. 3.19). The pillows exhibit several drain-out episodes, characterized by thin “floors” of metabasalt, which are E-W oriented. The size of the epidote-filled pillows ranges from 10x11 cm to 70x40 cm (Appendix 1). The whole sequence is represented by fine-grained material and a gray to dark gray color. This unit may also be defined as volcaniclastic rocks, but due to only one visible surface and no appearance of chert/finer-grained material, it is difficult to determine.

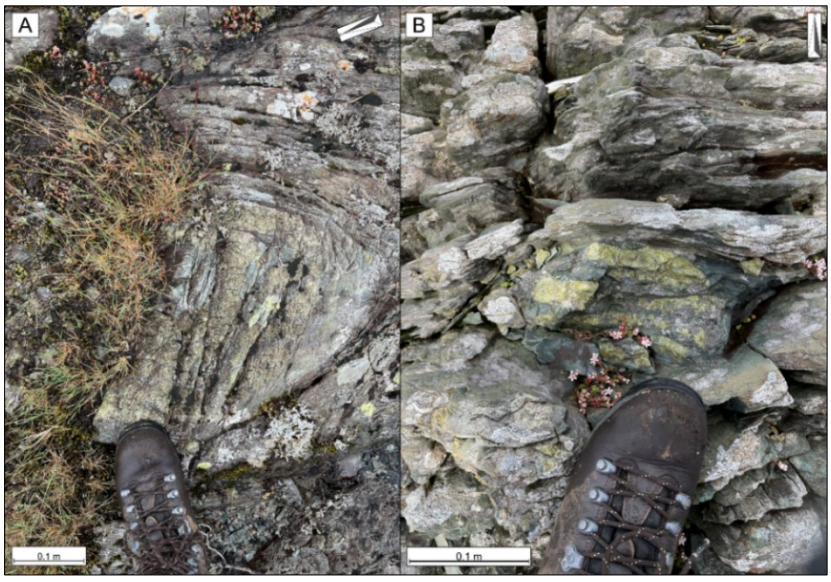

Fig.3.19: Pillow lava with epidote-filled cavities. A: five drain-out floors with NW-SE orientation. B: five drain-out floors E-W oriented.

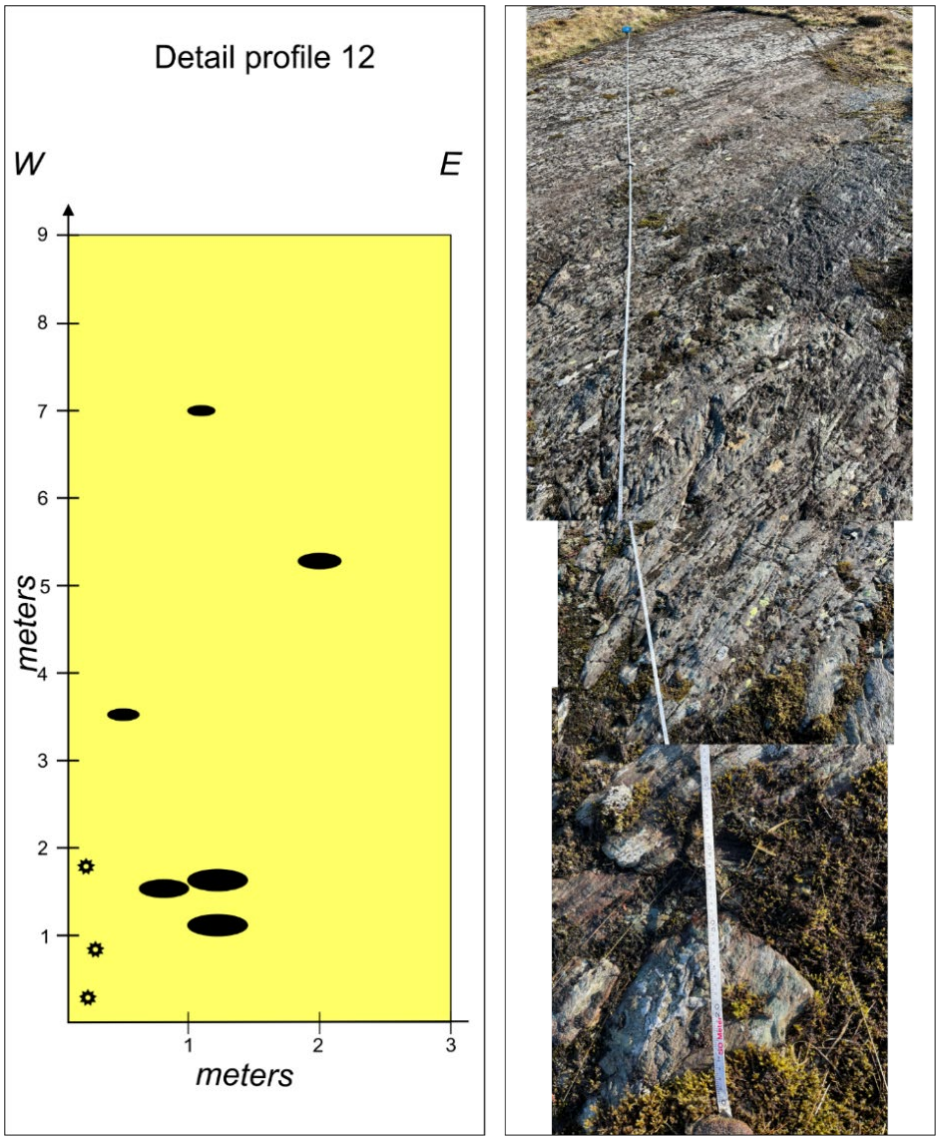

Fig.3.20: Sketch of detail profile 12 as well as live photos representing the different stages within the profile. The horizontal scale is not accurate for pillow and epidote measurements. This profile is dominated by a highly deformed volcanic breccia, with epidote-nodules with pillowy structures. Within the epidote-nodules drain-out floors are present and measured.

3.2.7 Detail profile 13

Detail profile 13 is located 1160 m stratigraphically (not adjusted) above the sheeted dike complex (Figs. 3.1 and 3.2), and the whole sequence represents pillows of different sizes, stacked on top of each other (Fig. 3.22). The in-situ pillows are very deformed, with some brecciated areas in between. These areas are slightly mineralized around the pillows. It is possible to observe hyaloclastites, but they are not measurable due to high deformation, which makes it difficult to define a clear start and end. From this stage of the sequence, towards the end of the profile, the pillows become larger and more distinct (Fig. 3.21). The pillows have an elongated lobe-shaped structure, defined as tortoise-pillows (Carracedo Sánchez et al., 2012) (Appendix 1).

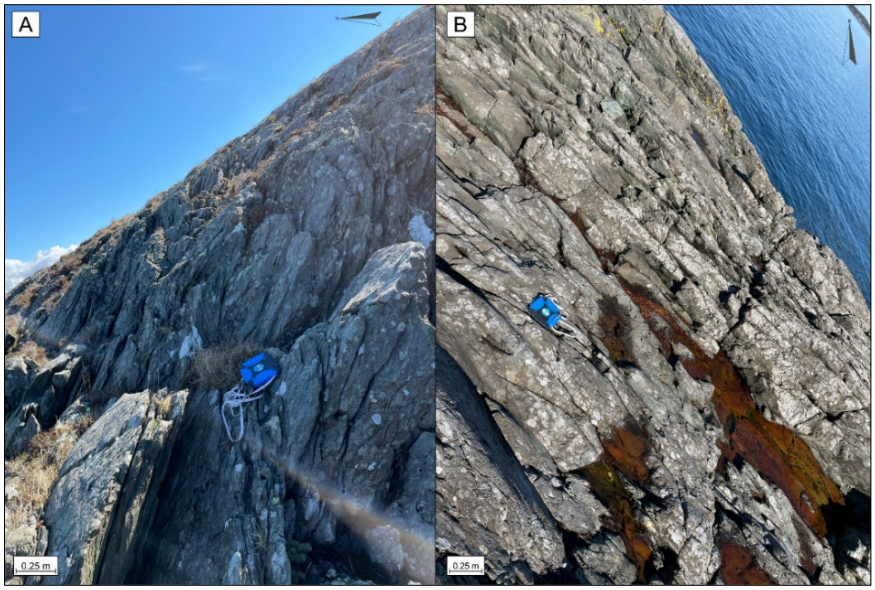

Fig.3.21: Tortoise-pillows from the top of the sequence. A: showing 3-dimentional tortoise pillows. B: the same tortoise-pillows further west of the sequence, only showing the top of the pillows.

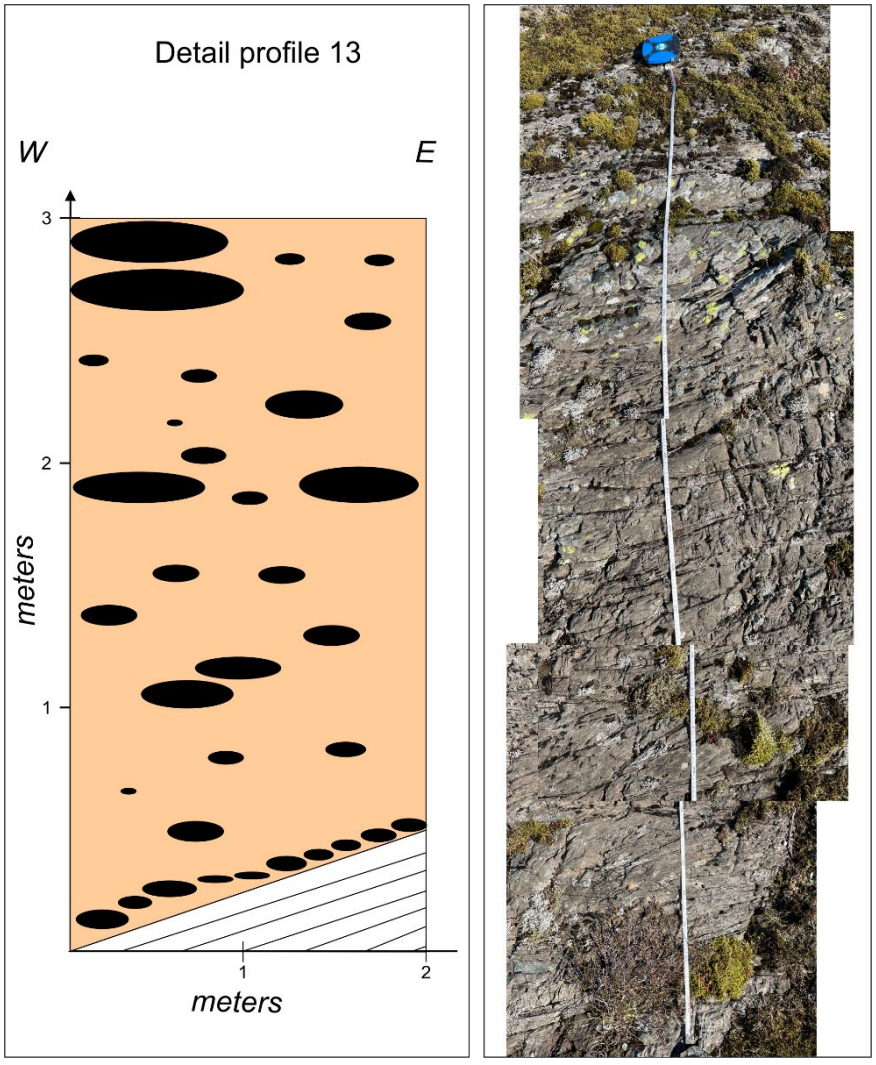

Fig.3.22: Sketch of detail profile 13 as well as live photos representing the different steps within the profile. The horizontal scale is not accurate for pillow measurements. This profile exhibits pillow lava with pillows of varying size and shape.

3.3 Volcanogenic Massive Sulfide Deposits (VMS)

The Grimelia mines occur at the lower part of the Volcanic sequence (Fig. 3.23). According to Korneliussen and Often (1980) the sulfide content and composition of ore mineralization varies greatly (Ch. 2.4.2). Through field observations, the goal is to predict an estimate of the amount of volcanogenic massive sulfide (VMS) deposits across the area, and is represented by part 1B of the master profile (Figs. 3.1 and 3.2). To accomplish this, thorough mapping of mineralized zones in proximity of the mines were conducted and is presented as two cross sections through the Master profile (Figs. 3.23 and 3.24). The cross sections do not consider the faults within the area and their possible impact (Fig. 3.25). However, field observations indicates that the VMS deposits in the area is delimited by faults.

Field observations confirms that the prevalence of mineralization varies greatly within the studied area. Some of the zones mapped with surface-mineralization extends up to 85 meters. The mineralized zones may be linked together based on mine entrances, and is explained in Table 3.1. The ore deposits seem to be parallel with the strike and the steep dip towards north. According to Rønning (1981) a reasonable estimate for the extent of the mineralized zones will be 600 $\pm$ 200 m, based on CP-measurements (charged potential, used to map the distribution of ore deposits), resulting in an optimistic calculation of ore-resources of 2 mill. tons.

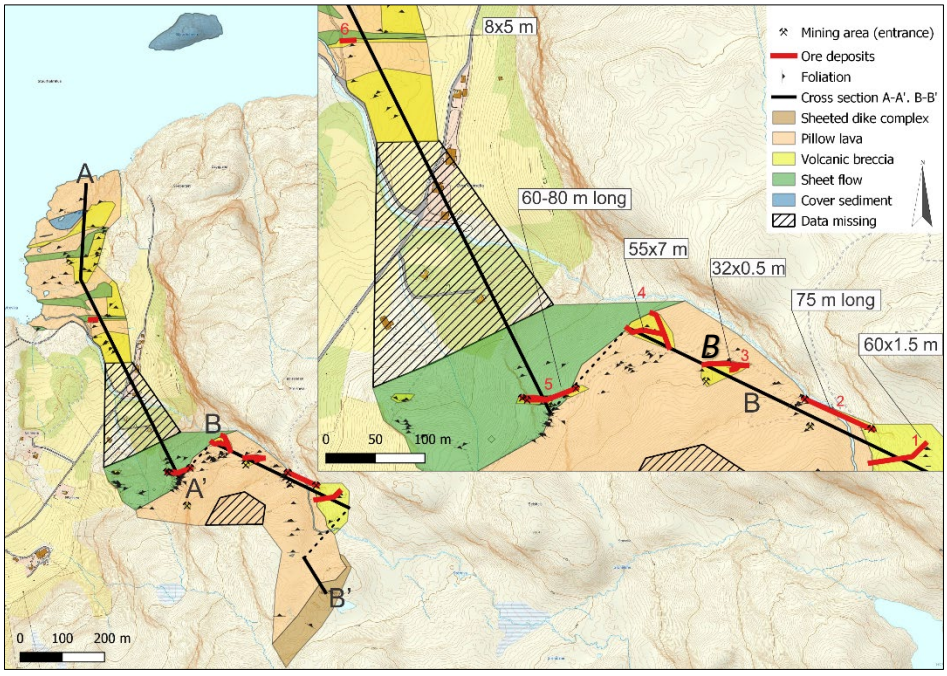

Fig.3.23: Geological map of the Solund-Stavfjord Ophiolite Complex including present work resulting in two cross sections through the Master profile (Part 1B) (Fig.3.24), to predict the amount of ore deposits within the volcanic breccia.

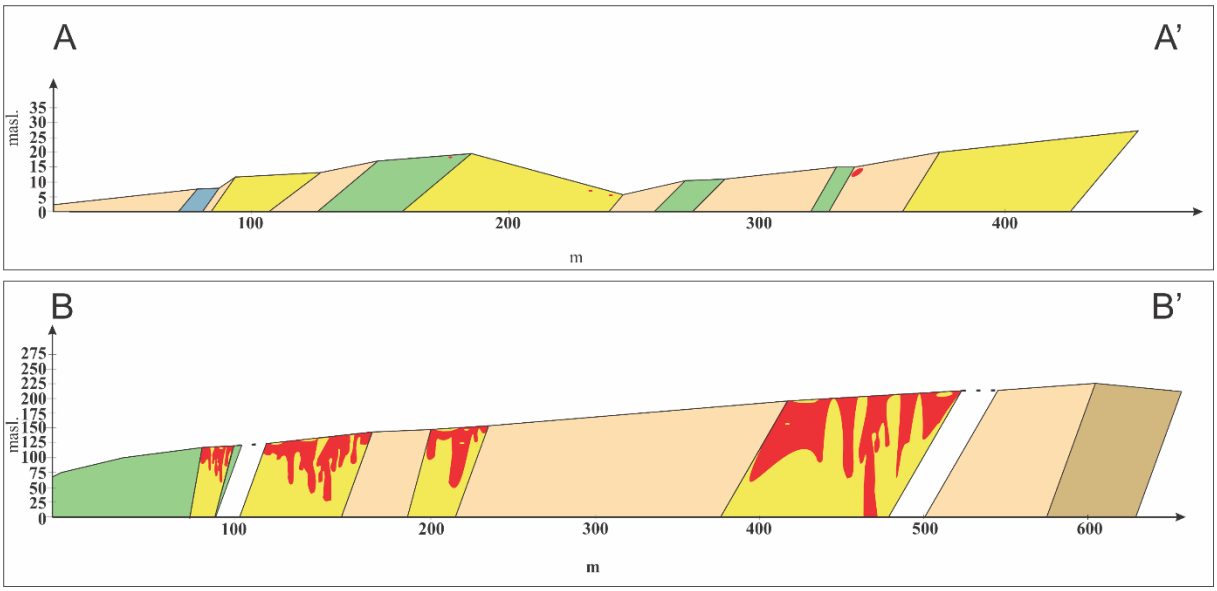

Fig.3.24: Cross section A-A' and B-B' illustrate the structure of the ophiolite as well as the mineralogical features within the volcanic breccia (indicated with red in the cross sections). The little red dot at 350 m in cross section A-A' represents location 6 in part 2 of the Master profile. The rest of the ore deposits in cross section B-B' is linked to the mines in part 1B of the Master profile. It is, however, important to highlight that the extent of the depicted mineralization-zones is not accurate.

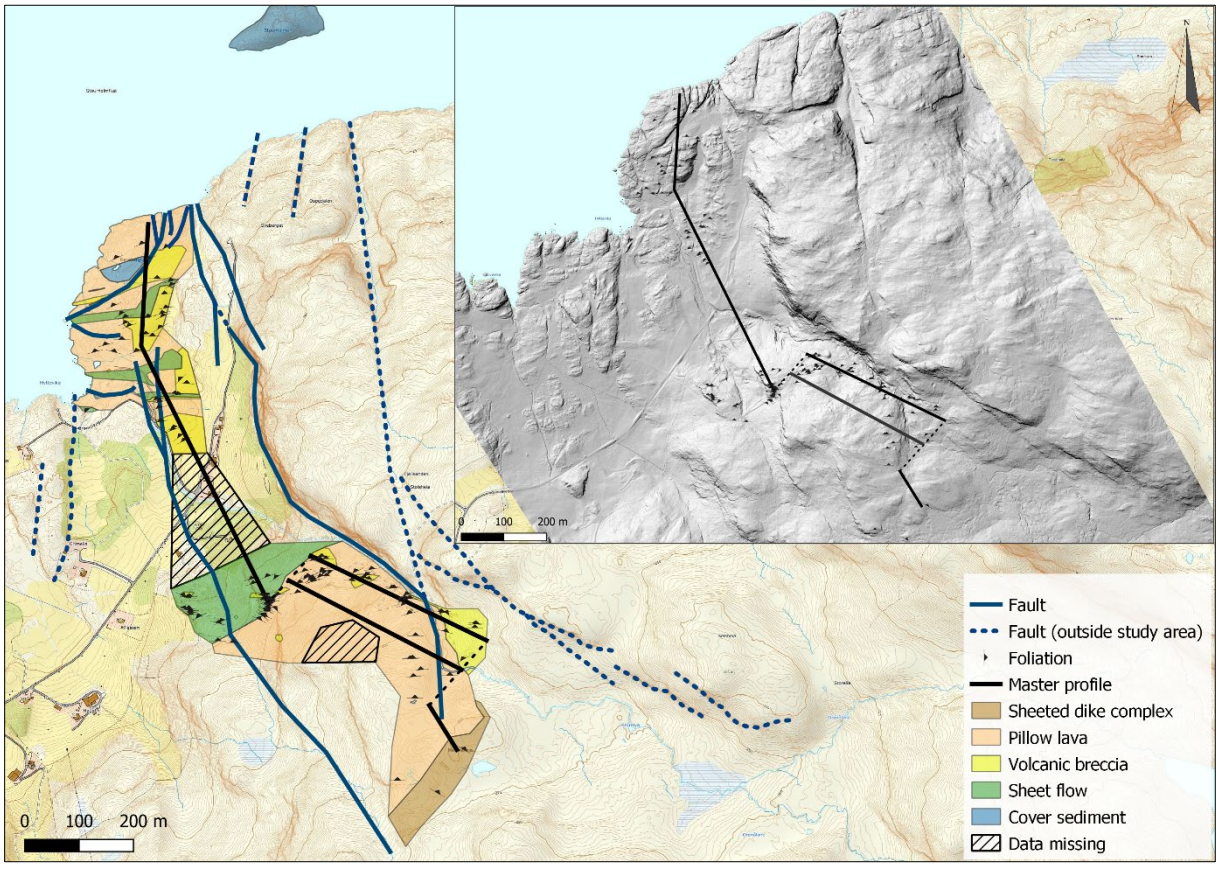

Fig.3.25: Geological map showing fault structures within and outside the study area. The main faults within the area of interest are marked with a dark blue line, whereas other larger and smaller faults outside the area is marked with dashed-blue line. The index-figure in the right corner, illustrating shadow features, is intended to give a better impression of the formations in the area.

Table 3.1: Table showing the size of the mapped mineralized veins/zones at the surface. See Fig.3.23 for the location of the different zones.

LOCATION	SIZE	COMMENT	FIGURE
1	Approx. 60 m long, 0.5 m at its thinnest, 1.5 m at its thickest	This vein is located on top of a mine and may be linked to the smallest mine in the area ("Øvre Gruve"), meaning the mine with lowest ore production a year (Bergvesenet., 1980).	Fig.3.3
2	Approx. 85 m in total.	Difficult to predict the size of the vein, other than length, as the vein connects two of the mine entrances in the area. The length of the vein is based on the mine entrances, not only surface observations. This vein is also linked to the smallest mine.	Fig.3.26 A
3	Vein with two branches of different sizes. The longest branch is approx. 32 m, 0.5 m at its thinnest, 3 m at its thickest, yet about 0.5 m wide all the way. The smallest branch is approx. 10 m, 1 m at its thinnest, 5 m at its thickest.	Mineralized zone at surface, cannot be linked to any of the mines in the area regarding the entrances. However, it is still located near one of the entrances.	Fig.3.8
4	Vein with some smaller branches. Main branch: 28 m long, 1 m at its thinnest, 10 m at its thickest, about 7 m wide throughout the zone.	Mineralized zone at the surface, which may be linked to the biggest mine in the area as it is placed on top of the mine, towards east. However, it is not linked to any of the mine entrances and, hence, not necessarily linked to one of the existing mines.	Fig.3.26 B
5	Approx. 60-80 m long in total.	Difficult to predict the size of the zone, other than length, as the vein connects three of the mine entrances in the area. This vein may be linked to the biggest mine in the area - "Nedre Gruve" (Bergvesenet., 1980).	Fig.3.10, Fig.3.11, Fig.3.26 D
6	Approx. 8 m long and 5 m wide.	Small, mineralized zone in the lowermost part of second part of profile 1. Impossible to predict whether this is connected to one of the mines or not. Nevertheless, it is not connected to one of the mine entrances.	Fig.3.26 C

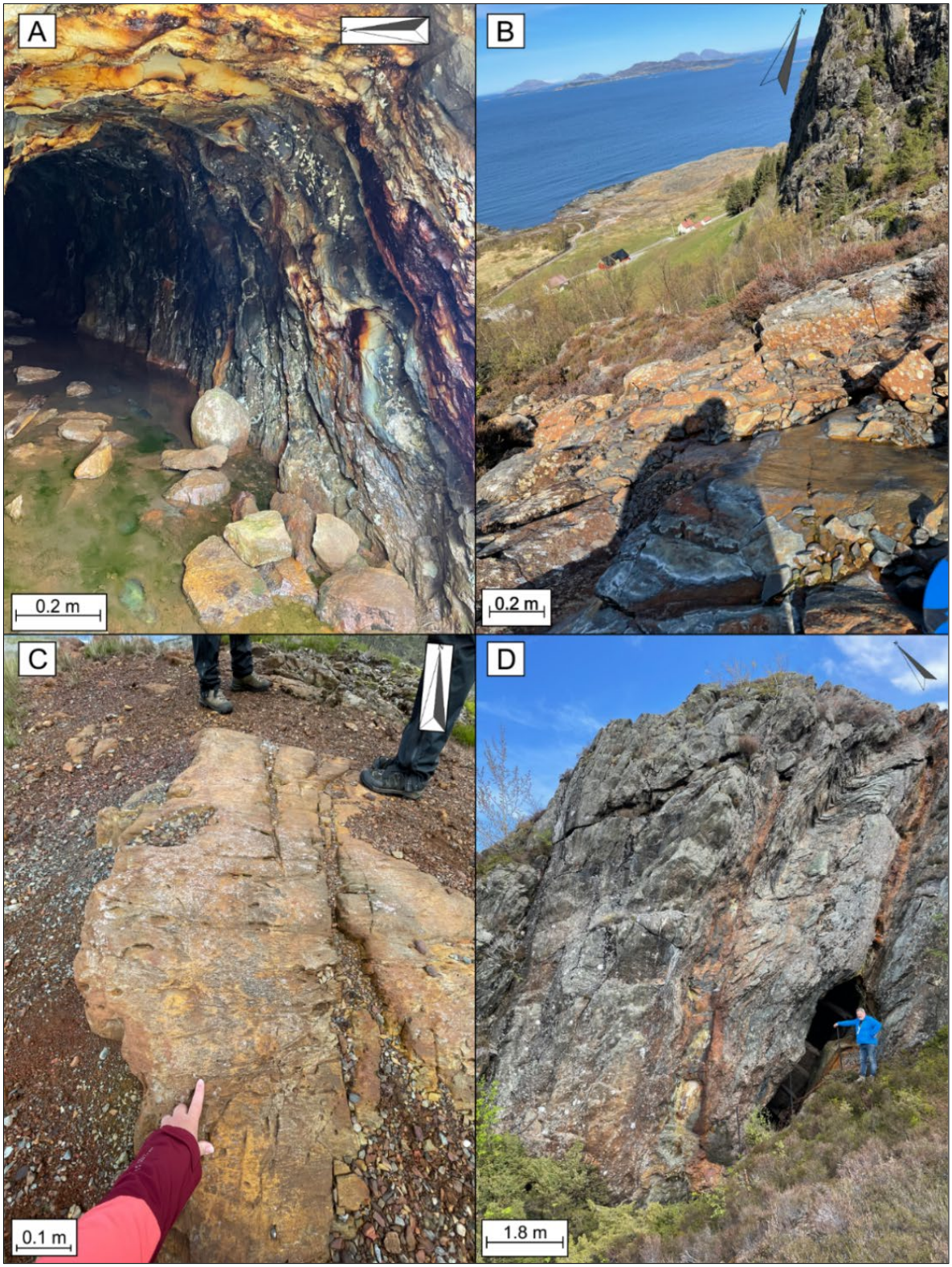

Fig.3.26: Pictures of different mineralized zones within the area. A: picture showing the entrance of one of the mines at location 2. The mineralization appears like lenses in the ophiolite. B: mineralized surface in location 4, showing the width of the vein. C: mineralized surface at location 6 (part 2 of profile 1). This is the only area with larger amounts of mineralization near the ocean. D: picture of one of the mine entrances at location 5, illustrating how the mineralized zones penetrated the ophiolite.

Chapter 4 – Interpretation of the volcanic sequence

In this chapter a discussion and interpretation of the physical properties related to each of the volcanic components will be presented. Also, measurements of the axial ratios of pillow lava and fragments of the various breccias will be presented and discussed for the purpose of adjusting the measured profile.

4.1 Morphology of the volcanic sequence

Several factors control the morphology of submarine lavas, such as 1) rate of cooling, 2) topography of the substrate, 3) viscosity, and 4) effusion rate. According to Griffith and Fink (1992) and White et al. (2002) the most important factors are the viscosity and the effusion rate of the lava flow. Thus, high effusion rate will result in sheet flows, whereas low effusion rate will favor the formation of pillows (e.g., Bonatti and Harrison, 1988; Furnes et al., 2003). Bonatti and Harrison (1988) presented a diagram, showing the relationship between spreading rate and lava type (pillow lava/sheet flow) (Fig. 4.1). Based on this study of Bonatti and Harrison (1988) demonstrating the relationship between spreading rate and lava morphology, and applying this to the entire volcanic sequence of the SSOC, it appeared that pillow lava and massive sheet flows represent 47% and 53% respectively, thus suggesting a spreading rate of 7-13 cm cm/yr. (Fig. 4.1). (Furnes et al., 2003; 2006).

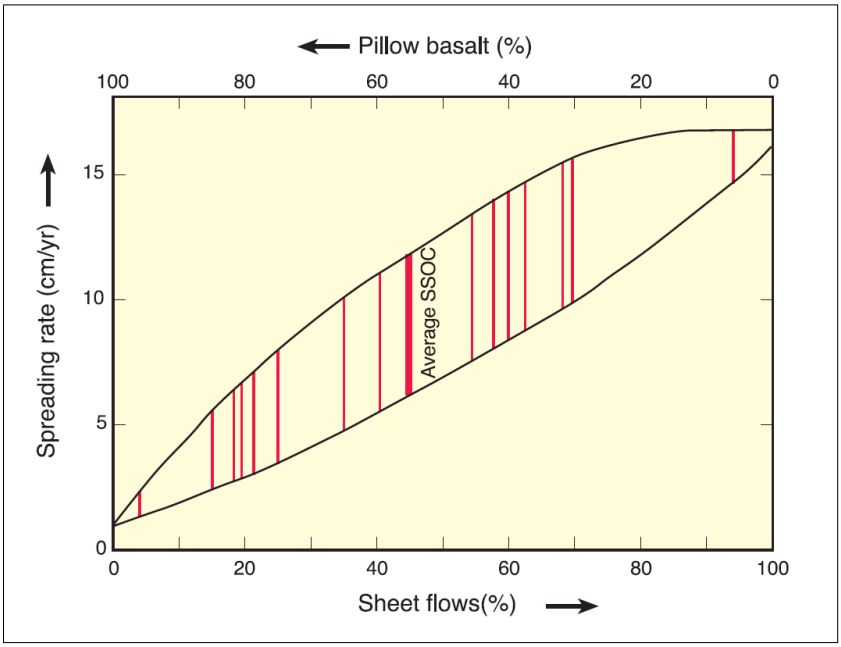

Fig.4.1: Diagram representing the relationship between spreading rate and whether the lava type is classified as pillow lavas or a sheet flow (modified from Bonatti and Harrison (1988)). The diagram indicates the proportion of pillow and sheet flows through numerous of stratigraphic sections of the SSOC (Furnes et al., 2003). Figure from Furnes et al. (2006).

In the investigated area of this research, lava morphologies such as massive sheet flows, volcanic breccia, and pillow lava, all appearing in an interconnected relationship, can be found. How these units are connected to each other is proposed by Carracedo Sánchez et al. (2012), by presenting a new propagation four-stage model for submarine basaltic lavas that accounts for the development of sheet flows, volcanic breccias and pillow lava along the same flow (Fig.4.2). The morphology of the volcanic sequence in the studied area of the SSOC, involves this four-stage lava flow propagation model, as well as the flow rate of emitted lavas. The four-stage model is presented below along with a modified version of the model (Fig. 4.2) (Carracedo Sánchez et al., 2012).

1) This stage represents a flowing stage, where a high-temperature sheet flow with low viscosity, is directly emitted from the vent at a high flow rate. It can also be emitted by inflation, where a moderate flow rate from the vent is generated by coalescences of various smaller and fluid (low viscosity) flow (Fig. 4.2 A).
2) This stage is represented by the cooling stage reasonable for the prismatic sheet flow section with columnar joints. The flow is starting to cool as the flow velocity decreases and we get thermal contractions of the outer parts, while the inner zone remains molten (Fig. 4.2 B).
3) This stage represents the drainage stage, where megapillows, prismatic joints, welded columnar breccias, and pillow lavas are formed due to rapid drainage and high magma pressure. Tunnels along the lava flow is developed by drainage of massive lava towards the megapillows. This is resulting in partial collapse of the tunnel roofs, which forms the prismatic joints (tortoise shell jointing). Further, columnar breccias are formed due to high temperatures in the tunnels, allowing warm piled fragments to weld and partly coalesce. At the end, the formation of the pillow lava section is developed. This results from various smaller lava flows and cooling units at progressively more restrained flow rates, contained in the largest tubes (Fig. 4.2 C).
4) This stage is represented by tunnel collapse due to water pressure, which is resulting in unwelded talus breccias where the collapse has occurred. The formation of these breccias is, according to Carracedo Sánchez et al. (2012), speculative as they were not preserved at the type locality at Meñakoz beach (Spain). However, such gravitational lava tunnel collapse is a common process within submarine environments (e.g., Francheteau et al., 1979) (Fig. 4.2 D).

This model can successively be applied to explain the field observations of the lava pile within the SSOC at Grimelia. Detail profile 6 is a suitable example for the section dominated by sheet flows and volcanic breccias (Figs. 3.10 and 3.11), whereas detail profile 11 is a good example of the transition zone including both massive sheet flows, volcanic breccias and pillow lavas (Fig. 3.18). The pillow dominated section is observed at the top of the Master Profile, and a suitable example for this section would be detail profile 13 (Figs. 3.21 and 3.22).

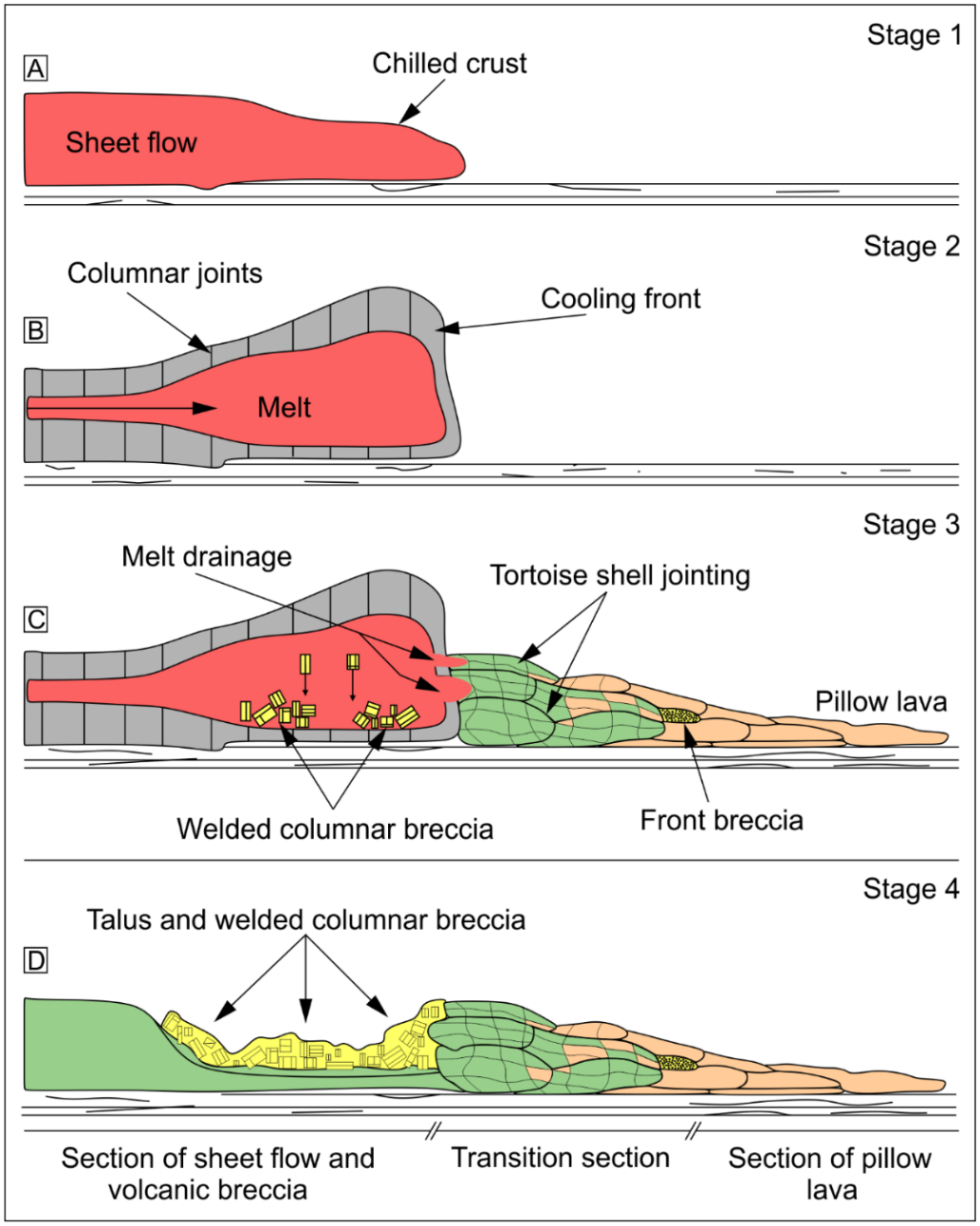

Fig.4.2: A: high emission rate near the vent resulting in the development of a sheet flow. B: a thick crust with columnar joints envelopes the sheet flow due to cooling and thermal contractions. A continuous magma supply progressively inflates the flow. C: Due to high magma pressure, the thick crust raptures and the formation of pillow lava, sheet flows and welded columnar breccias starts. D: As the flow stops, the sheet flow roof collapses due to water pressure, resulting in the formation of talus breccias. Modified sketch of the four-stage propagation model developed by Carracedo Sánchez et al. (2012), based on Erga, (2021).

Bonatti and Harrison (1988) proposed a model that favors different conditions and thus the morphology of the discussed components of the investigated volcanic rocks (Fig. 4.3). The formation of sheet flows is favored over pillows by 1) high temperature, 2) low crystals/ liquid ratio, 3) low viscosity, and 4) high discharge rate of the lava upon eruption. On the other hand, formation of pillow lavas and/or hyaloclastites is favored by the opposite conditions. These conditions, schematically presented in Fig. 4.3, is expected to vary in oceanic spreading centers and seamounts (Bonatti and Harrison, 1988).

	Pillow Basalts	Lobate Flows	Sheet Flows	
High	←———	Viscosity	←———	Low
High	←———	Crystal Content	←———	Low
High	←———	Composition (SiO_2 content)	←———	Low
Low	———→	Temperature at Eruption	———→	High
Narrow	———→	Conduit Width	———→	Wide
Long	———→	Conduit Length	———→	Short
Low	———→	**Effusion Rate**	———→	High
Low	———→	**Slope**	———→	High
Rough	———→	Surface Roughness	———→	Smooth
Low	———→	**Spreading Rate**	———→	High

Fig.4.3: Model of different eruption styles and products, and how they are related to factors such as thermal stress, initial temperature, viscosity, crystals/liquid ratio and spreading rate. Sheet flows, for instance, favors low viscosity and crystal content, as well as high temperature at eruption, effusion rate and spreading rate. From Bonatti and Harrison (1988), modified by Glancy (2011).

Another factor that is crucial to the morphology of submarine lava flows is the determination of paleo-effusion rates and the emplacement times for submarine lava flows, which has been experimentally determined by Gregg and Fink (1995). Typically, submarine flows are classified as pillowed, lobate (tortoise), or sheet flows based on their morphologies (e.g., Fox et al., 1987; Gregg and Fink, 1995). Generally, it is assumed that pillow lavas result from low effusion rates, whereas sheet flows form from high effusion rates. But, by using laboratory simulations, correlated to results from sea-floor observations, four submarine lava flow morphologies are

considered to characterize specific effusion rates. These are levees, folded, lineated sheets and striated pillow (Fig. 4.4). This model exhibits that the lowest effusion rates and slopes, including highest cooling rates, favors the formation of pillow lavas. By increasing the flow rates by the steepening of slopes, or decreasing cooling rates, a progression of flow types in submarine environments is equivalent to the transition from pillows to lobate (tortoise) flows, lineated flows, folded flows, and levees (jumbled flows) (Gregg and Fink, 1995). Their observations of laboratory and subaerial flows show that local morphologies are controlled by local flow conditions.

Laboratory morphology	Submarine morphology	Ψ 0° min	Cooling rate	Slope	Flow rate
pillows	pillows		↑	↓	↓
	lobate sheets				
rifts	lineated sheets	3			
folds	ropy sheets	10			
levees	jumbled sheets	30			

Fig.4.4. Model representing the correlation between laboratory simulations (ψ) and submarine flow morphologies. These values are accurate for flows emplaced on slopes <10°. As the slope increases, ψ values associated with rift flows decreases. The ψ values includes effects such as viscosity, heat capacity, thermal diffusivity, and density.

4.2 Pillow lavas

The purpose of this subchapter is to account for various aspects of pillow lavas and their significance. The relation between measured vertical (V) and horizontal (H) axis of pillow lavas in the SSOC will, compared to undisturbed pillow lavas in Iceland, give an indication of the deformation of the sequence in the area. Further, the shape and content of vesicles can be used to identify the stratigraphic right-way-up and give an indication of the eruption-depth of the volcanic sequence. Cyclic stratigraphic units are also investigated as they represent multi-eruptional events in the constructions of the volcanic piles.

4.2.1 V/H ratios

Basaltic pillow lavas may be characterized by measuring their axial ratios V/H, where V and H represents the vertical and horizontal axes, respectively, in cross sections perpendicular to the elongate direction of the flow. It should be emphasized, however, that the elongate direction of a pillow flow is not easy to determine in an area of strong deformation as in the Grimelid

area. The relationship between the chemistry and axial dimensions of pillow lavas with different chemical composition were studied by Furnes and Fridleifsson (1978). They conducted detailed mapping on pillows of alkaline olivine basaltic and olivine tholeiitic composition in some shallow water pillow lava sequence from Azores and Iceland, focusing on the relation between vertical (V) and horizontal (H) axes. As a result of this they concluded that the pillows of different chemical composition have rather similar V/H ratios that gradually decrease with the increasing size of pillows. The V/H ratios plotted in a frequency diagram suggest that the alkaline olivine basalt pillow is likely more flattened than olivine tholeiite pillows, and that the olivine tholeiite pillows may become larger and smaller than the other (Furnes and Fridleifsson, 1978).

The pillow lava in the studied area of the SSOC is compositionally comparable to the olivine tholeiite pillows at both Brimnes and Mosfell, Iceland (Furnes and Fridleifsson, 1978). Here the pillows from the SSOC in Grimelia, are compared with the olivine tholeiite pillows at Mosfell, Iceland. In total measurements of V and H were made on 254 pillow lavas, each attached to the 13 different detail profiles (Appendix 1). As stated above, some of the measurements of the pillows may be relatively inaccurate due to rather undefined elongate direction of the pillows. However, by comparing the V/H ratio of the measured pillows with the undeformed Icelandic pillow, an indication of the deformation within the area will be given.

Pillow lavas from detail profile 1-13, compared to the undisturbed measured olivine tholeiite pillows at Mosfell, are presented in Figs. 4.5, 4.6, and 4.7. The highest registered V/H ratio on the measured pillows originates from detail profile 3 (pillow lava sequence), and are 70 cm and 270 cm respectively. Compared to the maximum V/H of undisturbed measured olivine tholeiite pillows at Mosfell, which are 105 cm and 170 cm respectively, the deformation of the pillow lavas in the SSOC in Grimelia is demonstrated (Fig. 4.8). The measured V/H ratios in Grimelia gives an average size of 14 cm and 56 cm respectively. The average V/H ratios for the Icelandic pillow is calculated to be 29 cm and 38 cm respectively. The total ratio in the Grimelia area will therefore be 2 throughout the volcanic sequence (Fig. 4.8), indicating that the average pillow of Grimelia needs to be multiplied by 2 to get to the original size. However, this provides a slightly to high deformation ratio, and hence, an average line is placed on top of

the SSOC pillows to get a more accurate result (Fig. 4.8). The line indicates that the pillows of the SSOC needs to be multiplied by 1.75 to get to its original size.

The deformation is also calculated for the various detail profiles, to detect if any of the components are more/less affected by the deformation (Figs. 4.5, 4.6, and 4.7). These data's can also be compared to maximum V/H ratios of olivine tholeiite pillow lavas at the Våganes-area, ca. 1.5 km further west, with an average V/H ratio of 17 cm and 80 cm respectively (Erga, 2021). Compared to the undisturbed pillow at Mosfell, this gives a V/H ratio of 1.7, which indicates that the pillow lava sequence of the Våganes-area is slightly less deformed than the correlated sequence of Grimelia.

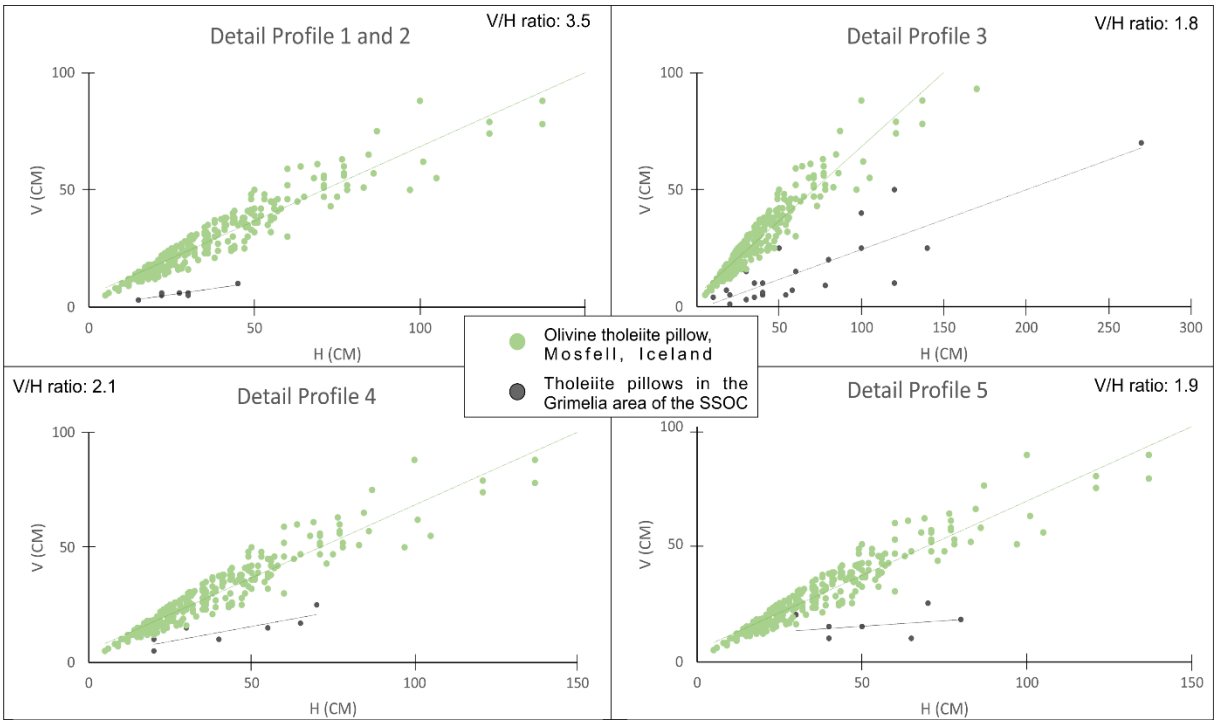

Fig.4.5: V/H ratios of olivine tholeiite pillow lavas within the SSOC in Grimelia from detail profile 1-5 (black dots), compared to undisturbed measured olivine tholeiite pillow lavas from Mosfell, Iceland. The green dots represent the undisturbed measured pillow lavas from Mosfell, Iceland, conducted by Furnes and Fridleifsson (1978).

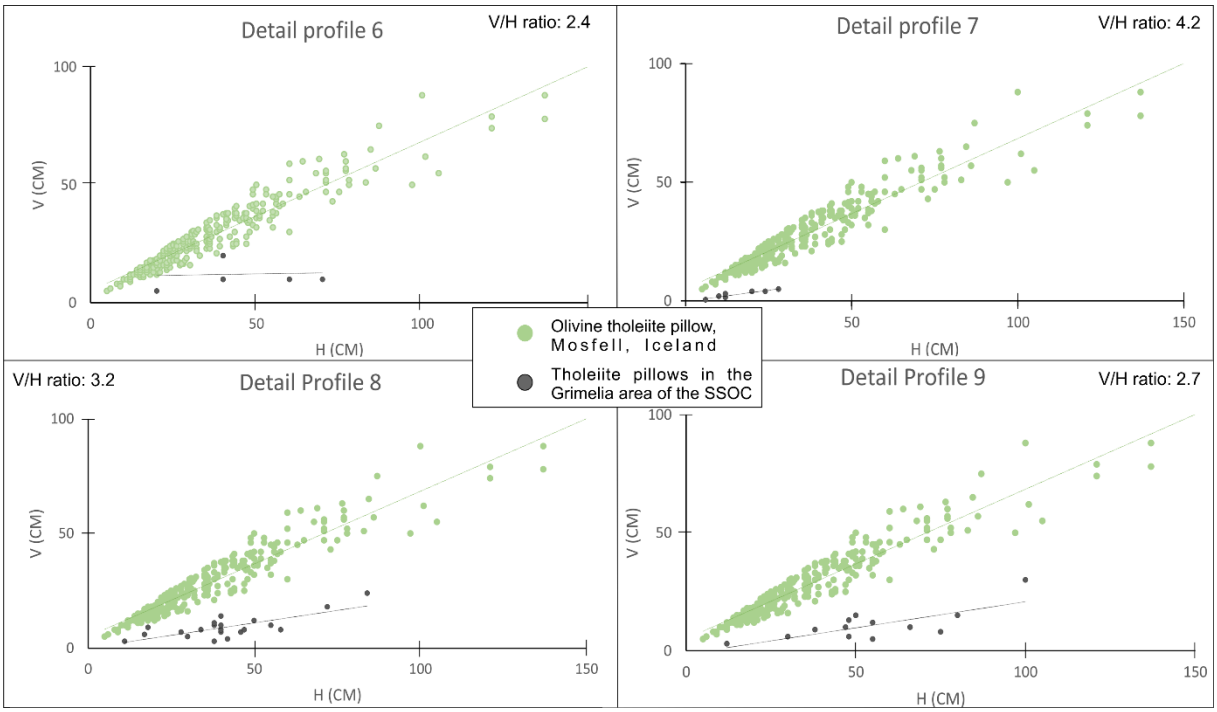

Fig.4.6: V/H ratios of olivine tholeiite pillow lavas within the SSOC in Grimelia from detail profile 6-9 (black dots), compared to undisturbed measured olivine tholeiite pillow lavas from Mosfell, Iceland. The green dots represent the undisturbed measured pillow lavas from Mosfell, Iceland, conducted by Furnes and Fridleifsson (1978).

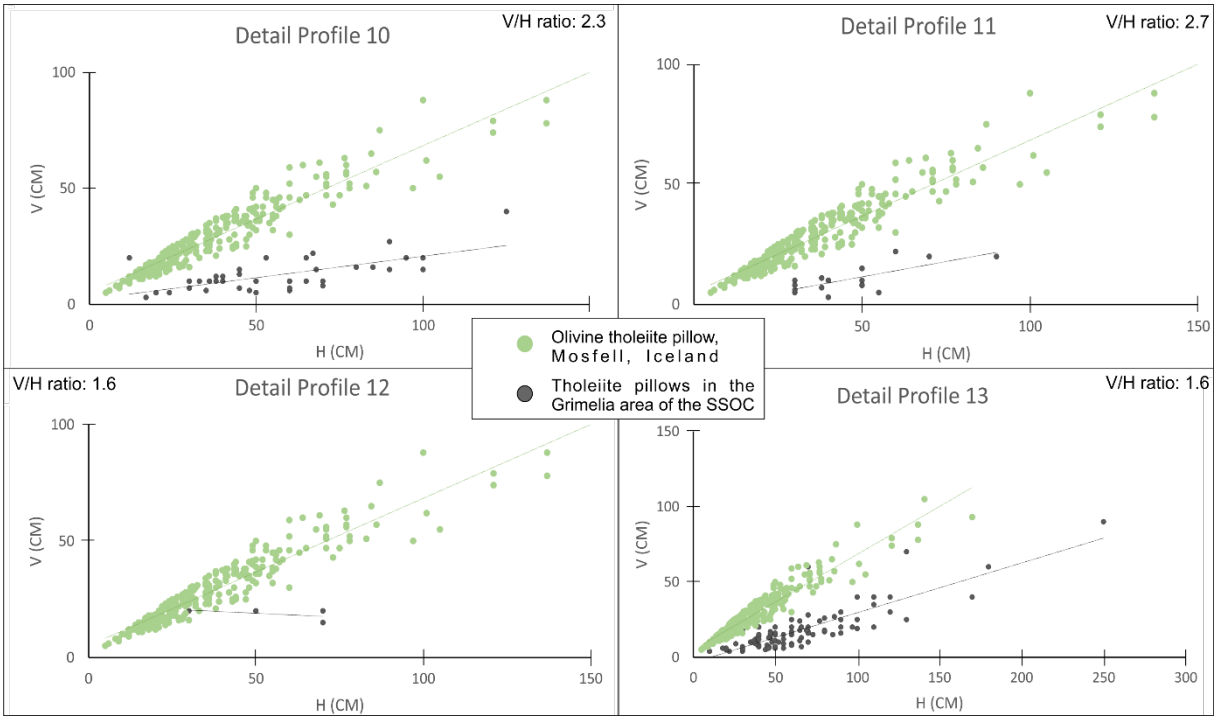

Fig.4.7: V/H ratios of olivine tholeiite pillow lavas within the SSOC in Grimelia from detail profile 10-13 (black dots), compared to undisturbed measured olivine tholeiite pillow lavas from Mosfell, Iceland. The green dots represent the undisturbed measured pillow lavas from Mosfell, Iceland, conducted by Furnes and Fridleifsson (1978).

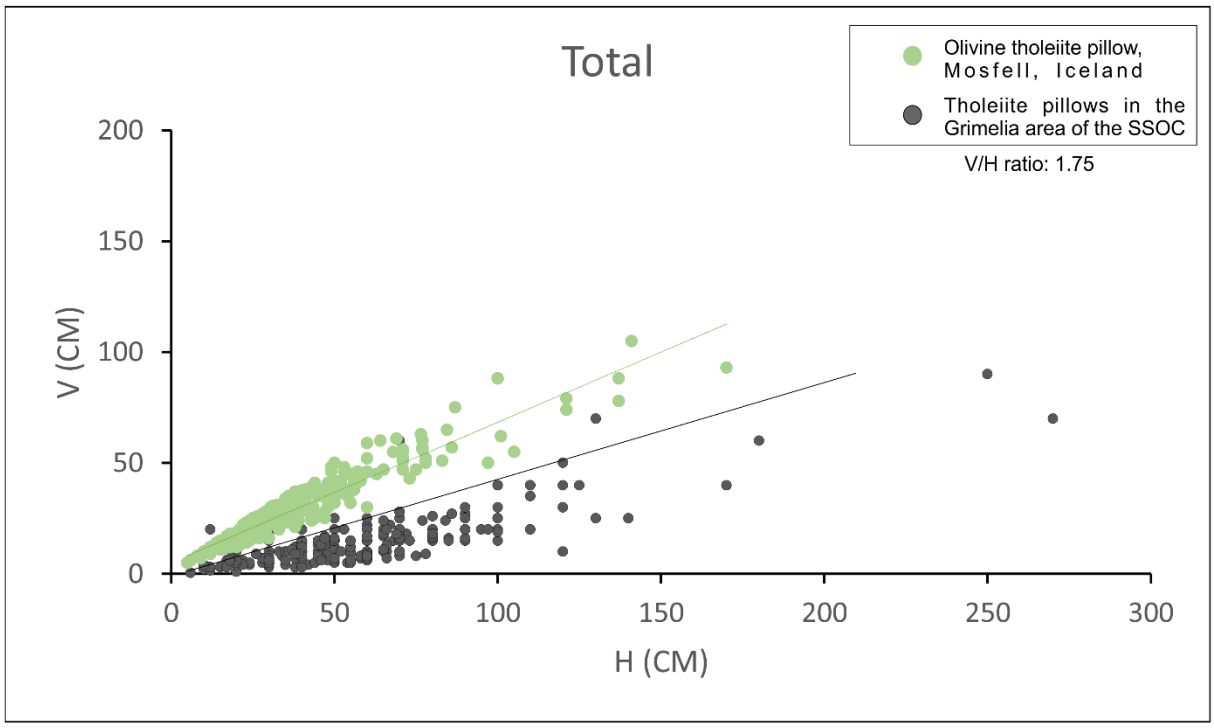

Fig.4.8: A total of measured V/H ratios of olivine tholeiite pillow lavas within the SSOC in Grimelia (black dots), compared to undisturbed measured olivine tholeiite pillow lavas from Mosfell, Iceland. The green dots represent the undisturbed measured pillow lavas from Mosfell, Iceland, conducted by Furnes and Fridleifsson (1978). By comparing the results, the total deformation ratio of the sequence is 1.75.

4.2.2 Stratigraphic indicator and vesicle content

Regarding pillow lavas and their morphology, the shape of the pillows can be used to identify the stratigraphic right-way-up of the sequence. The top of the pillow lavas is rounded with a convex shape, whereas the bottom of a pillow, that rests upon two underlying pillows, sometimes defines a V-shape. Due to high deformation this can be relatively difficult to observe in field, especially the V-shape. However, it is possible to recognize the morphological characters and determine the right-way-up in the SSOC. Within the volcanic sequence this particular feature has been observed at several locations, such as pillow lavas in detail profile 9 (Fig. 3.15), and detail profile 13 (Fig. 3.21). The pillow lavas within the volcanic sequence of SSOC in the Grimelia show that the way-up is stratigraphically towards north-northwest (Fig.4.9). Another method to determine the stratigraphic way-up is to observe drain-out structures with epidote-filled cavities (Chapter 4.3.4).

According to Jones (1969) the content of vesicles in pillow lavas can also be used to identification of right-way-up as well as the depth of the water and time of eruption. The content and size of the vesicles present in pillow lavas are primarly controlled by volatile content, when the pressure conditions allow volatiles to form as a separate gas phase in a

magma. Eruptions of pillow lava hardly form volatile content at a water depth of ca. 5000 m as a result of to high pressure. However, at shallow water eruptions with lower pressure, the vesiculatiry is high (de Wit et al., 2020). The vesicle content in the SSOC were investigated by Furnes et al. (2012), concluding that there are sparsely vesicular to nonvesicular content in the ophiolite. The pillow lavas within the SSOC are geochemichally similar to those reported by More (1965) from the Pacific Ocean. Hence, Furnes et al. (2012) concluded that the pillow lavas in the volcanic sequence likely erupted in deep-water environments, such as 2500-3000m (Furnes et al., 2012). The pillow lavas of the SSOC within the Grimelid area are vesicle-free, supporting the proposition of eruption in a deep-water environment, as previously proposed (Furnes, 1974; Furnes et al., 2012).

Fig.4.9: Picture showing pillow lavas with a rounded, convex top. Used to identify the right way up of the volcanic sequence. Scale: Geological hammer, ca. 25 cm long.

4.2.3 Cyclic stratigraphic units

Cyclic units through the Master profile of the volcanic sequence in Grimelia, is registered 8 times at a large scale (Fig. 3.2, Appendix 2). According to Furnes et al. (2003), beds of chert within cyclic units indicate several periods of volcanic quiescence. The present of chert in cyclic unit has not been found at a large scale, hence difficult to predict the number of eruptive periods (at a large scale) based on this. However, detail profiles 6 and 11 in this case, exhibits cyclic units examined at shorter intervals. Detail profile 6 (Fig. 3.11) is the best fit for a cyclic unit in this case, due to the extent of 15 meters and several eruptive units throughout one profile. Massive sheet flows are registered at the start of the eruptive unit and has a total thickness of 0.6 m. Further, the next 0.4 m is composed of volcanic breccia, which ends with massive sheet flows at one meter through the profile. Another eruptive episode starts with sheet flows at one meter, and has a thickness of total 4 m. Further, volcanic breccia occurs with a total length of 8 m. This eruptive unit ends with massive sheet flows towards the top. Beds of chert is not registered at minor cyclic units; hence these episodes represent single eruptions, or individual phases of an eruption (Furnes et al., 2003). However, it is likely to assume that the volcanic sequence in Grimelia represent multieruptional constructions, where the magma composition could change considerably (Furnes et al., 2003).

Cyclic units of the SSOC, especially in and/or nearby the area of interest, have been studied by e.g., Furnes et al. (2001; 2003) and Erga (2021). Cyclicity of the volcanic sequence of SSOC is typically composed of sheet flows and/or flows with large pillows at the base, followed by lavas with progressively smaller pillows and volcanic breccia. However, volcanic breccia may be absent in some cases (Furnes et al., 2003).

The internal structure of oceanic lithosphere is the result of interplay between the spreading rate, magma supply, tectonic extension, and thermal regime beneath and along a spreading axis (e.g., Macdonald, 1982; Smith and Cann, 1993; Phipps Morgan et al., 1994; Dilek, 1998; Karson, 1998; Furnes et al., 2001). Cyclic stratigraphic units in ocean crusts are a common occurrence recognized in volcanic and plutonic rocks (van Andel and Ballard, 1979; Kappel and Ryan, 1986; Staudigel et al., 1996; Ayadi et al., 1998; Natland et al., 1998; Furnes et al., 2001). From the base to the top of a cyclic stratigraphic unit, the extrusive sequence may contain sheet flows, pillow lavas and hyaloclastites (e.g., Staudigel et al., 1996; Furnes et al., 2001). The proportions between sheet flows and pillow lavas within the cyclic unit is likely to vary

markedly due to different spreading rate (Bonatti and Harrison, 1988; Furnes et al., 2001), and decreasing eruption rate, which leads to massive units/large pillows at the bottom, and finally minor pillows towards the top.

4.3 Volcanic breccias

The term "volcanic breccia" is in this case used as a main terminology to identify several types of volcanic lithologies, such as isolated and broken pillow breccia and volcaniclastic rocks composed of different volcanic rock fragments. Volcanic breccias is likely to form at any water depths due to several syn-eruptive and post-eruptive mechanisms (e.g., Carlisle, 1963; Honnorez and Krist, 1975; Wohletz, 1983; Bergh and Sigvaldason, 1991; Fouquet et al., 1998; Furnes et al., 2003).

According to Furnes et al. (2003) the dominant mechanism for brecciation in a subaquatic environment may be divided into 6 categories: 1) Expansion of magmatic volatiles in shallow water, 2) submarine lava fountaining at high eruption rates, 3) thermal shattering as a result of melt in contact with cold water, 4) spalling of glass rinds during inflation of pillows, 5) syn-eruptional disintegration and gravitational sliding, and 6) post-eruptional disintegration leading to distal bedded finer-grained volcaniclastic rocks and proximal talus (Furnes et al., 2003). Their systematic studies of the SSOC indicate that the formation of the volcanic breccias is a result of several of the above-mentioned categories (Fig. 4.10). The broken pillow breccia/hyaloclastites have likely formed during lava fountaining (mechanism 2), whereas the hyaloclastite matrix of broken pillow breccia exhibits thermal shattering features (mechanism 3). Inter-pillow hyaloclastites are formed due to spalling of pillow rinds during pillow growth (mechanism 4). As a result of syn-eruptional and post-eruptional disintegration (mechanism 5 and 6), broken pillows, pillow-fragments and hyaloclastites are formed. A fine-grained laminated, or bedded volcaniclastic rock have formed due to post-eruptional disintegration (mechanism 6) and is likely to represent resedimented hyaloclastites (Furnes et al., 2003).

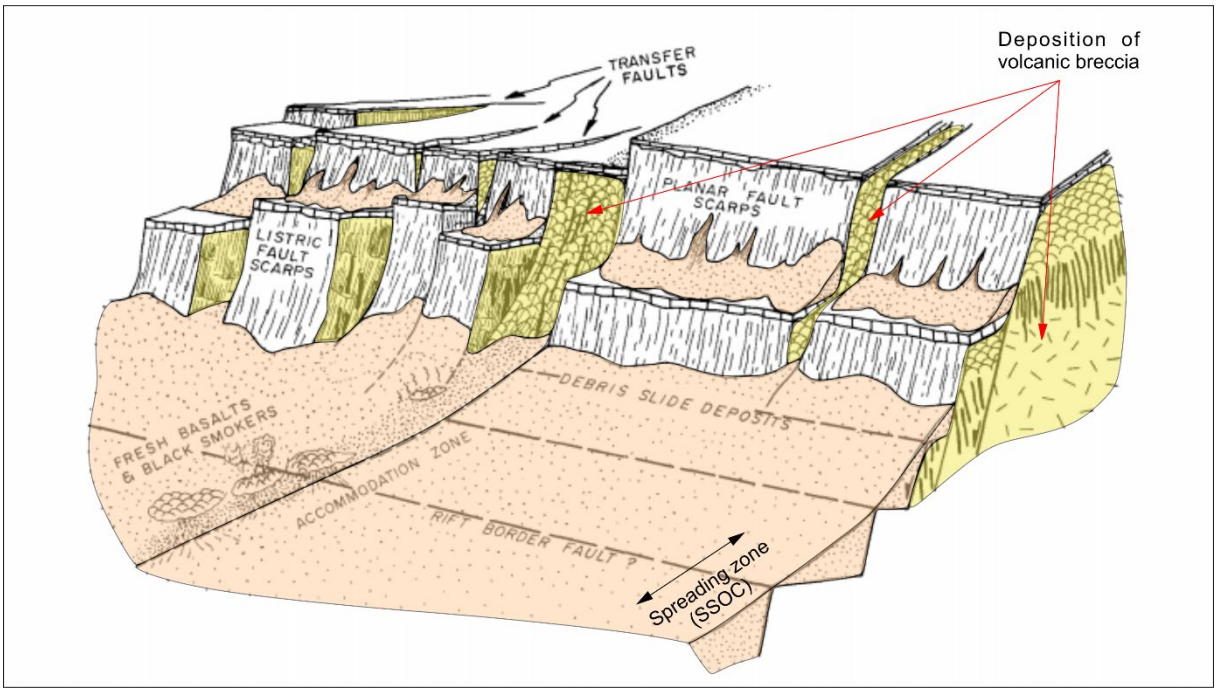

Fig.4.10: Proposed model of inferred geological relationships, based on Karson and Rona (1990) study of the Trans-Atlantic-Geotraverse area (Mid-Atlantic Ridge). This model is proposed to represent the development of the volcanic breccias in the area of SSOC, represented by transported sediments from different volcanic sources deposited to more stable areas.

4.3.1 Types of volcanic breccias

Furnes (1972) distinguished between two main types of volcanic breccias, isolated pillow breccias, and broken pillow breccias (Fig. 4.11), first described by Carlisle (1963) and Jones (1970). Isolated pillow breccia consists of whole pillows in a tuffaceous matrix (Furnes, 1972), whereas broken pillow breccia is dominated by whole or disaggregated pillows, set in a matrix of cogenetic basic tuff, which is likely to be confused with other volcanic breccias (Carlisle, 1963). The broken pillow breccia in Grimelia is only registered at one location (detail profile 10, Figs. 3.16 and 3.17), and is made up of a mixture of whole pillows with varying size, fragments of pillows, hyaloclastites, and irregular fragments of greenstone (Furnes 1972). Furnes and Fridleifsson (1979) further proposed a name for volcanic breccias associated with pillow lava and hyaloclastite, called pillow block breccia. Its characteristic features fit the volcanic breccia in Grimelia, predominantly consisting of dominantly pillow fragments with minor matrix components. Pillow block breccia typically show features such as 1) division into steeply dipping tabular units, and 2) transition from pillow lava into breccia (Furnes and Fridleifsson, 1979). The volcanic breccia occurring in Grimelia is predominantly interpreted as pillow block breccia (e.g., detail profile 1 and 2, Figs. 3.3, 3.4, and 3.5), with broken pillow breccia appearing once.

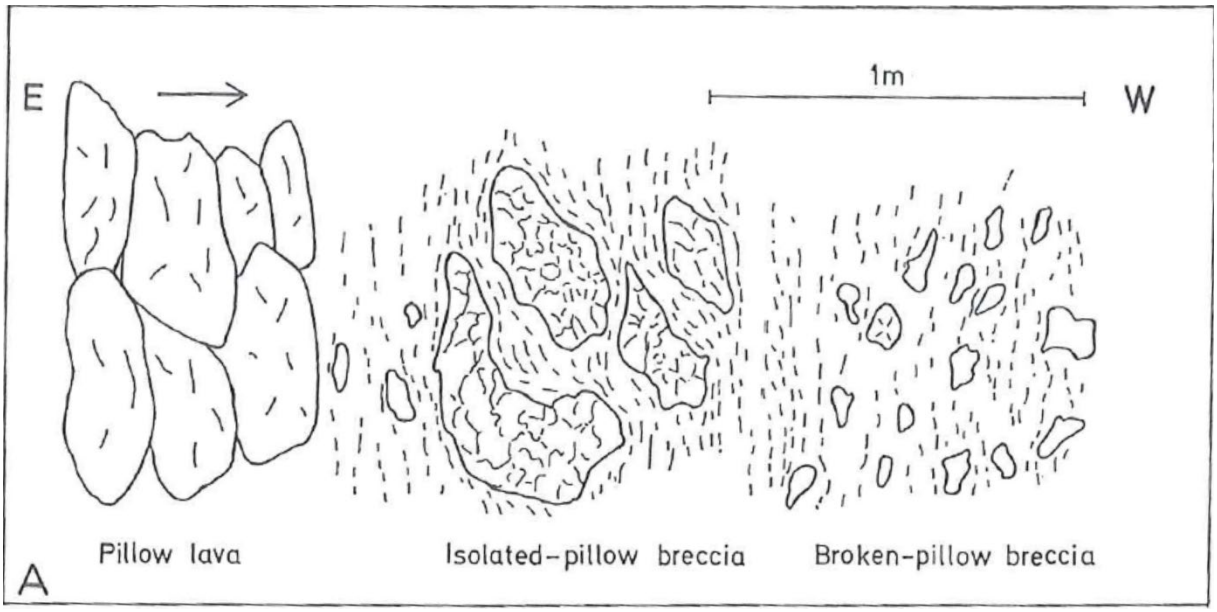

Fig.4.11: From Furnes 1972, illustrating the development from pillow lavas to isolated pillow breccia, to broken pillow breccia. This development is based on the SSOC in Oldra, Solund, approx. 41 km from Grimelia.

4.3.2 Hyaloclastite and pillow fragments within the breccia

Hyaloclastites are defined as volcaniclastic rocks that are generated by non-explosive granulation of volcanic glass and are common products of deep submarine environments (Honnores and Krist, 1975). Studies of modern seafloor exhibits that hyaloclastite are glassy clastic deposits, which is formed by non-explosive thermal granulation and/or spalling of solidified lava rinds due to deformation (White et al., 2015). The hyaloclastites observed in Grimelia is interpreted as original glass fragments (long chlorite lenses) and fits the description of White et al. (2015) (Fig. 4.12). Whole pillow-shaped fragments are also registered within the different volcanic breccia sequences, example from detail profile 1: Figs. 3.3A and 3.4. The axial ratio of these fragments is predominantly larger than the hyaloclastites (Appendix 1).

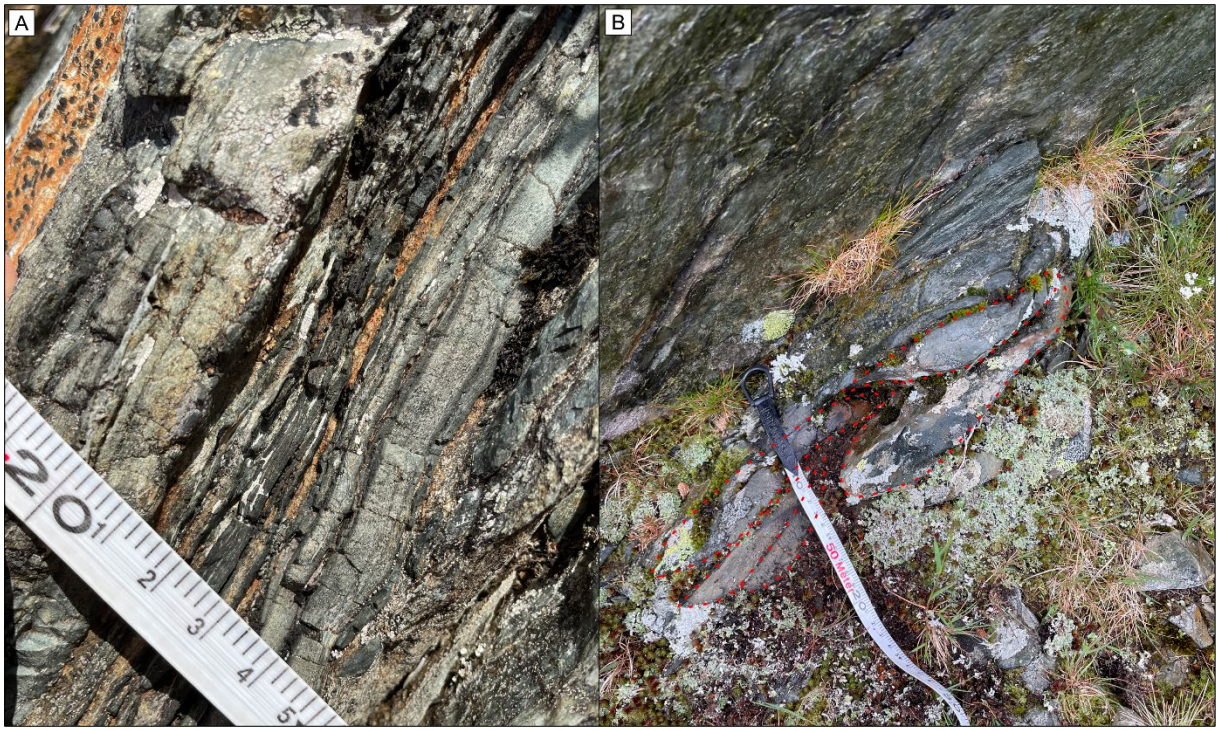

Fig.4.12: A: elongated hyaloclastites from part 1 of the Master profile, only a few mm thick and black colored. Difficult to distinguish clear ends due to high deformation, hence relatively inaccurate measurements. B: elongated hyaloclastites from part 2 of the Master profile, a few cm thick.

4.3.3 Volcaniclastic rocks

Volcaniclastic rocks usually occurs as fine-grained laminated or bedded rocks and are composed of different volcanic rock fragments, often with a presence of chert and siliciclastic sediments. Especially the presence of chert indicates that the accumulation occurred during several volcanic episodes. The material of the volcaniclastic rocks is probably resedimented hyaloclastites formed due to post-eruptional disintegration (Furnes et al., 2003). Within the study area in Grimelia, volcanic breccias defined as volcaniclastic rock occurs at detail profile 7 (Fig. 3.13) predominantly, where black chert is observed (Fig. 3.12 B). Detail profile 12 may also be defined as volcaniclastic material, due to the presence of epidote nodules (Fig.3.20). Commonly the epidote nodules are enveloped by sheared greenstone skin, and regarded as originally representing hollow pillows, and they commonly appear in areas defined as volcaniclastic rocks.

The occurrence of pillows with epidote-filled cavities with several drain-out episodes and different orientations of the drain-out floor (s) (Fig. 4.13), indicates that the volcaniclastic rocks are formed due to post-eruptional disintegrations connected with steep slopes and fault scraps (Furnes et al., 2003). A study done by Karson and Rona (1990) disclosed important

information of spreading centers connected to tectonic, magmatic, and hydrothermal activity. A post-eruptional disintegration resulting in proximal talus deposits and distal bedded finer-grained volcaniclastic rocks (Furnes et al., 2003), is likely to represent this proposed model (Fig. 4.10). Material from the slopes adjacent to the magmatic spreading center gets released as a result of tectonic activity, forming talus deposits. The fragments forming from talus deposits are both broken and whole fragments remaining their original shape. This is easily recognized as whole pillows, epidote nodules or pillow lavas with drain-out structures, completely or partially filled with epidote. Some of the rocks is probably transported from different sources due to the post-eruptional disintegration (Erga, 2021).

4.3.4 Drain-out structures

Towards the top of the volcanic sequence, predominantly concentrated within the volcanic breccia in detail profile 12, several drain-out features in pillow lavas occur (Fig. 4.13). The pillow lavas contain epidote-filled cavities with several drain-out episodes, with five drain-out episodes at most (Figs. 3.19 and 3.20). Due to various episodes of drain-out in the pillows, in which the cavities are filled with epidote, the drain-out structures can indicate the stratigraphic top of individual lava flows as well as the paleo-horizontal (Ballard and Moore, 1977; Fonneland-Jørgensen et al., 2005).

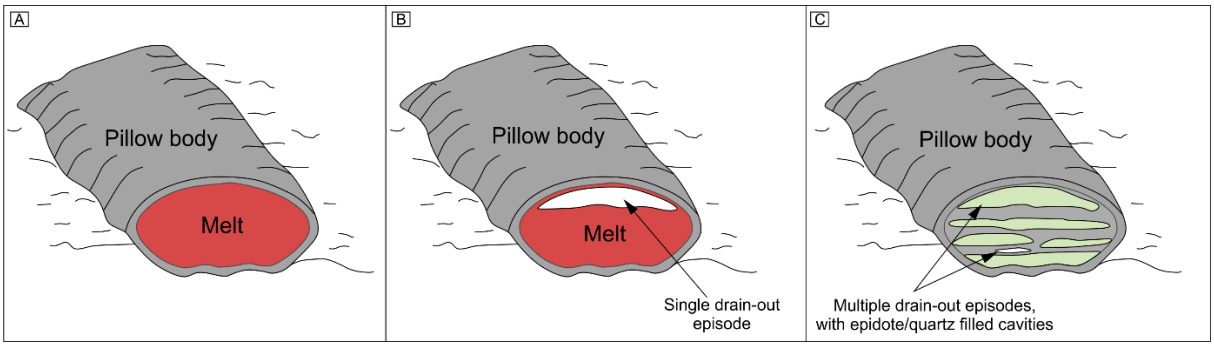

Fig.4.13: Model showing the different stages from melt to multiple drain-out episodes in hollow pillows. A: Solidified skin within a pillow lava. B: The solidified skin cracks, resulting in one to several drain-out episodes of the melt. C: multiple drain-out episodes with epidote and/or quartz filled cavities. From Harris and Rowland (2015), redrawn and modified from Erga, 2021.

The pillow lavas and their drain-out generation in the Grimelia area are, commonly epidote-filled, but quartz-filled cavities have been observed. As the drain-out features are concentrated within a minor part of the Master profile, only six drain-out features were measured. However, this gives an indication on the orientation of the floor of the drain-out generations within the sequence (originally represent the horizonal orientation), compared to

the foliation of the different layers (Fig. 4.14 A). Due to a relatively narrow cluster, this allows the suggestion of only minor and/or no block tilting of successive pillow lava horizons (Fonneland-Jørgensen et al., 2005).

Drain-out structures towards the top of the volcanic sequence of SSOC have been measured and presented in previous work near by the study area and can be compared with the results presented in this work. Fig. 4.14 A, shows drain-out orientations in the Grimelia area (black dots) as well as the average foliation of different units (yellow dot). Fig. 4.14 B, presents drain-out orientations in the Våganes area (red dots), ca. 1.5 km further west, as well as the foliation within the area (green dot) (Erga, 2021). Fig. 4.14 C, exhibits drain-out orientations in the Oldra area, Solund, approx. 41 km further south-west (Fonneland-Jørgensen et al., 2005). All plots are characterized by relatively narrow cluster, suggesting minor and/or no tilting of successive pillow lava horizons of the SSOC (Fonneland-Jørgensen et al., 2005).

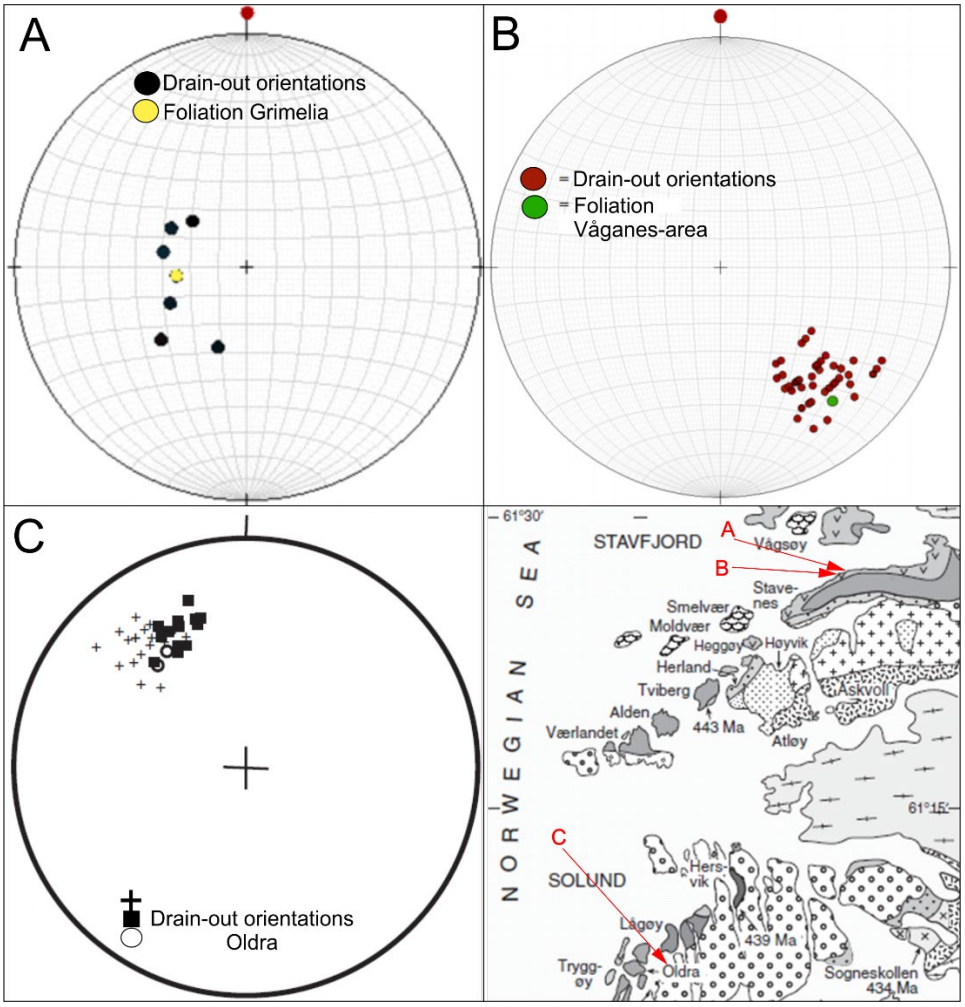

Fig.4.14: A: drain-out orientations and average foliation within the volcanic sequence of Grimelia area. B: drain-out orientations and average foliation within the volcanic sequence of the Våganes-area (Erga, 2021). C: drain-out orientations of the Oldra area in Solund (Fonneland-Jørgensen et al., 2005). Map: Furnes et al. 2012 (modified from Furnes et al., 1990).

4.3.5 Axial ratios of epidote nodules, hyaloclastites, and pillow fragments

The longest and shortest axis of fragments within the volcanic breccias have been measured. This implies fragments of the hyaloclastites and pillow-shaped fragments, as well as epidote nodules predominantly observed in the volcanic breccia (Appendix 1). Characteristic features for the hyaloclastites are strong deformation of the original glass fragments, now appearing as chlorite lenses. The purpose of this kind of measurements is to compare the axial ratios of the deformed breccias with equivalent and undeformed breccias. In total 39 hyaloclastite fragments and 10 pillow-fragments were measured. Maximum registered lengths for pillow-shaped fragments are 15 cm and 7 cm, whereas the maximum lengths for hyaloclastites are 40 cm and 1 cm respectively. The average size of the longest and shortest axis of pillow-fragments and hyaloclastites are 8.5 cm and 0.5 cm, and 10.5 cm and 3 cm respectively. This gives an average axial ratio of 0.29 for pillow-fragments, and 0.06 for hyaloclastites.

The pillow-shaped fragments are usually less deformed than the fragments of the hyaloclastites, yet still elongated. Measured epidote nodules, however, seems to be less affected by deformation as it is registered high axial dimensions in the area. Field observations indicates that the foliation has gone around the nodules, instead of deforming them. This indicates that the epidote nodules have a higher resistance to deformation than the other fragments within the area. Maximum registered lengths for epidote nodules are 90 cm and 20 cm respectively. In total 15 epidote nodules were measured, giving an average size of longest and shortest axis at 34 cm and 14 cm respectively and a ratio of 0.41.

To get an impression of the deformation in the area, these results are compared to a study done by Franzson et al. (2011), and Furnes and Fridleifsson (1979). Franzon et al. (2011) investigated undisturbed hyaloclastite formations in Iceland. Some of their results exhibits BEI (Backscattered Electron Image) photographs of hyaloclastite tuff samples with very small dimensions. Their result is therefore multiplied by 1000 and compared to the measured hyaloclastites within the volcanic breccia of SSOC (Fig. 4.15 A). The shortest and longest axis of hyaloclastite fragments within the SSOC are significantly smaller compared to the hyaloclastites from Iceland. By comparing the results, it gets implemented that the hyaloclastite fragments of SSOC needs to be multiplied by 97 to get the original size. However, the degree of deformation of hyaloclastites in SSOC cannot be reliable as they are compared

to hyaloclastites presented in a thin section. The comparison in Chapter 7 is more reliable, suggesting a deformation-ratio of 2.7 (Fig.7.3).

Further, the pillow fragments and epidote nodules are compared with pillow fragments within the pillow block breccias at Mosfell, Iceland (Furnes and Fridleifsson, 1979) (Fig. 4.15 B). The average lengths of these fragments are measured to 5.9 cm and 4.2 cm, giving an average ratio of 0.7. The pillow fragments of the SSOC are also significantly smaller and elongated compared to the pillow fragments from Iceland, whereas the epidote nodules are larger. The pillow fragments of the SSOC needs to be multiplied by 2.5 to match the undeformed pillows of Mosfell (Iceland), whereas the epidote nodules need to be multiplied by 1.7 (Fig. 4.15 B). This confirms the interpretation that the epidote nodules are less affected by deformation.

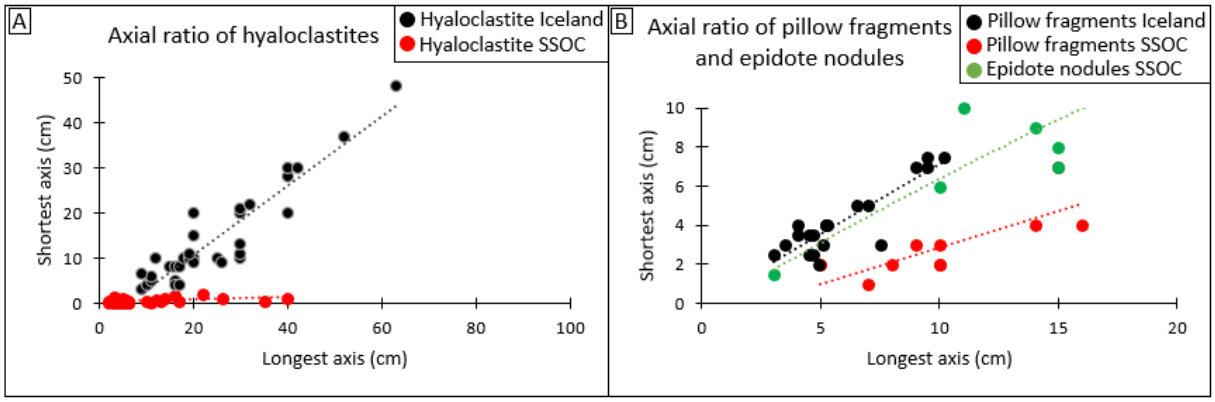

Fig.4.15: A: Results from the measured axial ratios of hyaloclastites in the volcanic breccia sequence of the SSOC, compared to data from undisturbed hyaloclastite fragments of Iceland (Franzson et al., 2011). The red dots represent hyaloclastite from SSOC. The black dots represent data from Franzson et al. (2011) study on undisturbed hyaloclastite fragments from Iceland and is multiplied by 1000. B: Results from the measured axial ratios of pillow fragments, compared to measured pillow fragments in the pillow block breccia formation in Iceland (Furnes and Fridleifsson, 1979 (Fig.1)). Green dots exhibit measured epidote-nodules from the SSOC, which seem less affected by deformation, compared to the black dots.

Chapter 5 – Profile comparisons

For this chapter, the Master Profile will be compared to previous work in the area. The lowermost parts of the Master profile will be represented by both version A and B (Fig. 3.2).

5.1 Previous work in the area

Based on 29 detail profiles, each one less than 1 km apart, Furnes et al. (2003) provided a complete picture of the volcanic evolution of the oceanic crust in the SSOC (from Solund (SW) throughout the Stavenes peninsula) (See Fig. 1 of Furnes et al., 2003, and Fig. 5.1). In Fig. 5.1 the volcanic construction along the Stavenes peninsula is shown. A total of 16 sections, of which 9 reach the sheeted dike complex, exhibit large variations in their thicknesses (mainly ca. 470-800m), as well as in the proportions of the main components, i.e., 1) sheet flows, 2) pillow lavas and 3) volcanic breccia. Thus, the volcanic products can, over laterally short distances, change from e.g., predominantly sheet flows to pillow lavas, or to volcanic breccias. As their profiles 18 and 19 are the closest profiles to this study, these are used for comparison, as well as Profile 1 of Erga (2021), located only 1.5 km west of this study.

Profile 18 from Furnes et al. (2003) is composed of more pillow lavas and volcanic breccias than profile 19, both profiles contain roughly the same amount of sheet flows, whereas in profile 19 there is a mixture of sheeted dikes and volcanic rocks through the first 150 meters. Profile 1 from Erga (2021) is, to a large extent, composed of volcaniclastic rocks, in situ volcanic breccias and sheet flows, for about 300 meters, whereas the uppermost 100 meters predominantly contains pillow lavas and minor areas with sheet flows. Profile 19 exhibits a minor section of cover sediments, consisting of metagraywacke and phyllite (Furnes et al., 2003), likewise to the Master profile of Grimelia. In profile 18 and 19 it is observed metagabbro intrusions at several levels, which is not registered at the Master profile nor Profile 1 of the Våganes-area (Erga, 2021). Profile 18 and 19 exhibit a volcanic sequence slightly larger than 500 m (Furnes et al., 2003), profile 1 extends for 400 m (Erga, 2021), whereas the Master profile of Grimelia shows a volcanic sequence with a total extend of ca. 1200 m (Fig. 3.2). This will be the longest registered volcanic sequence of the Stavestranda area, hence plotted and compared to the 3-dimensional, topographic interpretation of Furnes et al. (2003) (Fig. 5.1).

Studies of the metabasalt geochemistry of the SSOC through the above-mentioned profiles (Furnes et al., 2006), demonstrated stratigraphic variation in the volcanic components within

short distances. This observation led to the conclusion that the lava sequences did not form through eruptions from one large, homogenous, axially persistent magma chamber, but were more likely fed from small, separate magma chamber that evolved independently (Furnes et al., 2006).

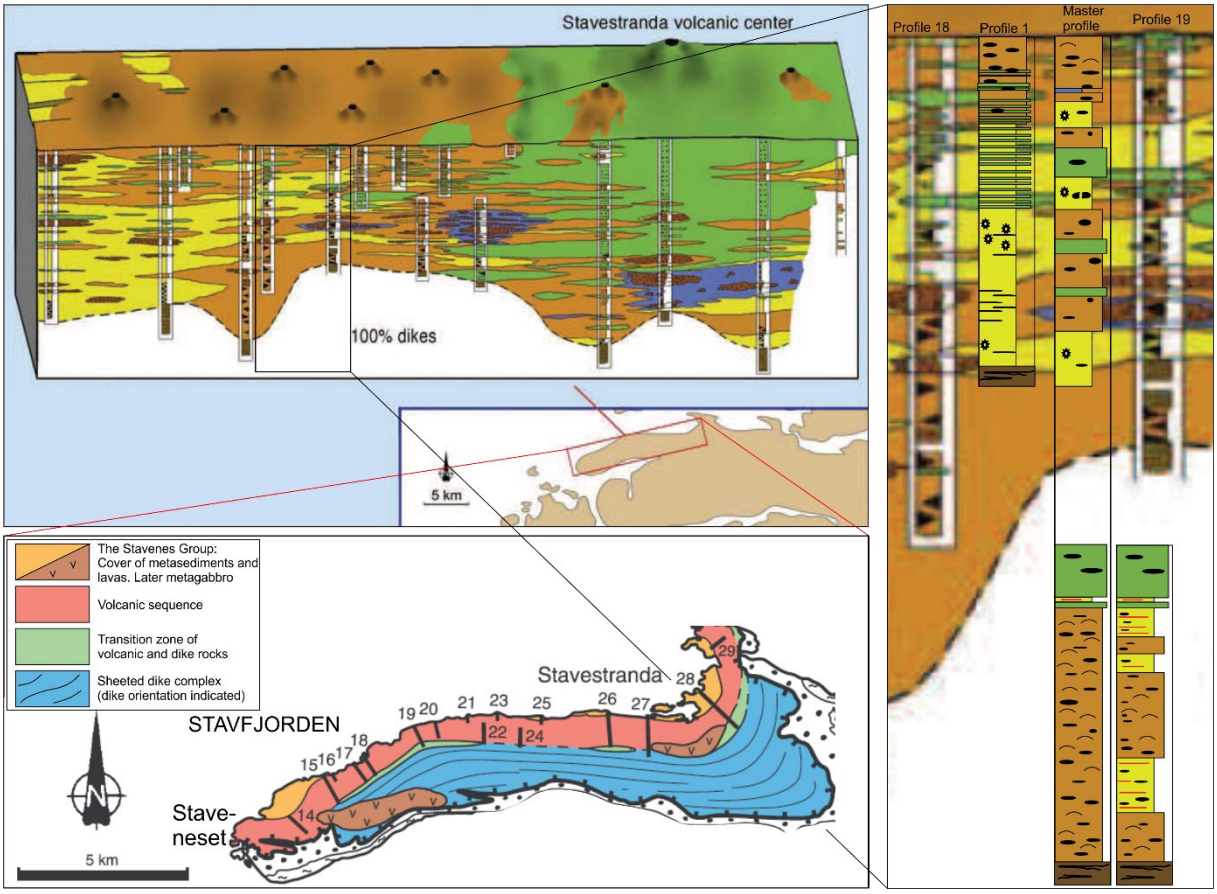

Fig.5.1: Volcanic stratigraphy of the Solund-Stavfjord Ophiolite Complex from Stavestranda, excluding the cover sediments at top. The figure illustrates a 3-dimensional, topographic interpretation from Furnes et al. (2003), modified to compare the Master profile of Grimelia with their profiles 18 and 19, as well as profile 1 of the Våganes-area (Erga, 2021). For explanation to legend, see Fig.5.2. This is just to illustrate the differences within the profiles located with short distances. The vertical scale is slightly inaccurate.

5.2 A proposed model for the Stavenes peninsula

The fact that there are major variations in the thickness (from cover sequence to the sheeted dike complex) of the volcanic sequences within short distances, indicates that the location of the different measured sections with respect to the spreading centers and volcanic centers differs from profile to profile. Profile 18 and 19 conducted by Furnes et al. (2003) exhibits a volcanic sequence slightly larger than 500 m, whereas Profile 1 from the Våganes-area is 400 m (Erga, 2021). As the Master Profile of this study exhibits a 1200 m extrusive sequence, the

question is why this profile is significantly larger than the other profiles in the area, even though all profiles are uncorrected in terms of deformation and foliation.

A proposed model to this question is made, indicating that the volcanic sequence of Grimelia is located at the magmatic spreading center. As the volcanic sequence of the Master Profile has a total extent of 1200 m, on average 500 m longer than the rest, it is suggested that this sequence has formed at, or close to, the magmatic spreading center of the SSOC. This is also in accordance with the occurrence of the VMS deposits at the lowermost parts of the Master Profile, as such deposits most likely form at the spreading center. This sequence is the only registered sequence within Stavestranda containing VMS deposits, indicating an ocean-floor hydrothermal activity during formation (Fig. 5.2). Based on the composition of the volcanic sequences in profile 14-18 (Furnes et al., 2003), and Profile 1 (Erga, 2021), it is likely to assume that these sequences have been located adjacent to the fault slopes forming talus deposits of volcanic breccia and volcaniclastic material. The shorter profiles, profile 16 and profiles 20 – 25, is interpreted to represent sections of the SSOC located farthest away from the spreading center.

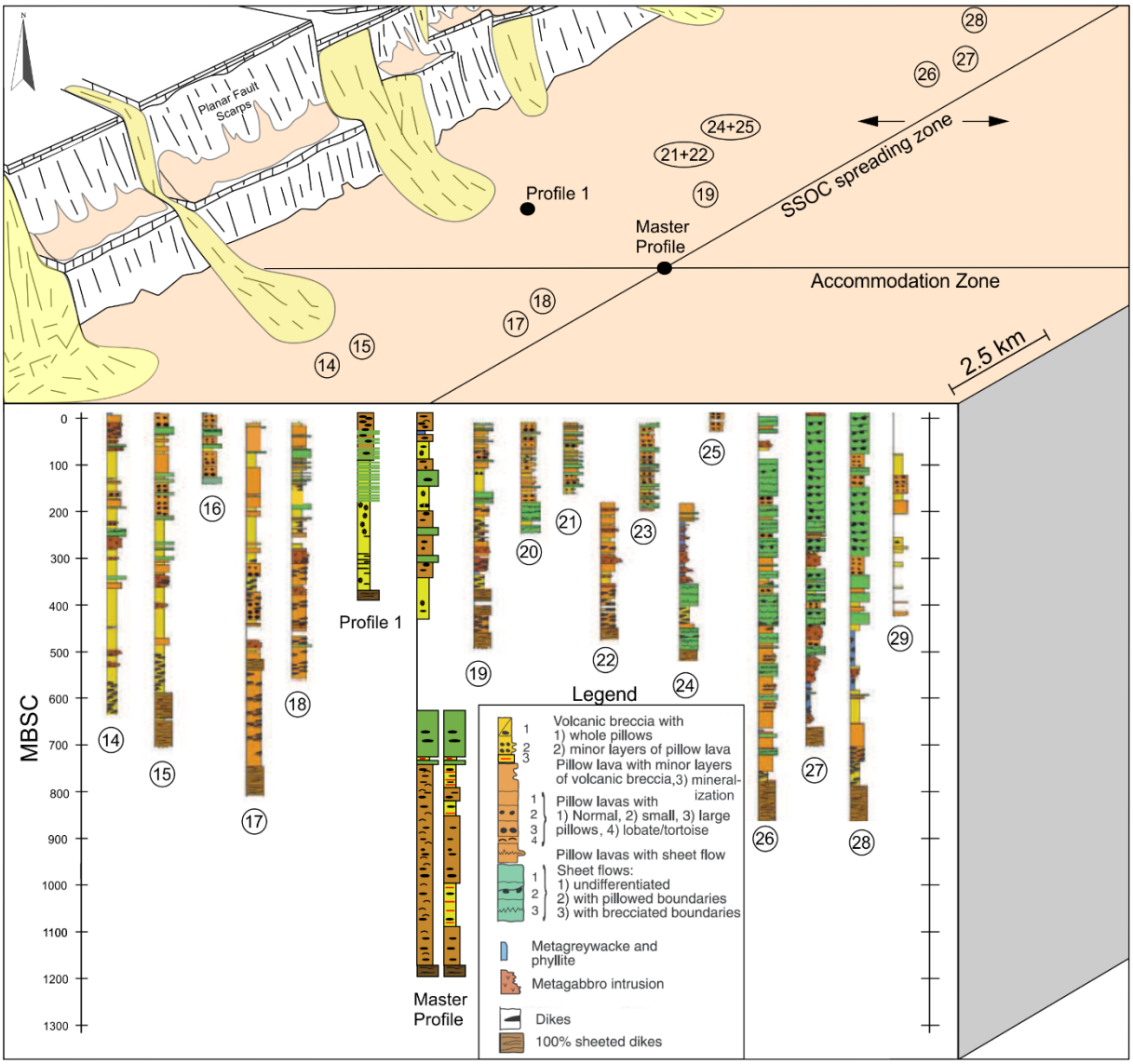

Fig.5.2: A proposed model of the location of the different extrusive sequences at the Stavestranda volcanic center during formation. As the Master profile of this study is the largest registered profile in the area, as well as the only profile composed of VMS deposits, the location during formation is interpreted to be at the magmatic spreading center. MBSC: Meter below sedimentary cover. Model inspired by and modified from Karson and Rona (1990), and Furnes et al. (2003). Profile 1 from Erga (2021). The scale might be slightly inaccurate.

Chapter 6 – Volcanogenic massive sulfide (VMS) ore deposits

In the SSOC, mining for Cu and Zn has been conducted in the Grimelia area through several mining periods (Stensrud, 1976; Korneliussen and Often, 1980) (Chapter 2.4.2 - Solund Stavfjord Ophiolite Complex - Ore deposits). The Grimelia ore deposit is located within the defined field area and is hence treated as part of the thesis. It is, however, important to highlight that this is not the focus of the thesis but considered with general knowledge about circulation of hydrothermal fluids and mineralization at spreading ridges. A geological map of the area, through the Master profile, part 1B, exhibits the extent of the volcanic breccias and the associated mineralization in this area (Fig. 6.1). Field observations indicates that the VMS deposits are linked to the volcanic breccias in the area, and further that they are delimited by major faults in the area (Fig. 3.25).

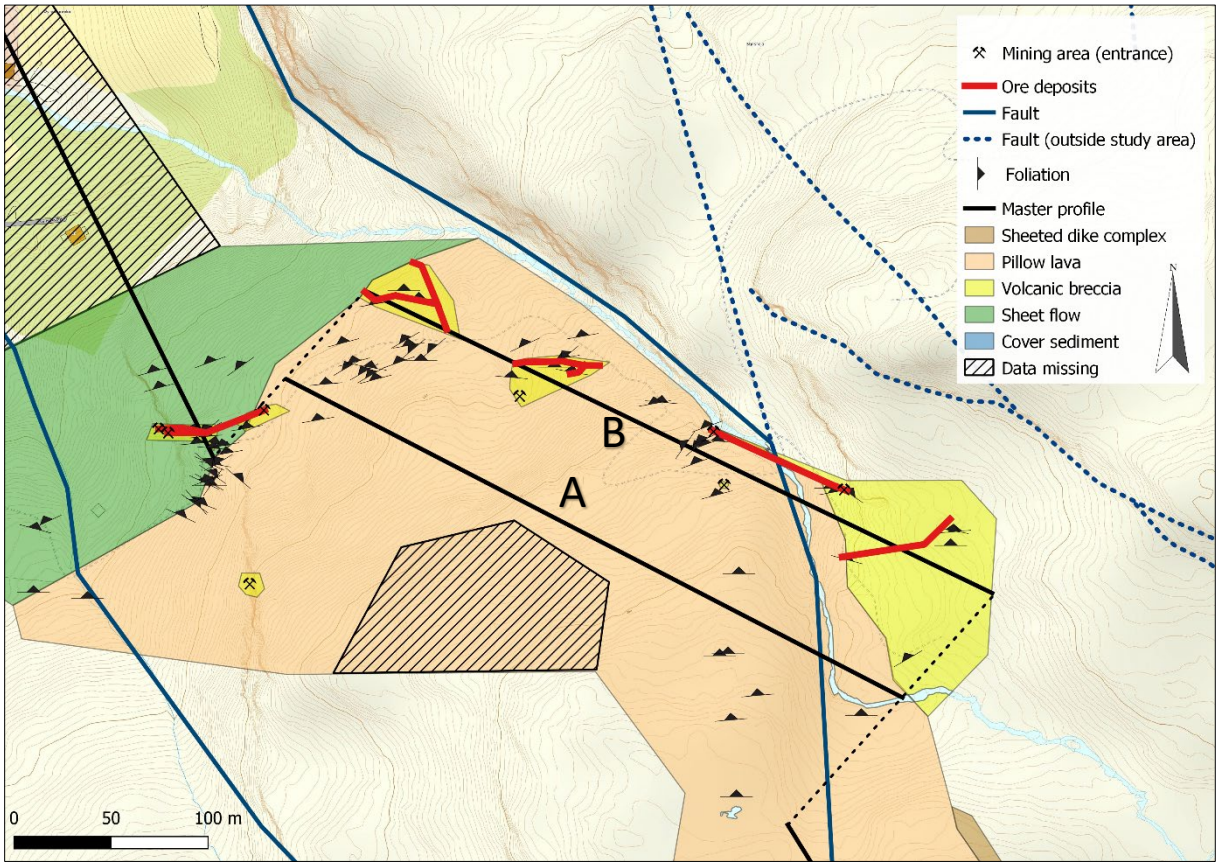

Fig.6.1: Geological map of the Solund-Stavfjord Ophiolite Complex showing the extent of the volcanic breccias and the associated mineralization. A cross section through the Master profile, part 1B (Fig.3.24), predicts the amount of ore deposits within the sections of volcanic breccia.

The genesis of ore deposits within ophiolites may be linked to the presence of epidosites, as the epidosites may play a fundamental role in the conditions of the hydrothermal solutions (Richardson et al., 1987). Epidosites, or epidote- and/or quartz-filled cavities in this case,

within an ophiolite can give an indication on the presence of VMS deposits elsewhere, due to episodes of high temperature circulation of hydrothermal fluids (Richardson et al., 1987). According to Alt (1995) zones of epidosites are restricted to the lower section of a sheeted dike complex and lower volcanic section, localized below large, massive sulfide deposits, which will form a deep upwelling feeder zone for the deposit (Fig. 6.2). However, the presence of epidote nodules within the SSOC in Grimelia is restricted to the upper section of the volcanic sequence (Fig. 3.2). Nonetheless, their presence leads to the assumption that they may be connected to the origin of the VMS deposits.

VMS deposits are major sources of Zn, Cu, Pb, Ag, and Au, as well as significant sources of Co, Sn, Se, Mn, Cd, In, Bi, Te, Ga and Ge. Formation of VMS deposits occurs at or near the seafloor from hydrothermal fluids in submarine volcanic environments and typically formed as lenses, and classified based on their metal content, gold content or host-rock lithology (Galley et al., 2007). The VMS deposits typically occurs within volcano-sedimentary stratigraphic succession and associated with volcanic rocks (Barrie and Hannington, 1997). The size-range of the hydrothermal mineral deposit varies from small to large, depending on the speed of the spreading centers. Large VMS deposits favor slow- rather than intermediate- to fast-spreading centers, yet the largest deposits commonly occur in sediment-hosted settings, rather than volcanic hosted setting (Rona, 1988).

6.1 Subsea mineralization at Mid-Ocean Ridges

Subseafloor hydrothermal conventions systems displays a spectrum in terms of intensity, size, and depth of circulation, located at and adjacent to seafloor spreading centers (Rona, 1988). Hydrothermal activity of intermediate to high intensity, is characterized by temperatures between 200-400°C, high thermal gradients, relatively fast flow rates, lower mass ratios, and production of greenschist metamorphic facies (Rona, 1988). Periodic repetition of geologic events, which rejuvenates the hydrothermal activity, may superimpose products of multiple ore-forming episodes (Rona, 1988). It is likely that this is the case of Grimelia, represented by at least four major episodes of eruption (Chapter 6.2, Fig. 6.5).

The mineral deposits and the size of hydrothermal fields are to a certain extent independent of the spreading rate, as the range of hydrothermal mineral deposit sizes occurs at all spreading rates. However, it is dependent on extremely localized physical and chemical

conditions (Rona, 1988). Processes occurring during the formation of VMS deposits, can be divided into three main zones, 1) recharge, 2) reaction and 3) discharge (Fig. 6.2). The recharge zone is dominated by descending seawater along faults and cracks, where the seawater undergoes progressive reactions when penetrating the crust. Reactions occurring at low temperatures and shallow depths is affecting the fluid-composition, which successively will affect reactions at higher temperatures and greater depths. Further, this process is controlled by oxidation and alkali fixation, both occurring during open-system alteration in the upper volcanic section, as well as fixation of seawater Mg in the crust (Alt, 1995).

In reaction zones the lower dikes and uppermost gabbros lose sulfur and metals to hydrothermal fluids during alteration at higher temperatures. The critical point of seawater controls the physical conditions, where fluids become buoyant and rapidly rise to the surface through upflow zones (Fig. 6.2). Deep focused upflow zones, characterized by the presence of epidosites through quartz-epidote-sulfide veins, are only observed in ophiolites. Disseminated sulfide mineralization on top of the sheeted dikes, is formed by diffuse discharge when high-temperature hydrothermal fluids mix with seawater in the subsurface in areas with focused flow or diffuse upflow (Alt, 1995).

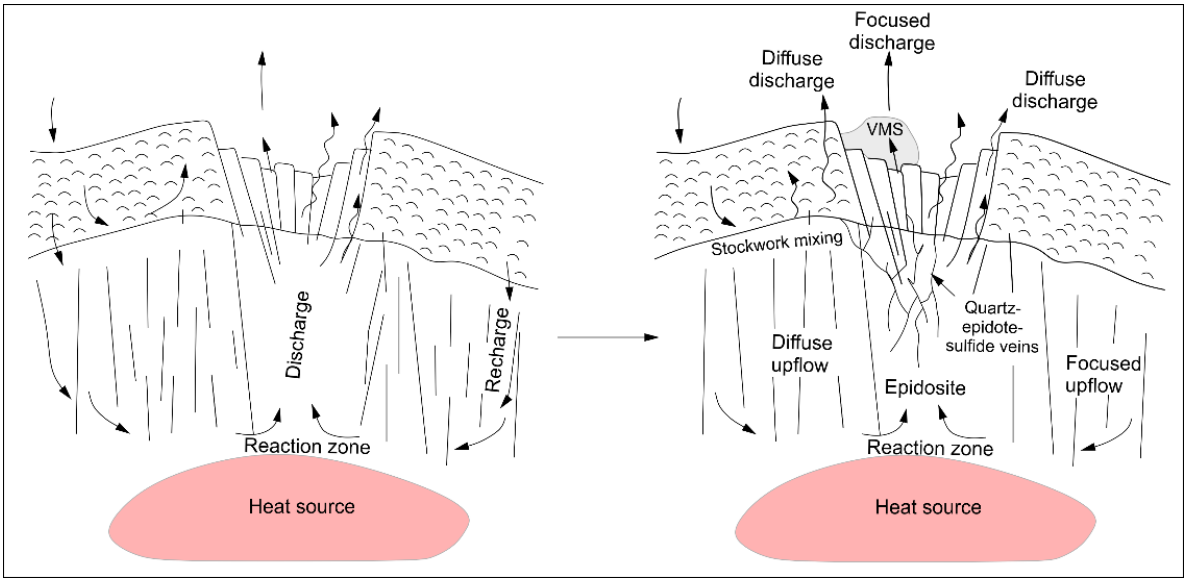

Fig.6.2: A general model representing the hydrothermal evolution of the volcanic sequence in Grimelia. Modified from Alt (1995).

According to Galley et al. (2007) two main components occur in most of the VMS deposits. The first is typically a mound-shaped/tabular body composed of more than 40% massive sulfide, quartz, and subordinate phyllosilicates (Galley et al., 2007) (Fig. 6.3), located in the focused discharge zone with focused upflow (Alt, 1995). The next component is iron oxide

minerals and altered silicate wall-rock (Galley et al., 2007), also located in the focused discharge sone (Alt, 1995). These components are typically underlain by stockwork veins/pipes and disseminated sulfides, where the pipes are enveloped in distinctive alteration halos. In turn, this may result in a hanging-wall strata above the VMS deposit (Galley et al., 2007).

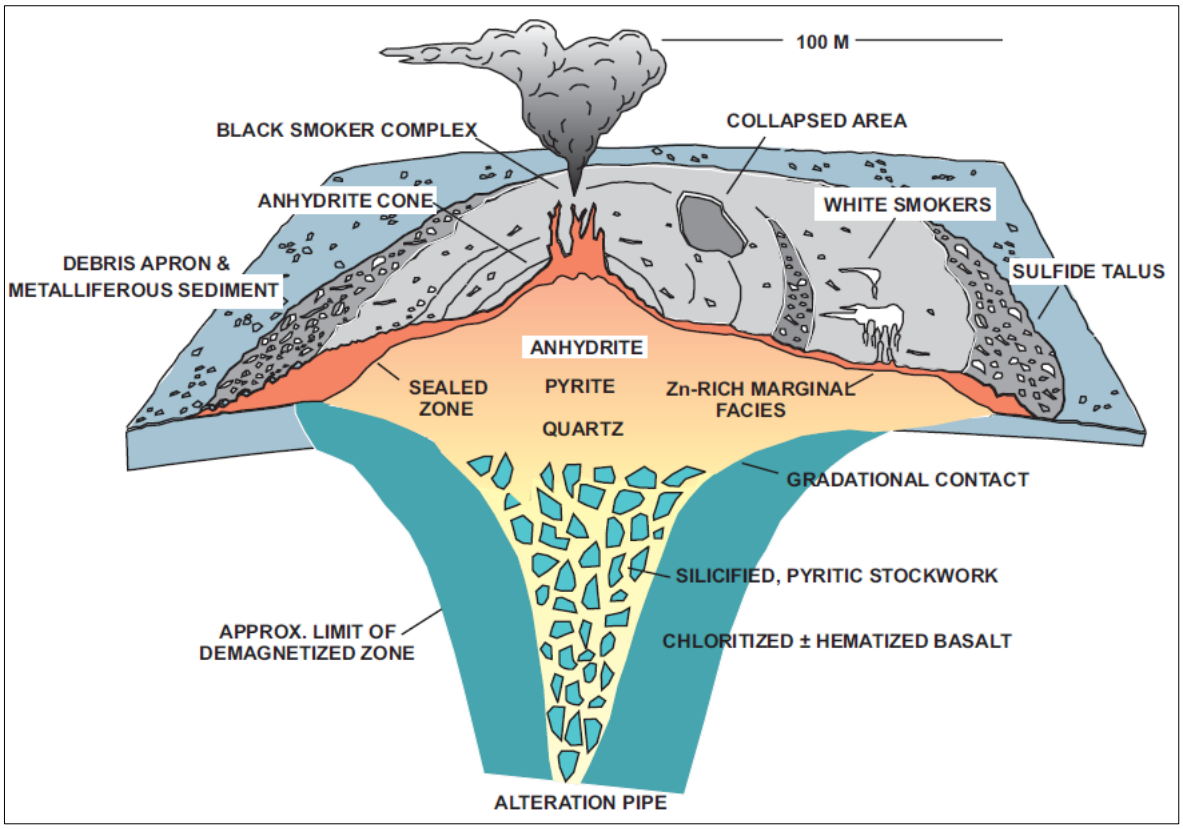

Fig.6.3: A detailed model of a classic cross section of a VMS deposit, showing a schematic diagram of a modern sulfide deposit on the Mid- Atlantic Ridge (TAG: Trans-Atlantic-Geotraverse). The diagram exhibits semi-massive to massive sulfide lenses underlain by a discordant stockwork vein system and associated pipes. From Galley et al. (2007) modified from Hannington et al., 1998.

Hannington et al. (1995) provided detailed studies of mineral assemblages and their physical and chemical conditions that prevails during seafloor mineralization, which gave the conclusion that a variety of parameters have a major impact on the bulk composition of a deposits and the mineralization. Based on this, and the fact that the VMS deposits in Grimelia are delimited by faults (Chapter 3.3), a model of the deposits in the area is made (Fig. 6.4). The model indicates various distributions and how they are intended to form at seafloor, depending on the source rock, hydrology and subseafloor replacement. The size of the deposits is also depending on the degree of permeability. In Grimelia, the VMS deposits are bounded by the volcanic breccia-zones, with originally high permeability. The massive sheet

flows and pillow lavas represent more impermeable materials and will hence not contain VMS deposits. The characteristic shape of most massive sulfide deposits, including the VMS deposits in Grimelia, are mounded shaped with a convex-up top (Rona, 1988). It is, however, likely that the deposits are interfingering with the other components as presented in Fig. 6.4C.

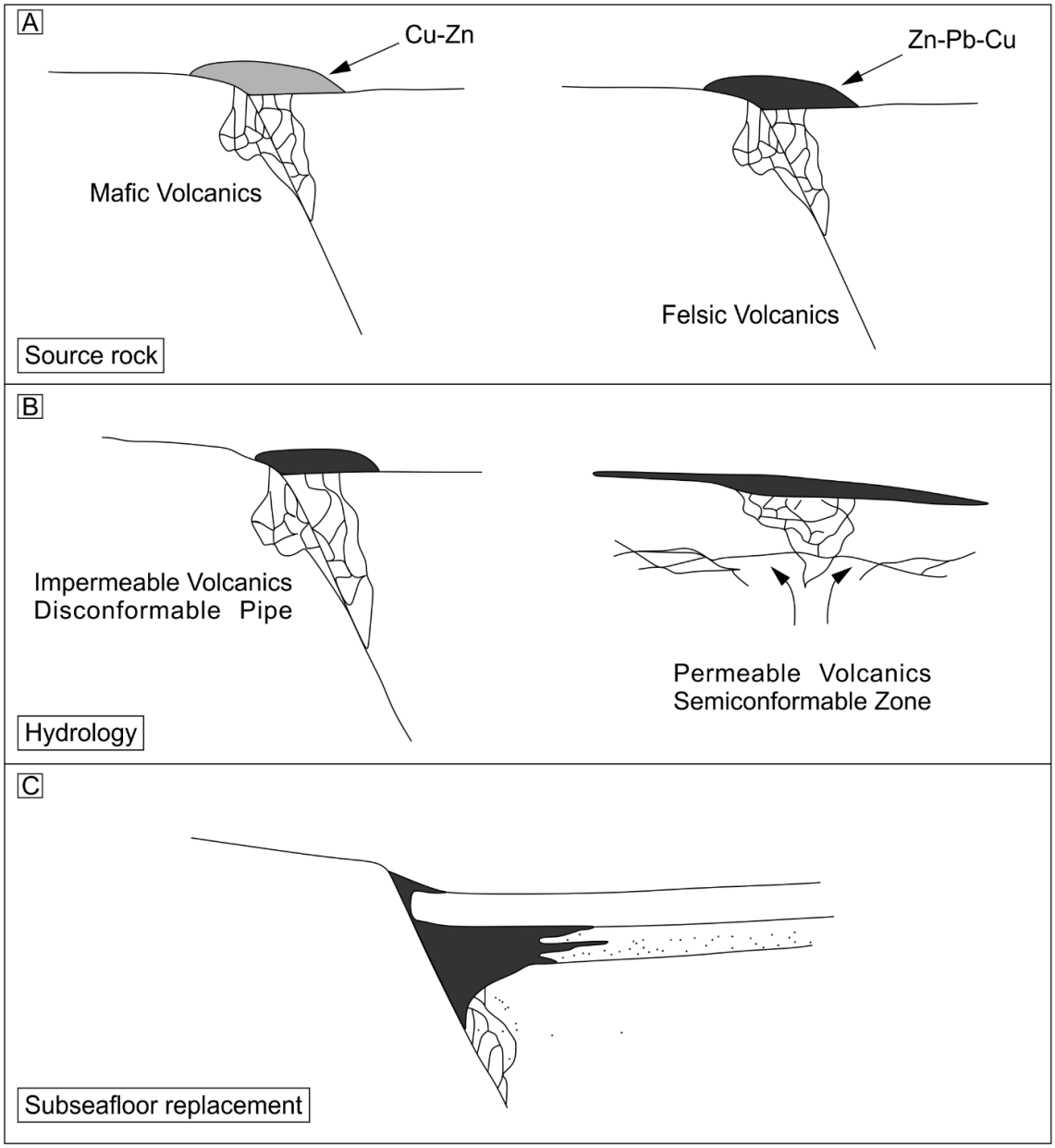

Fig.6.4: Model suggesting formation of VMS deposits located in Grimelia, depending on various physical and chemical conditions. A: the formation is controlled by the source rock, giving different mineral assemblages when depositing. B: the formation is controlled by hydrology and whether the source rock is permeable or impermeable. The degree of impermeability controls the size of the deposits. C: the formation is controlled by subseafloor replacement, e.g., determined by faults. Modified from Hannington et al., 1995.

6.2 A proposed model for the Grimelia deposits

Based on field observation and general knowledge about mineralization at spreading ridges, a proposed model of the VMS deposits in Grimelia is made (Fig. 6.5). Field observations

indicates that the VMS deposits are limited to part 1B of the Master profile, located approximately 65 m further north of part 1A. As the deposits occur at four different levels, it is suggested that the area has undergone four stages, and/or continuous stages of focused flow and focused discharge. The suggested model indicates that the deposits of Grimelia is bounded by a large fault in the area, giving extremely localized physical and chemical conditions, which in turn controls focused flow of hydrothermal fluids and resulting focused discharge zones. Fig. 6.5B suggest how the VMS deposits interfingers with the other components in the volcanic section. Hence, based on surface observation, it is impossible to predict the extent of the subsurface deposits. It is, however, known that when the mines in Grimelia were operational, the ore production were 300-1100 tons ore a year with a Cu average of 3.5-4.5% (Stensrud, 1976; Korneliussen and Often, 1980). As the internal structure of the SSOC infer an intermediate spreading rate for the magmatic evolution (e.g., Dilek et al., 1997; Furnes et al., 2003; Furnes et al., 2012), combined with general knowledge of mineralization at spreading ridges, it is likely to assume that the extent of the VMS deposits in the area of Grimelia is of minor to intermediate size.

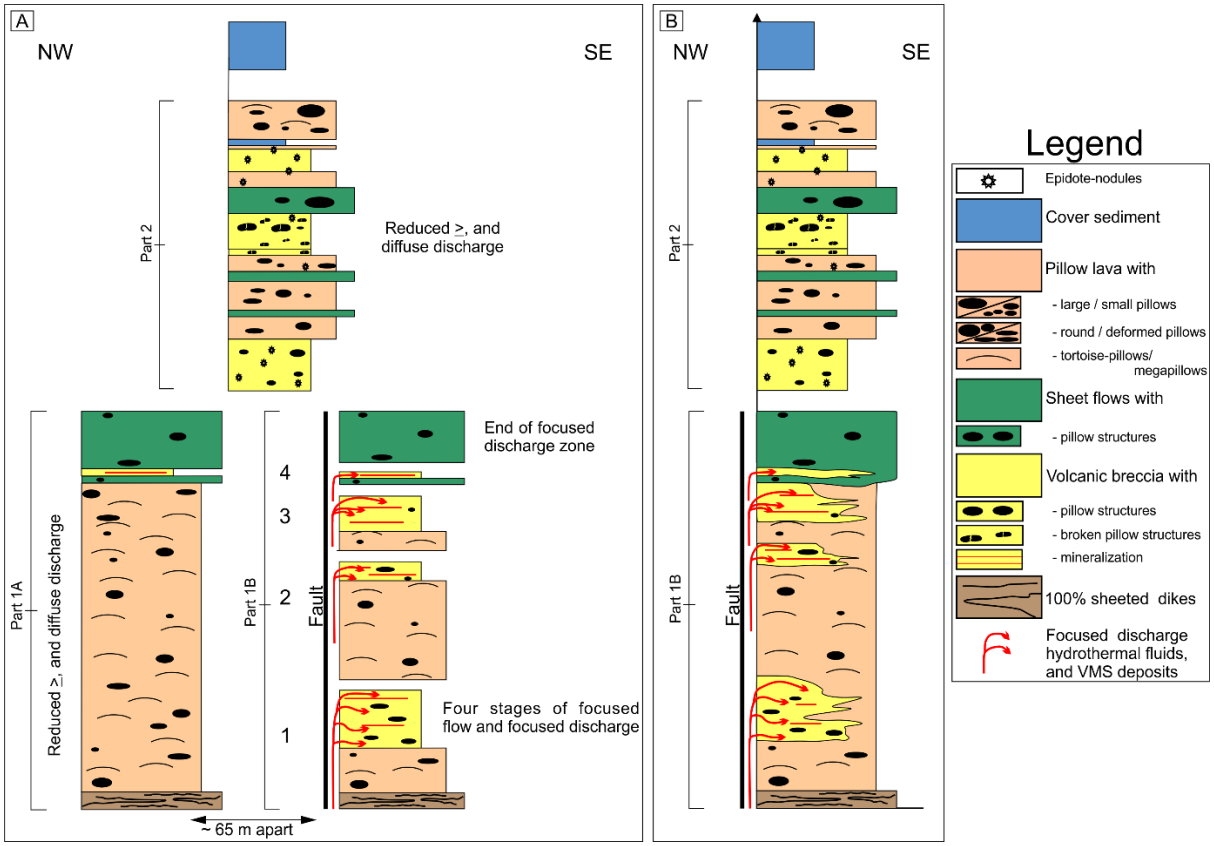

Fig.6.5: Proposed model representing the evolution of VMS deposits in Grimelia. A: Indicates that the formation of VMS deposits is restricted to part 1B of the Master profile, controlled by focused flow and focused discharge in the volcanic breccias. The mineralization is also bounded by one of the larger faults in the area (Fig.3.25), giving extremely localized physical and chemical conditions. B: suggested appearance of the VMS deposits interfingering the other components in the area.

Chapter 7 – Petrography

As a result of late Caledonian orogenesis, the rocks of the SSOC have been affected by sea-floor alteration and lower greenschist-facies metamorphism (Furnes et al., 2000; 2006; Fonneland-Jørgensen et al., 2005). The different components in the studied area have an expected composition of the main assemblage of greenschist facies conditions, which is actinolite, epidote, albite, chlorite, and leucoxene, as have been reported elsewhere in the SSOC (e.g., Fonneland-Jørgensen et al., 2005).

For the petrographic characterization of the investigated rocks, 13 thin sections were made, representing the different volcanic components within the studied area. Twelve of them were collected from part 1 of the Master profile, whereas one is from part 2 (Fig. 3.2). Five of the thin sections exhibit the mineralogical and textural features of sheets flows, four thin sections represent the volcanic breccia, whereas the last four represent pillow lavas. Three of the best-suited thin sections have been selected for the characterization of the texture and hence the estimate of the extent of deformation. One thin section is from a sheet flow (Fig. 7.1 A), one from a pillow lava (Fig. 7.1 B), and the last one is from one of the volcanic breccias (Fig. 7.2). These can be used to reinforce the hypothesis of a less deformed sheet flow-sequence, and intermediate to strongly deformed pillow lava and volcanic breccia- sequences.

As mentioned above, the main mineral assemblage is actinolite, epidote, albite, chlorite, and leucoxene, typical of lower greenschist facies conditions. All of these minerals appear within the thin sections, but their proportions vary greatly. As minor constituents, minerals such as quartz, muscovite, biotite, and garnet also occur. According to Strekeisen (2020), the primary rock composition is essential for the mineral assemblage, which in this case can be interpreted to mafic and pelitic protoliths. Yet, the mineral assemblage of a pelitic protolith is only observed in one thin section, which in this case is from the volcanic breccia sequence. Sulfide minerals is present in 8 out of 13 thin sections and occurs as opaque minerals or gold-colored minerals in reflected light. Since the ore deposits appear to be concentrated to the volcanic breccias, it is likely to expect that the sulfides are predominantly concentrated to these areas as well. However, traces of sulfides are observed in all three components.

7.1 Description of thin sections

The texture of the examined sheet flow shows chaotic and randomly oriented plagioclase crystals, set in a finer-grained groundmass of chlorite, actinolite, epidote and leucoxene (Fig.7.1 A). Based on this partly preserved primary magmatic texture, it is reasonable to assume that the occurrences of massive sheet flows are relatively little affected by deformation, compared to the other examined volcanic lithologies. In some of the larger crystals (plagioclase) it is possible to observe swallow-tale texture, which is a primary quench structure. Fig. 7.1 B exhibits the same minerals in a fine-grained groundmass as the previous thin section, except leucoxene. However, in this case the rock sample is represented by a pillow lava, where the crystals have become larger and is more parallel oriented. This suggests that the pillow lavas are affected by deformation to a higher extent than the sheet flows. Nevertheless, it is possible to observe that the foliation to a certain extent bends around the largest crystals, confirming deformation of pillow lavas at the microscopic level. In this thin section it is also observed swallow-tail texture, as well as chlorite-glass rinds around some of the crystals.

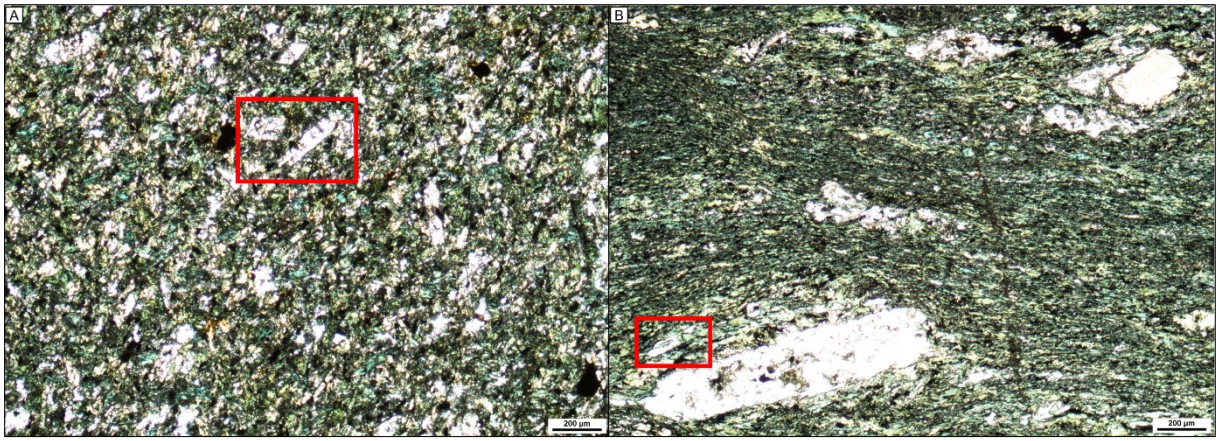

Fig.7.1: A Thin section from massive sheet flows showing larger, randomly oriented plagioclase crystals, in a finer groundmass of chlorite, actinolite, epidote, leucoxene and sulfides (opaques). The irregular texture indicates that the area is less affected by deformation. B: Thin section from pillow lavas showing larger plagioclase crystals in a finer groundmass of chlorite, actinolite and epidote. The crystals are more parallel oriented in this case, indicating influence of deformation. The large plagioclase crystal within the red squares in both pictures shows a primary quench texture, known as swallow-tail texture.

The thin section from the volcanic breccia is mainly composed of the same minerals as the previously mentioned minerals, but additionally lenses of quartz as well (Fig. 7.2 A). This sequence seems to be more affected by deformation processes as the crystals are parallel oriented. Here the crystals, especially chlorite lenses are larger and more well developed than in the previous thin sections. These are likely to represent the originally glass fragments of the hyaloclastite component of the volcanic breccia (Fig. 7.2 B). Some of the chlorite lenses of the

hyaloclastites observed in thin sections of the SSOC are measured and compared to the data from Fig. 4.15 A, representing hyaloclastites from subglacial deposits in Iceland and measured hyaloclastites in the field area at Grimelia. The longest and shortest axis of the hyaloclastites within the thin sections are 27.5 cm and 5 cm respectively (multiplied by 1000) (Fig. 7.3), with an average value of 14 cm and 3 cm. The average ratio of hyaloclastites in Iceland is 0.58, whereas the average ratio of hyaloclastites in SSOC is 0.21 (based on thin sections). This indicates that the hyaloclastite fragments of Grimelia needs to be multiplied by 2.7 to get to the original structure compared to supposedly similar type of deposit, studied by Franzson et al. (2011).

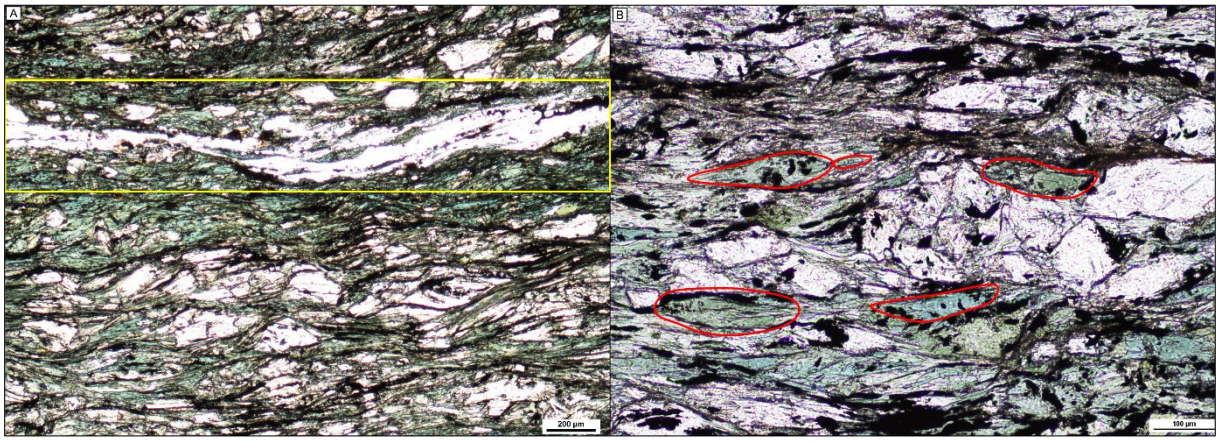

Fig.7.2: Both images are from the same thin section representing volcanic breccia. Mineral assemblage is actinolite, chlorite, epidote, quartz, and sulfides (opaques). A: overview showing how the different crystals are parallel oriented due to high deformation. The white mineral-band within the yellow box represents the quartz. B: More detailed/zoomed picture of the minerals within the thin section. The red envelopes represent some of the well-developed chlorite minerals, constituting the presumed original glass fragments of the hyaloclastites.

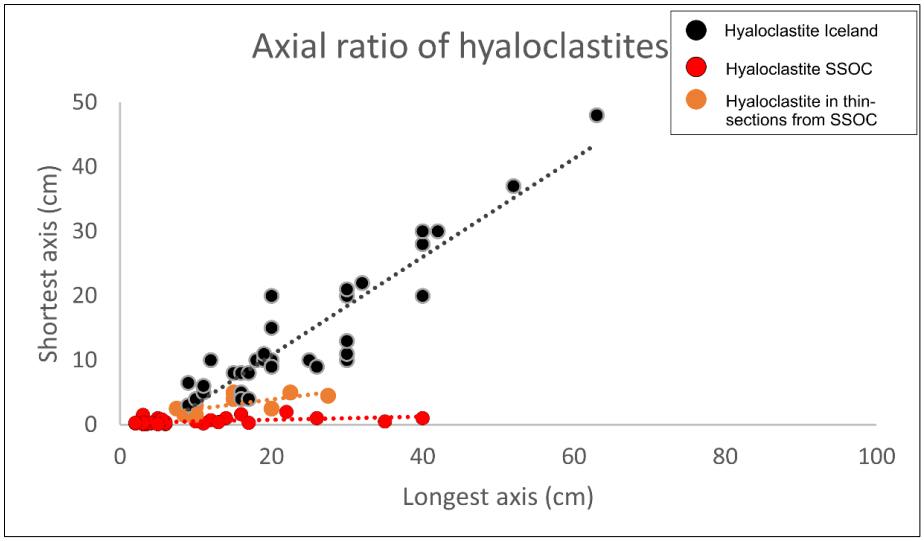

Fig.7.3: From Fig.4.15A, combined with measured hyaloclastites in thin sections from SSOC. The red dots represent hyaloclastite from SSOC, measured in field. The black dots represent data from Franzson et al. (2011) study on undisturbed hyaloclastite fragments from Iceland and is multiplied by 1000. The orange dots exhibit data from hyaloclastites in thin sections from SSOC and is multiplied by 1000.

Chapter 8 – Reconstruction and evolution of the volcanic sequence

A reconstruction of the volcanic sequence in the Grimelia area can be predicted, subject to the consideration of several parameters. The first step concerning adjustments of the thickness of the sequence relates to the altitude of the dip-angle of the strata, which, in this case, will slightly reduce the thickness. The next step, with respect to adjustments due to deformation, will increase the maximum thickness of the sequence and present an estimate of a reconstructed maximum thickness. These parameters can be calculated by trigonometric formulas and the correlation between V/H ratios on measured pillow lavas compared to undisturbed pillow lavas in Iceland, as well as comparison of axial ratios of fragments in the deformed volcanic breccias with undeformed equivalents. This chapter will provide the above-mentioned two steps concerning the reconstruction of the volcanic sequence (Appendix 3), provide a reconstructed profile, a profile-comparison with modern oceanic crust, as well as a presumption of the evolution in the area.

8.1 Step 1: Adjustments regarding dip of strata

To calculate the true thickness of the measured strata, the dip of strata within the different sequences is used. For the section with missing data an average dip of 59°, taken to represent the original bedding of the lava units, is used. Excluding the sedimentary cover, the profile thickness before reconstruction is 1205 m. In total, the adjustments have been made for 16 parts of the profile (Appendix 3, Figure 2), excluding the sedimentary cover. By using trigonometric formulas, a calculation of the actual thickness regarding the dip of the strata can be made. Table 3.1.1 shows the calculations how to adjust the thickness of the various components within the volcanic sequence of Grimelia, where the new total length (thickness prior to adjustment for deformation) is **957 m**.

8.2 Step 2: Adjustments regarding deformation

The extent of deformation within the volcanic sequence of Grimelia is predicted based on V/H (vertical/horizontal) ratios on measured pillows in the area, compared to various undisturbed pillow lavas (Furnes and Fridleifsson, 1978), as well as maximum and minimum axis of hyaloclastite fragments (Franzson et al., 2011), both from Iceland. The calculations are presented in Appendix 3, Table 3.2.1.

The deformation ratio is, however, difficult to calculate as multiple factors control the deformation. As for the deformed pillows of the SSOC in Grimelia, it is the measured sections that constitutes uncertainties with the measurements. Initially, the lava flow/direction of the pillows has a slightly different orientation. As the measured pillows are all from the same section, statistically there will thus be a small part that only represents the true cut of a pillow, meaning that only a few will represent a cut perpendicular on the lava flow (Fig. 8.1). Hence, most of the measurements will provide an inaccurate V/H ratio, resulting in a higher deformation-ratio than it should be.

Chapter 4.2.1 predicts the deformation within the different detail profiles in the area, stating i.e., pillows from part 1 of the Master profile is more deformed than the pillows of part 2 (Fig.3.2). Yet, field-observations displays the opposite as the pillows of part 1 is more massive (Fig. 8.2), compared to the pillows at part 2 (Fig. 3.21). To get the right estimate for a reconstructed maximum thickness, the total deformation ratio of 1.75 (Fig. 4.8) would hence give a slightly larger thickness than originally. Therefore, the deformation ratio of detail profile 13 (Fig. 4.7) is used for pillow lavas in part 2 of the Master profile, as this deformation ratio is based on 98 measurements within the same sequence. A slightly decreased deformation ratio of 1.3 is used for pillows in part 1 of the Master profile, as field observations and the texture of the pillow- thin section indicates a partly deformed area.

The deformation ratio of the hyaloclastite fragments is calculated to be 2.7 (Fig. 7.3) and is used for volcanic breccias throughout the entire volcanic sequence. The components consisting of sheet flows do not need to be adjusted due to minor deformation (Chapter 7).

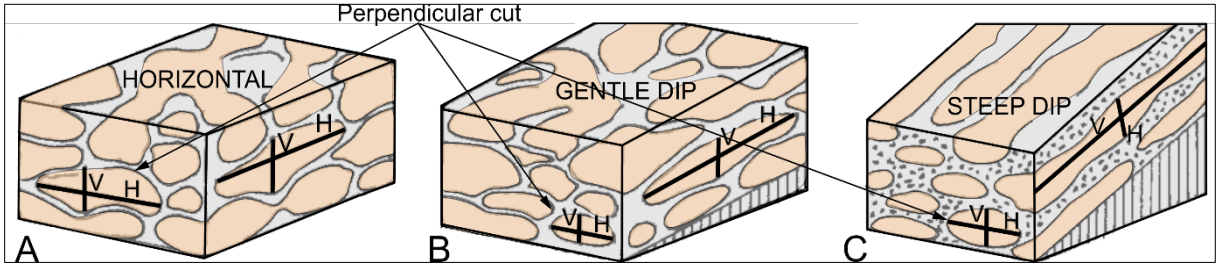

Fig.8.1. Showing pillow lavas with the same flow direction, different dip-angle, different crosscuts, and likely measured parameters in field. A crosscut like the different options (A-C) will provide measurements perpendicular on the flow direction, when measured from the front. The crosscut on the sides, however, will provide measurements less than 90° on the flow direction. This will result in a higher V/H ratio than it should be, and hence provide somewhat inaccurate results. Modified from Walker (1992).

Fig.8.2: Massive mega-pillows from the pillow lava section of the master profile, part 1. These are less deformed than the pillows of the master profile, part 2. These pillows can easily be misinterpreted as massive sheet flow, but the lobate surface defines them as pillows.

8.3 Reconstructed maximum thickness

Based on step 1 and step 2 of adjustments concerning dip of strata and deformation, a new estimated profile thickness is made. Profile thickness before reconstruction: **1205 m** (excluding cover sediments). Estimated profile thickness after reconstruction regarding dip of strata and deformation: **1430 m** (Appendix 3). It is, however, important to highlight that this is only an estimate for the reconstructed maximum thickness. It is also important to keep in mind that the calculation of the estimated thickness is based on homogeneous degree of deformation for all three components throughout a sequence. However, it is known that the deformation will not be homogeneous throughout one sequence and hence, the estimated thickness may be slightly overestimated.

8.4 Comparison to modern oceanic crust

The volcanic sequence of the reconstructed Master profile from Grimelia and adjacent profile of the Våganes-area (Profile 1, Erga, 2021) of the SSOC, will be compared with two profiles through the oceanic crust of the Costa Rica Rift. This modern oceanic crust represents

formation at intermediate spreading rate, which has also been interpreted for the formation of the SSOC crust (Dilek et al., 1997; Furnes et al., 2000; 2003; 2006). During Ocean Drilling Program (ODP) Leg 149, Hole 504B and Hole 896A were drilled into a 5.9 Ma old ocean crust, 200 km south of the Costa Rica Rift in the eastern Pacific (Alt et al., 1996; Torsvik et al., 1998). The study of Alt et al. (1996) focuses on 1) differences in the volcanic stratigraphy and geochemistry within these two holes, 2) examination of the heterogeneity of the basement alteration in the different parts, and 3) drill across a fault to detect possibly differences. Hole 504B is drilled into a hangingwall, through two possible faults, whereas Hole 896A is drilled into a footwall, only ~1km further south (Alt et al., 1996). The volcanic stratigraphy of these holes is compared to the volcanic stratigraphy of the SSOC, represented by the Master profile of Grimelia, as well as Profile 1 in the Våganes-area only 1.5 km further west (Profile 1, Erga, 2021).

Hole 504B penetrates a 571 m volcanic section and consists predominantly of pillow lavas (47%), alternating with massive sheet flows and volcanic breccia (Fig. 8.3). Detailed measurement of the drill core reveals that 6% of volcanic breccia appears in the upper parts, whereas 19% emerges within the lower section. Hole 896A penetrates a 290 m volcanic section, where the volcanic stratigraphy comprises 51.4% pillow lava, 40% massive flows as well as 8.6% volcanic breccia (Alt et al., 1996). The alternation between the different components is relatively great in both of these profiles. Profile 1 from the Våganes-area penetrated a 730 m volcanic sequence and consists predominantly of volcaniclastic rocks (Fig.8.3). Slightly above the middle of the profile massive sheet flows and in situ volcanic breccia occur, and pillow lavas towards top. In this profile, the alternation between the different components occurs frequently for the last 300 m (Erga, 2021).

The above-mentioned profiles, compared to the Master profile of Grimelia, provides less than half of the thickness of the Master profile. The distance between the profiles from SSOC is approx. 1.5 km, and ca. 1 km respectively between the profiles from the Costa Rica Rift (Fig.8.3). This illustration (Fig. 8.3) exhibits that the appearance of the different components varies greatly in the last part of Profile 1, and to a lesser extent in the other profiles. However, detail profiles 1-13 (Figs. 3.4 - 3.22) from the Master profile shows in situ different variations within the different sequences. This indicates that the alternation between the different components in the SSOC occurs more frequently, compared to the section of the Costa Rica

Rift, which can be explained by 1) difficulties distinguishing between the different lithologies in both areas, and 2) formation conditions were different. Characteristic to all profiles is that they have major lithology changes within short distance, which also is the case for the profiles provided by Furnes et al. (2003) (Figs. 5.1 and 5.2).

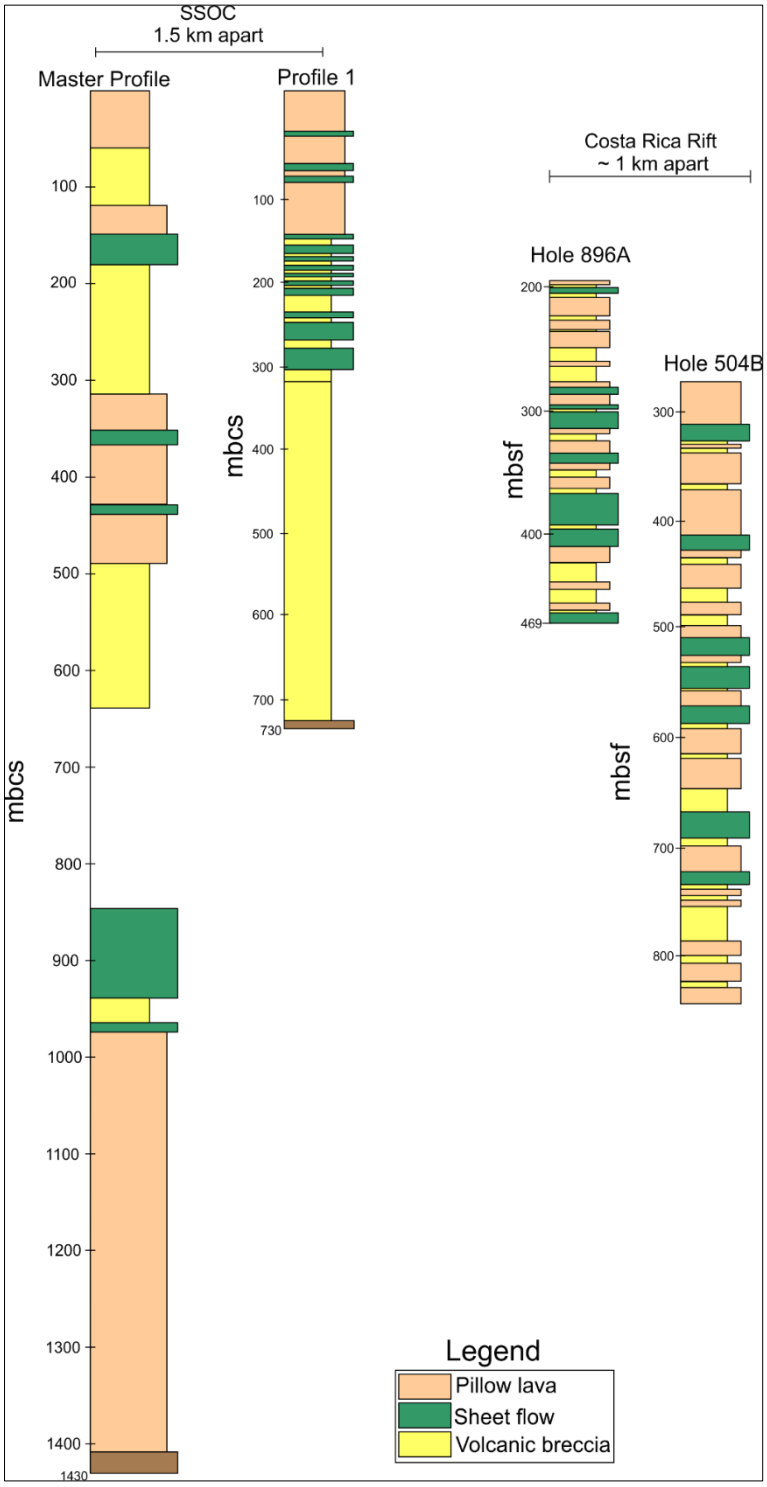

Fig.8.3: Representing stratigraphic varieties in the volcanic sequence through simplified profiles from the SSOC and the Costa Rica Rift. Profile 1 from Erga (2021), Hole 896A and Hole 504B from Alt et al. (1996). Mbsf: meter below sea floor, mbcs: meters below cover sediment.

8.5 Evolution of the SSOC's volcanic sequence in Grimelia

The evolution of the magmatic sequence of Grimelia represents repeated volcanic stages of different development, and which can be summarized in Fig. 8.4. First, the registered and not further discussed sheeted dike complex, representing feeders to the volcanic sequence, occurs as a psuedostrategraphic magmatic unit below the volcanic sequence. The lowermost part of the Master profile, part 1 A&B (Fig. 3.2), representing mineralized zones, is developed at the magmatic spreading center with ocean-floor hydrothermal activity (Fig. 8.4 A). As stated in chapter 6, the formation of VMS deposits depends on several factors. The deposits in the volcanic sequence of Grimelia is suggested to be bounded by a major fault, and related to different upflow zones, which in turn is depending on spreading rate, and physical- and chemical conditions. Note that the reconstructed part 1B is slightly inaccurate, and only illustrative for the proposed model. Further, the formation of volcaniclastic rocks as part of the volcanic breccias, can be related to their locations near fault slopes (Fig. 8.4 B). Volcaniclastic rocks are related to a post-eruptional disintegration resulting in proximal talus deposits and distal bedded finer-grained material (Furnes et al., 2003).

The different lava components appearing in the volcanic sequence are classified by their morphology and are controlled by several factors. One of the factors involves a four-stage lava flow propagation model, presented by Carracedo Sánchez et al. (2012). This is a model for submarine basaltic lavas that accounts for the development of sheet flow, in- situ volcanic breccias and pillow lavas along the same flow. The two last stages are presented in Fig. 8.4 C, representing a section of sheet flows and volcanic breccias, transition zone of all three components, as well as a pillow section at the end. However, conditions such as 1) rate of cooling, 2) topography of the substrate, 3) viscosity, and 4) effusion rate, are also important for the development of the different components.

The volcanic sequence of Grimelia with a thickness of 1430 m, has the longest registered profile compared to the profiles of a modern oceanic crust. This is not necessarily realistic when proposing that the sequence is developed at the magmatic spreading center, with ocean-floor hydrothermal activity, in an oceanic crust with intermediate spreading rate.

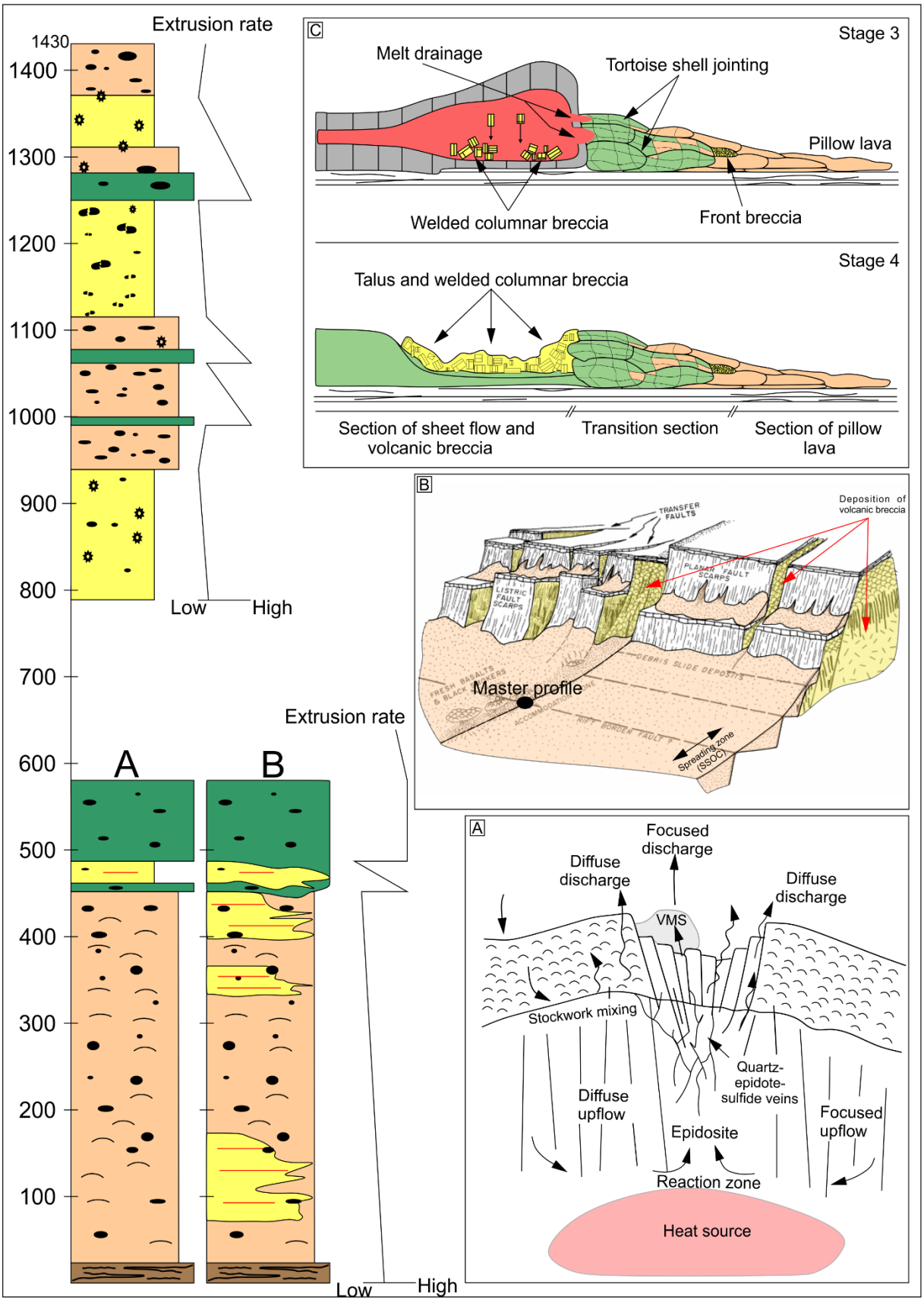

Fig.8.4: A reconstructed profile showing the evolution of the volcanic sequence of Grimelia, with both versions A and B from part 1 of the profile. A: a general model representing the hydrothermal evolution of the volcanic sequence in Grimelia. Modified from Alt (1995) (see Fig. 6.2). B: Development of volcanic breccias and volcaniclastic rocks (see Fig. 4.10.). Modified from Karson and Rona (1990). C: Formation of pillow lava, sheet flows and volcanic breccias (see Fig. 4.2). Modified and based on Carracedo Sánchez et al. (2012) and Erga (2021) respectively.

Chapter 9 – Geochemical investigation

The geochemical investigation is intended to reflect the geochemical signatures of the metabasalts in Grimelia (Appendix 4) and will be compared with previous work in the area defined by the SSOC (e.g., Furnes et al., 2000; 2003; 2006; 2012; 2020; Erga, 2021). Detailed evolutionary models, that can be correlated with the tectonic evolution of the SSOC, are previously presented from the above-mentioned studies, as well as studies related to ophiolites elsewhere and in general, published by Dilek and Furnes (2009; 2011; 2014), Furnes and Dilek (2017), and Furnes and Safonova (2019). Hence, the aim of this chapter is to predict if the geochemical signatures of the metabasalts in Grimelia support the earlier proposed tectonic evolutionary models of the SSOC.

The first presented diagrams are intended to predict the magmatic character of the samples, by distinguishing between subalkaline and alkaline basalt, and further between tholeiitic and calc-alkaline character, based on immobile elements (Fig. 9.1). Furthermore, the fractionating mineral assemblage is reflected from Bowen diagrams from several different elements (Fig.9.2). The samples are further plotted with respect to chondrite-normalized REE and N-MORB normalized elements, demonstrating element behavior in terms of enrichment or depletion (Fig. 9.4). Stratigraphic variation in the geochemistry is also presented (Figs. 9.7 and 9.8), followed by a petrological history. The tectonic evolution of the metabasalts in Grimelia is then presented, based on the results from the discrimination diagrams (Figs. 9.9 and 9.10), indicating the magmatic evolution.

9.1 Analytical procedures

The purpose of this subchapter is to provide an account of the fieldwork and sample collection, the various analytical techniques applied, and to the final geochemical results.

9.1.1 Fieldwork and sampling

In total 44 samples were collected by using hammer and chisel, during two field seasons in the period of 2020-2021. The first field season was conducted from June to July 2020, with a duration of 9 days, and 18 samples were collected. The last field season had a duration of 10 days from April to June 2021, where 24 samples were collected. In total 40 samples were analyzed, and 13 thin sections made. Predominantly, the samples are collected from part 1 of the Master profile (Fig. 3.2), whereas four samples represent the metabasalts from part 2 of

the profile. The samples are concentrated to part 1 of the Master profile, due major lithological varieties in this area.

9.1.2 Sample preparations and analytical techniques

Sample preparations

A diamond saw located at UiB is used to preparate the samples in respect of removing the weathering skin and divide the material into smaller pieces. Some of the pieces is further used to make thin sections, whereas the rest of the material is crushed with a hammer down to the size of 2 mm. To avoid contamination with the hammer and the underlaying metal plate, thick plastic bags are used when crushing. In total, approx. 10-15 ml of the 2 mm material is milled to powdered material by using a planetary ball mill (PM100). Further, ca. 2 g of the powdered samples, is heated in a furnace (1000°C) for 2 hours, due to removal of volatiles and potential organic material. The loss on ignition (LOI) for all samples is subsequently calculated, representing the percentage of removed material.

The last step of sample preparations involves the conversion of the powdered rock samples into glassy beads for XRF-analysis (X-ray fluorescence spectrometer). In order to achieve this, 0.96 g of the rock powder is mixed with 6.72 g of dried flux (lithium tetraborate, $Li_2B_4O_7$). The mixed material is placed in a Claisse-Fluxy instrument (furnace) for about 30 minutes with a temperature of 1000°C, while rotating the sample, to make the glass beads.

ICP-MS and ICP-AS

The prepared glass beads were supposed to be analyzed by a S4 PIONER XRF, but the instrument at UiB is currently out of order. The analysis was supposed to account for the concentration of the major elements Al, Ca, Fe, K, Mg, Na, Mn, P, Si and Ti. Instead, these major elements, except Si, are measured by using a Thermo Scientific ICap 7600 ICP-AS. The total sum of the concentration of the major elements will be 100. Si is therefore calculated by adding all the major elements, and further subtracted with 100.

The concentration of the trace elements e.g., Cs, Th, Ta, Nb, Pb, Zr, Y, Ti etc., including Rare Earth Elements (REE), are measured by a Thermo Scientific Element XR High-Resolution ICP-MS (HR-ICP-MS).

Both procedures involve the same approach. Prior to the instrumental analysis the samples are diluted to an appropriate level by 2 % w/v HNO_3. Quantification is done by external

calibration curves, a multi element standard solution prepared for certified single element solutions from Spectrapure. The concentration of trace elements is internal standardized by In, whereas the concentration of major elements is internal standardized by Sc. A quality control is done by USGS CRM BCR2 (Basalt, Columbia River) (Appendix 4). During the analytical run, the synthetic water CRM SPS-SW-2 (Spectrapure Standards AS) is analyzed repeatedly. This provides a direct control of the calibration curves and the monitoring of the performance.

Corrections for Zr

Prior to the different conducted analysis, the prepared samples were stored for a longer period of time, due to instrumental problems at UiB. As the powdered samples are mixed with a salty matrix (lithium tetraborate flux), the determination of Zr concentrations may give somewhat unreliable results (Pechishcheva et al., 2018), due to precipitation of Zr. As a result of this, the given Zr values were incorrect and first noticed with strongly negative anomalies in the N-MORB normalized multi-element diagram (Chapter 9.2.4), where the curve is expected to be relatively flat between Nd and Sm. Corrections for Zr have, hence, been necessary to conduct. This is done manually by getting the Zr value on the same line as Nd and Sm. Furthermore, the Zr values are denormalized with respect to N-MORB normalization values from Sun and McDonough (1989), and further used in the thesis (Appendix 4, Table 4.1.3).

9.2 Geochemical characteristics of basaltic rocks from the SSOC

9.2.1 Element mobility

Through various studies of alteration and metamorphism of basaltic rocks, it has been established that some elements are relatively immobile, whereas others are variably depleted or enriched relative to their original concentration. Whether an element is mobile or not, is controlled by the extent of water-rock interactions during reactions (Kelly and Delaney, 1987; Bickle and Teagle, 1992; Furnes et al., 2006). Other controlling factors of the alteration and metamorphism circulates through the upper crust, controlled by the composition and stability of mineral phases, volume of fluid phases, and temperatures (Furnes et al., 2020). Through experimental studies of the relation between basalt and seawater, it is demonstrated minor leaching of Fe and Si, enrichment of Na and Mg, varying Ca depletion, and that Al, Ti and P are the least mobile major elements (Scott and Hajash, 1976; Seyfried et al., 1978; Furnes et al., 2006). During alteration it is acknowledged that Ti, V, Y, Zr, Nb, REE (particularly HREE), and

Th are relatively immobile (e.g., Humphris and Thompson, 1978; Seyfried et al., 1988; Hofmann and Wilson, 2007; Furnes et al., 2020). To avoid unreliable results, a combination of major and trace elements is used for this petrogenetic analysis, as well as the mentioned immobile elements. The distinction between subduction-related and subduction-unrelated character is determined by the most critical element thorium (Th) (Furnes et al., 2020). In this case, subduction influence of the SSOC can be indicated by weak to moderate enrichments of Cs, Pb, and Th in its geochemical fingerprints (Furnes et al., 2012).

9.2.2 Magmatic character

To distinguish between alkaline, tholeiitic, and calc-alkaline magmatic series, a total iron-magnesium (AFM) (Irvine and Baragar, 1971) and total alkali-silica (TAS) diagram (Le Maitre, 1989) is used. As all the metabasaltic samples presented in this thesis are altered and metamorphosed, a classification based on the major elements including Na, K, and Mg, may give unreliable result. Therefore, the relative immobile elements Ti, Zr, Y, Nb, Th and Yb, is used to examine the magmatic character (Furnes et al., 2020).

Starting by plotting the data in the Nb/Y-Zr/Ti diagram of Winchester and Floyd (1977), this first step distinguishes between subalkaline and alkaline basalt, and all the samples plot on the boundary between subalkaline basalts and basaltic andesite (Fig. 9.1 A). Further, all the subalkaline basalts are isolated and potted in the Zr/Y-Th/Yb discrimination diagram of Ross and Bedard (2009) (Fig. 9.1 A_1-C_1), to distinguish between calc-alkaline and tholeiite character.

In the Nb/Y-Zr/Ti, all samples plot within a narrow areas within the field of subalkaline basalt, straddling the boundary to basaltic andesite. One sample from the volcanic breccia, however, plots within the subalkaline basalt alone. This sample have a Zr/Ti ratio of 0.009, whereas the other ratios range from 0.010 to 0.013. The samples with the lowest Zr/Ti ratios, approx. 0.010 (mainly pillow lavas and one volcanic breccia), plots slightly outside from the rest (Fig. 9.1 A). In the Zr/Y-Th/Yb diagram, all samples plot within the tholeiite section with a narrow field, except for one pillow with a Zr/Y ratio of 0.010, and one volcanic breccia with a ratio of 0.05, whereas the other ratios range from 0.017 to 0.036.

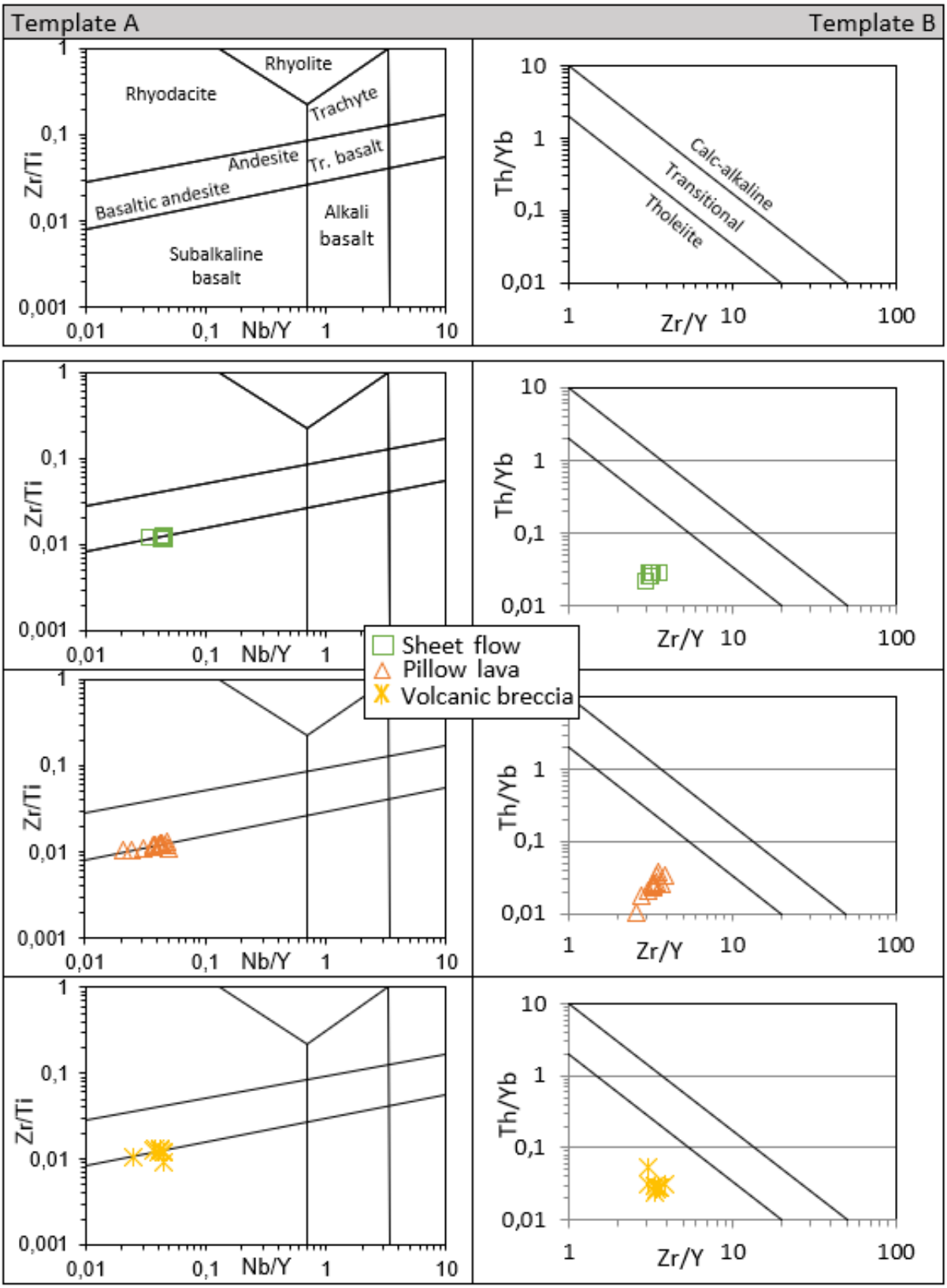

Fig.9.1: A, B, C: Nb/Y-Zr/Ti diagram distinguishing between subalkaline and alkaline basalts. Modified from Winchester and Floyd, 1977. A1, B1, C1: Zr/Y-Th/Yb diagram distinguishing between calc-alkaline and tholeiitic character. Modified from Ross and Bedard, 2009.

9.2.3 Bowen diagrams and other element-element relationships

The Bowen diagrams (Fig. 9.2) show the relationship for MgO vs. SiO_2, TiO_2, Al_2O_3, Fe_2O_3, V, Cr, Zr and Y, demonstrating the variations in the magma composition. As stated in the previous subchapter, MgO may give somewhat unreliable concentration due to experienced alteration- and metamorphic processes of the sequence and should hence be interpreted with caution. However, the results may nevertheless provide useful information.

The metabasaltic samples presented in the Bowen diagrams define a MgO range of 5 to 9 (Fig.9.2) and display relatively scattered patterns for all components. Yet, the pillow lavas and sheet flows plot narrower than the volcanic breccias, which tend to display a larger spread than the rest. SiO_2 vs. MgO displays a clear negative correlation, whereas Al_2O_3, Fe_2O_3 and Cr reflects a clear positive correlation against MgO. TiO_2, V, Zr and Y display a slightly positive correlation vs. MgO. According to Furnes et al. (2003) the wide spread in the data strongly suggest modification by fractional crystallization, as well as different degrees of partial melting and mixing (Furnes et al., 2006), as will be further discussed below.

In Fig. 9.3 different plot is displayed to determine whether fractional crystallization has been the only magma-modifying process or not. The relation between the presented diagrams is intended to reflect that factional crystallization alone cannot explain the compositional variations. The first two presented diagrams (Fig. 9.3 A-B) represented by Zr - Y and Zr - TiO_2 respectively, reflects that Zr shows strong positive correlations with Y and TiO_2. Further, the relation between Zr - TiO_2 (Fig. 9.3 B) reflects fractionation of Fe-Ti oxides (Zr = 225 ppm, TiO_2 = 3.3 wt.%). The Cr - Zr, and Ni - Zr diagrams displays a relatively strong negative correlation (Fig. 9.3 C-D). It is, however, poor correlation between those two diagrams and their trace elements. If fractional crystallization were the only magma-modifying process, it can be expected that the Cr - Zr and Ni – Zr diagrams would show a hyperbolic trend as well. However, the poor correlation between the diagrams indicates that fractional crystallization alone cannot explain the compositional variations. According to Furnes et al. (2006) magma mixing can account for much of the scatter seen in the two last mentioned diagrams.

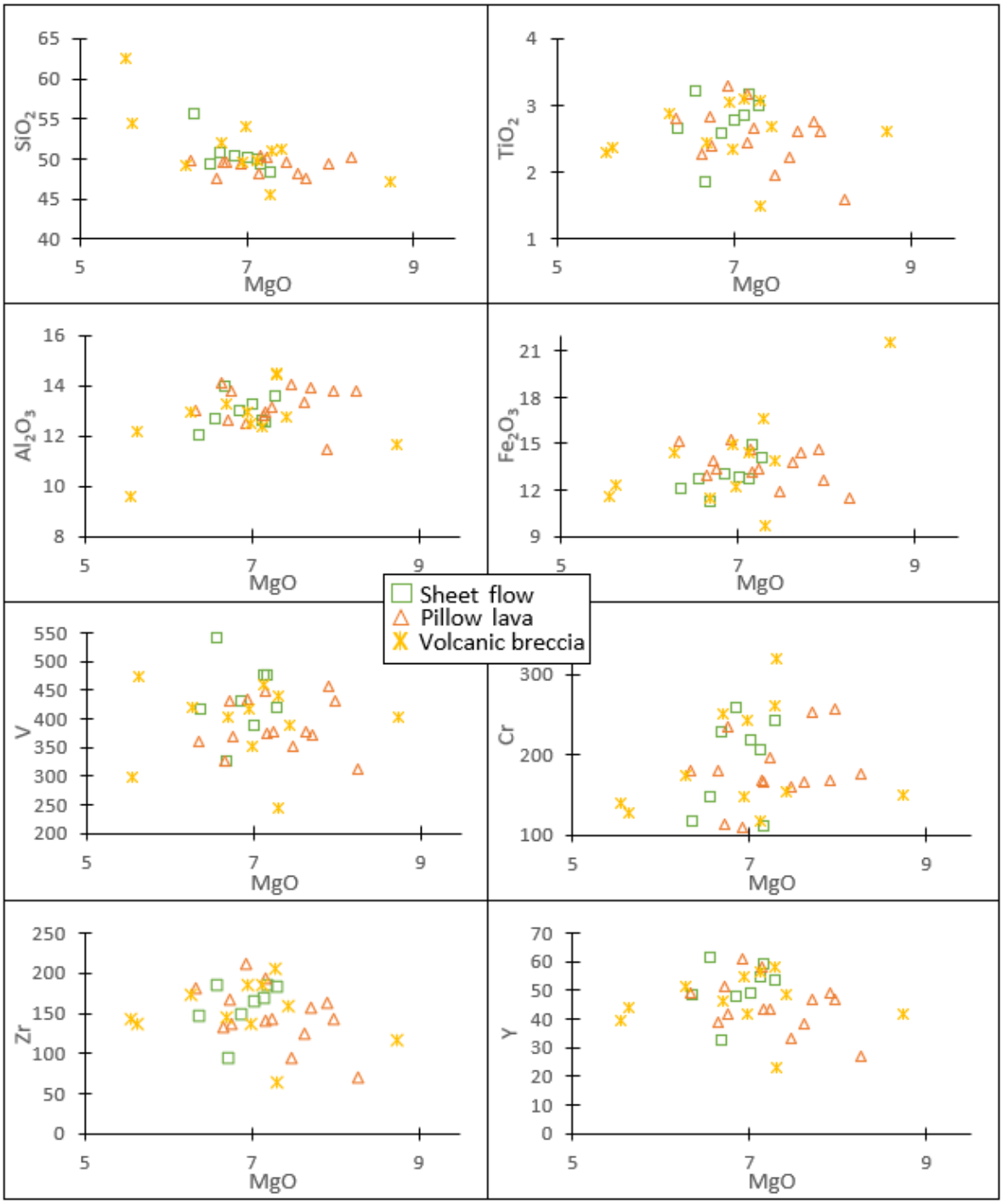

Fig.9.2: Bowens diagrams represented by MgO vs. SiO_2, TiO_2, Al_2O_3, Fe_2O_3, V, Cr, Zr and Y, showing the geochemical evolution of the different components in a minor area of the SSOC. Trace elements are measured in ppm, whereas major elements in wt.%.

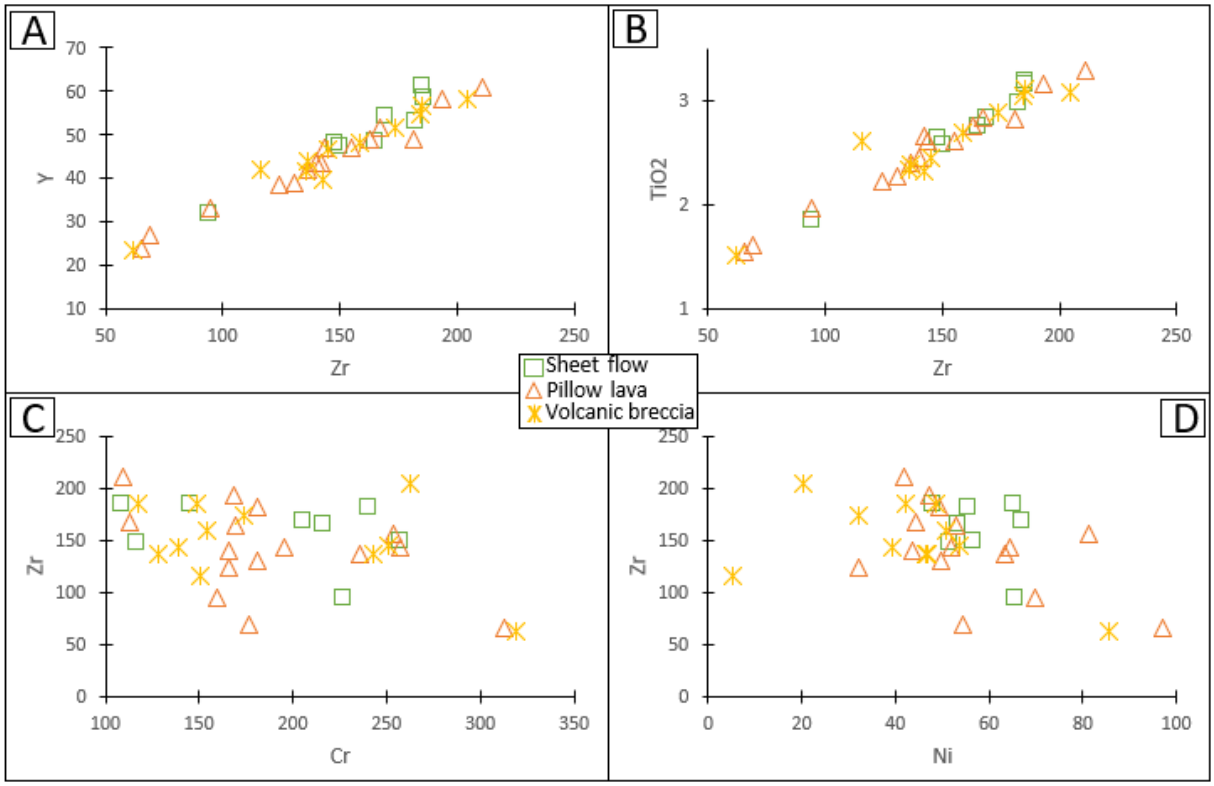

Fig.9.3: A: Zr vs. Y. B: Zr vs. TiO_2. C: Cr vs. Zr. D: Ni vs. Zr. Trace elements are measured in ppm, whereas major elements in wt.%.

9.2.4 Multi-element character of the metabasalt in Grimelia

Rock/Chondrite

REE patterns is normalized to chondrite for all three components (sheet flow, pillow lava, and volcanic breccia) and illustrated in Fig. 9.4 A-C, with normalization values from Sun and McDonough (1989). All samples exhibit a progressive depletion in LREEs from La through Sm, and generally a slightly convex to flat pattern from this point through Lu. Most samples have either a slight positive or negative anomaly for Eu. For the sheet flows seven out of eight samples display negative anomalies (depletion) for Eu (Fig. 9.4 A), and one sample with a positive anomaly (enrichment). For pillow lavas three of the samples reflects a positive anomaly for Eu, ten samples display a negative anomaly, whereas two of the samples do not show any increase nor decrease of Eu. The majority of the volcanic breccias reflects a negative or slightly negative Eu anomaly, where only three of the samples show no signs of Eu-depletion with either a positive anomaly or a flat curve for Eu. The majority of the samples also reflects a tiny enrichment in Lu.

Rock/N- MORB

N-MORB- normalized multi-element diagrams are displayed in Fig. 9.4 A_1-C_1, and the normalized values are from Sun and McDonough (1989). Characteristic for all samples is a strong enrichment in Pb, as well as relative strong depletion in Ta, and Nb. One of the samples from the pillow lavas and one from the volcanic breccias, reflects a strong depletion in Th, whereas the rest is in line with La. The sheet flows and pillow lavas display a more consistent pattern than the volcanic breccia. However, the pattern of the volcanic breccias is quite consistent, except for one sample that has a relatively strong depletion in Eu. This differs from the rest of the samples, that is characterized by slightly negative or positive anomalies for Eu, or a flat curve.

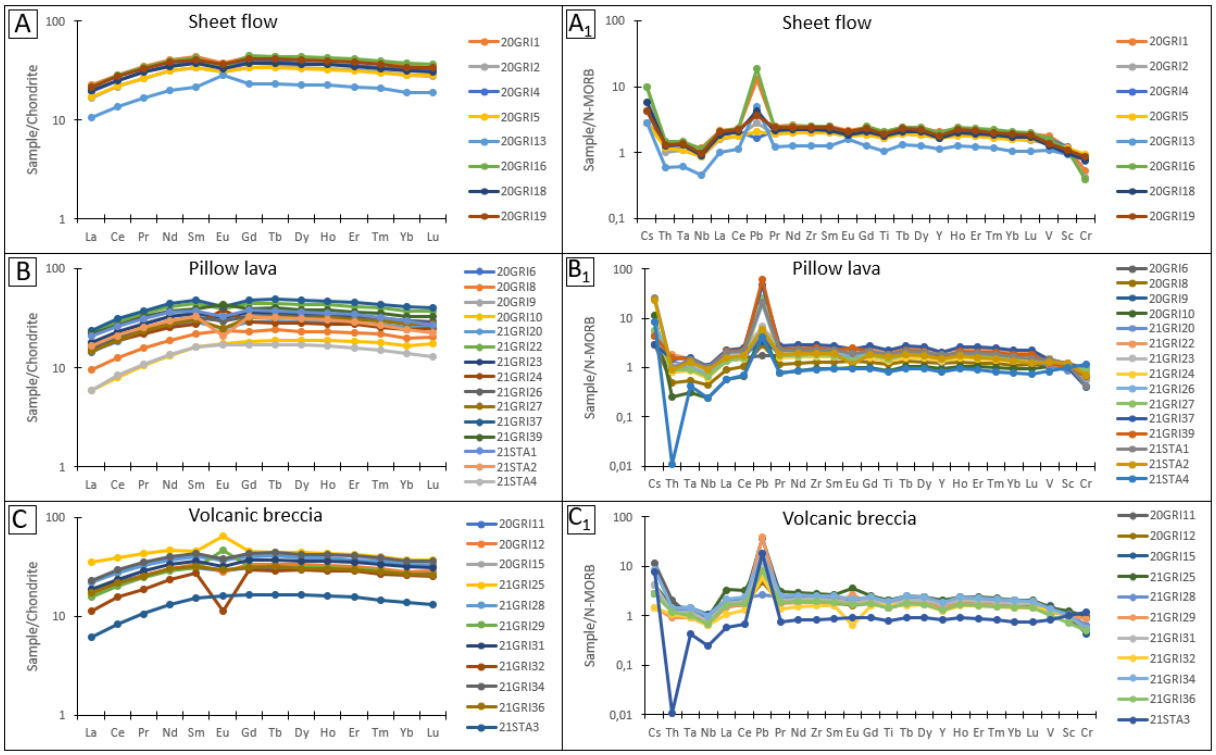

Fig.9.4: A, B, C: Chondrite normalized REE plots of sheet flows (A), pillow lavas (B), and volcanic breccias (C). Normalized values from Sun and McDonough (1989). A_1, B_1, C_1: N-MORB normalized multi-element diagram of sheet flows (A_1), pillow lavas (B_1), and volcanic breccias (C_1). Normalized values from Sun and McDonough (1989).

9.2.5 Chemical stratigraphy

The Master profile with stratigraphic positions of the 34 representative samples of metabasalt, is presented in Fig. 9.5, and reflects some compatible (Cr, Ni) and incompatible elements (Zr, Y, TiO_2) plotted against the stratigraphic height. As a result of this, the geochemical changes during the volcanic evolution can be interpreted. These compatible and incompatible elements are taken as predominantly immobile during hydrothermal alteration

and metamorphism, thus giving the elements a covariation in the diagrams that is taken to represent the original trends. Zr and Y are averagely reflected by an upward decreasing trend, whereas Ni, and to some extent Cr, are represented by a generally upwardly increasing trend. However, both components alternate between increase and decrease, thus giving them a scattered appearance. TiO_2 reflects a slightly negative trend. According to Furnes et al. (2006) the various concentration of the different elements is to some limited extent controlled by melting processes.

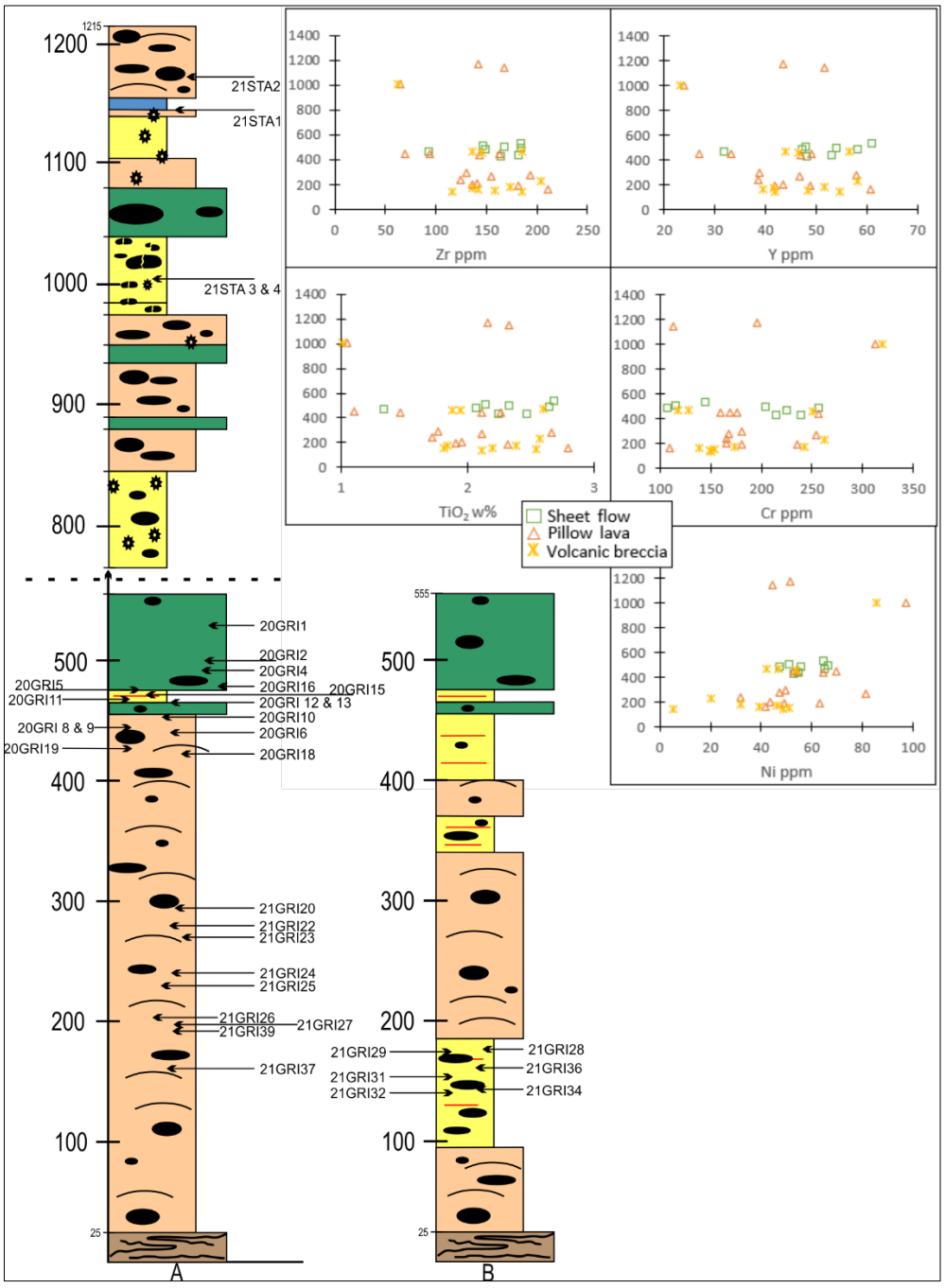

Fig.9.5: Zr, Y, TiO_2, Cr and Ni plotted against stratigraphic highest to predict the volcanic evolution in the Grimelid-area. The geochemical samples are mainly retrieved from the lower parts of the Master profile.

In Fig. 9.6 two different sections displaying Zr and Cr contents, plotted against stratigraphy, is presented. Fig. 9.6 A, mainly representing the upper part of the volcanic sequence, reflects a slightly upward decrease of Zr and increase of Cr from the samples 20GRI26;27, and 21STA1;2;4. Fig. 9.6 B, however, representing the lower part of the volcanic sequence, shows the opposite, with an increasing Zr and generally decreasing Cr trend. This example consists of samples 20GRI5;10;12;13;15;16 and is retrieved from/nearby detail profile 6 which is the best fit of a cyclic unit in the area. Both versions appear scattered, but the example from detail profile 6 (Fig. 9.6 B) has more of a saw-toot pattern than the other.

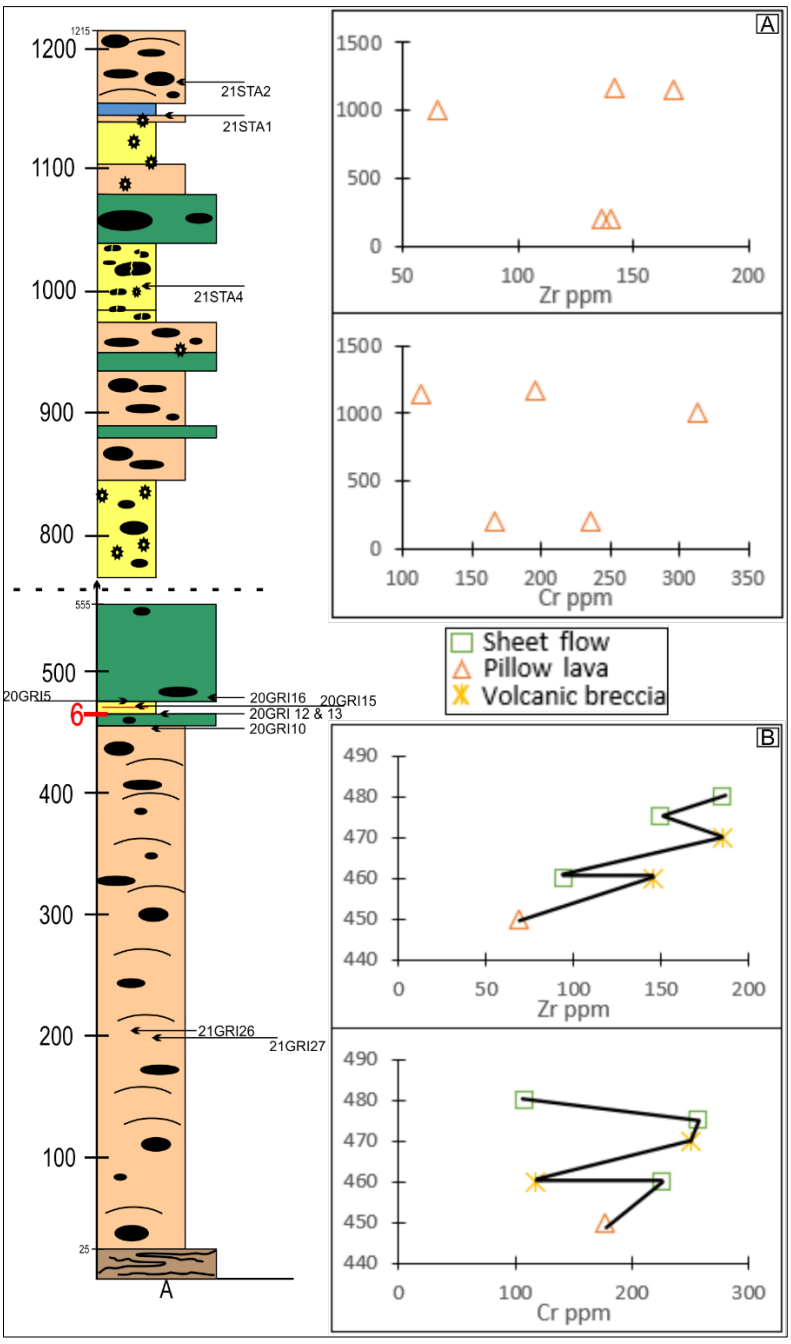

Fig.9.6: Zr and Cr plotted against stratigraphic heights, represented by A: pillow lavas of varying size and B: a cyclic unit from detail profile 6.

9.2.6 Petrogenesis

As stated above, the geochemical data of the 34 representative metabasalt samples are presented in various diagrams to predict the fractionating minerals during the magmatic evolution of the SSOC. The samples show good correlation between Zr-Y, Zr-TiO_2, Cr-Zr and Ni-Zr (Fig. 9.3), indicating that factional crystallization is the dominant magma-modifying process throughout the volcanic evolution, as previously proposed by Furnes et al. (2003; 2006).

The different trends of the various components presented in the Cr - Zr and Ni - Zr diagrams, however, may indicate that the components are differently affected by hydrothermal water circulations. From e.g., Fig. 9.3 C-D, the sheet flows plot narrower compared to the volcanic breccias and pillow lavas. This may be explained by more extensive water circulation in the volcanic breccia and pillow lava section, as these piles, especially the volcanic breccias, are more permeable compared to the sheet flows. As a result of extensive water circulation in these components, the pillow lavas appear with cavities, glass rinds around the pillows, and with inter-pillow hyaloclastites, whereas the volcanic breccias display variably degree of mineralization, which is differently affected by ocean-floor hydrothermal activity (Chapter 6).

Fig. 9.7 displays Cr plotted against Zr in a modeled hybridization-fractional crystallization diagram from Furnes et al. (2006). Their interpreted line is representing the degree of hybridization-fractional crystallization of the SSOC, where also the representative samples of metabasalt from Grimelia is plotted. The diagram reflects a scattered pattern of both sheet flows, pillow lavas, and volcanic breccias, where all the samples except four, plots along, or slightly to significantly above the line exhibiting different degrees of gabbro fractionation. The remaining four samples (three pillow lava and one volcanic breccia), plots below the fractionating line. The majority of the samples plot within the region of 40-50% gabbro fractionation, whereas the others plot within 20-40% or 50-60% fractionation. Some of the samples reflects gabbro fractionating slightly below 20%, and none higher than 60%. Two of the samples represents approximately 10% troctolite fractionation (21STA3;4) and is therefore the samples considered to be most influenced by the primary magma.

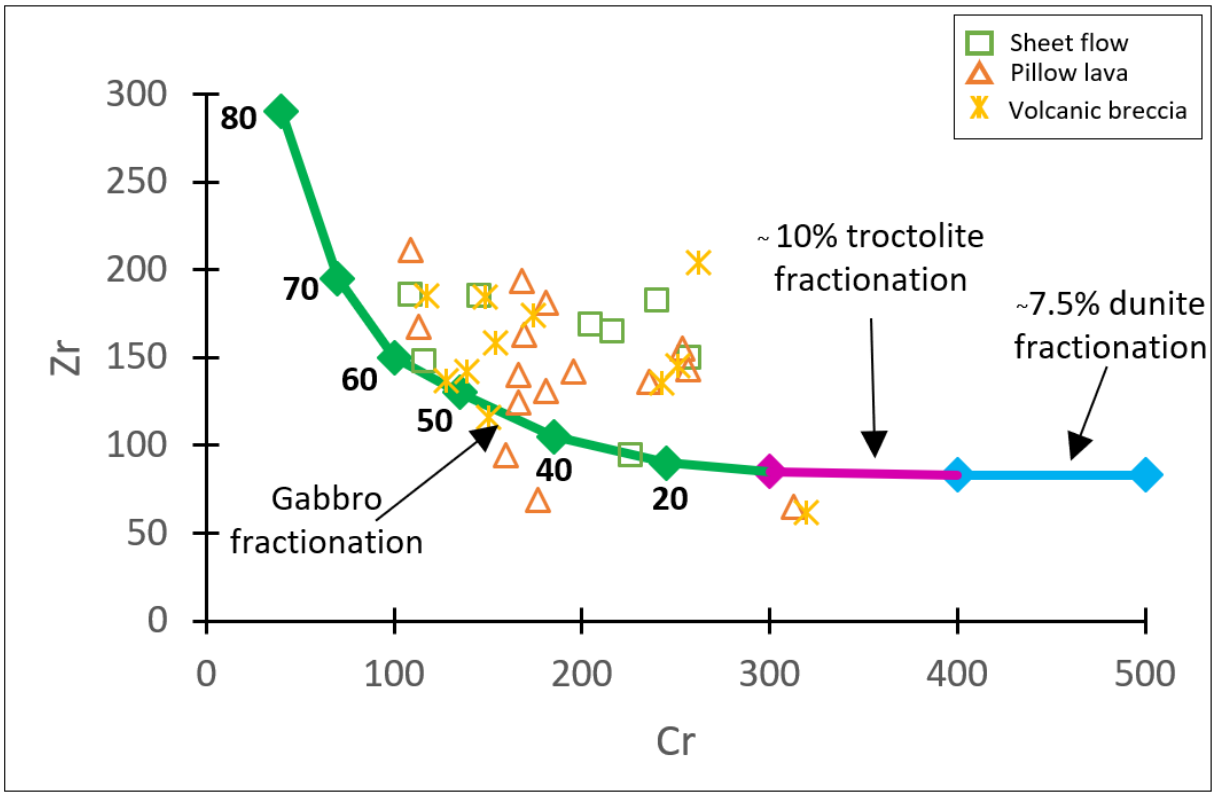

Fig.9.7: Modeled Cr-Zr concentrations compared to an interpreted hybridization-fractional crystallization line from Furnes et al. 2006. The percentage of fractionating is represented by the green/purple/blue line.

The majority of the chondrite normalized REE plots, as well as the N-MORB- normalized samples defining the multi-element diagrams (Fig. 9.4), show a weak to strongly negative anomaly for Eu, indicating fractionation (Furnes et al., 2012). A positive Eu anomaly suggests accumulation of plagioclase in the magma, whereas a negative anomaly for Eu will indicate depletion of plagioclase (Furnes and Dilek, 2017). The diagrams also strongly exhibit enrichments of Pb and Cs (Fig. 9.4 A_1-C_1), and depletion in i.e., Ta and Nb, which is characteristic features for backarc basin ophiolitic crust with subduction influence (Pearce and Stern, 2006).

A study conducted by Furnes et al. (2006) reflects five types of covariations for Zr- and Cr increase/decrease. The different types of covariations reflect 1) Zr increase, Cr decrease, 2) Zr decrease, Cr increase, 3) Zr and Cr increase, 4) Zr and Cr decrease, and 5) almost constant Zr and Cr (Furnes et al., 2006). Displayed in Fig. 9.6, covariation type 1 and type 2 are reflected at different stratigraphic heights of the Master profile. However, Fig. 9.8 indicates that type 2 is the dominant covariation of the samples in Grimelia on an average basis. Type 2 covariation is a result from mixing of an evolved magma resident in a chamber with large increments of less differentiated magma (Furnes et al., 2006). Although the second type is the dominant

type of covariations of the samples in Grimelia, all of the above-mentioned types are present. The other types are represented by 1) successive small additions of a less evolved magma to a resident magma, 3) and 4) repeated mixing of resident magma with batches of primary Cr-rich magma, followed by fractional crystallization after each mixing event, and 5) eruptions of batches of magma in rapid succession from a magma chamber that contained magma from fractional crystallization of magma mixing (Furnes et al., 2006).

The different diagrams presented in Figs.9.4, 9.6, and 9.8, exhibits the petrological history of the SSOC in Grimelia, and indicates differences in the magma-modifying process. The process in Grimelia is predominantly controlled by fractional crystallization for all the components, based on various Zr, Cr, and Ni concentrations. All samples from the multielement diagram (Fig. 9.4 A_1-C_1), display negative Nb anomalies, as well as positive Pb anomalies. Together with a large range from MORB-normalized Cr-values (from 0.3-1.1.6), and high Cs and Th values, a suggestion that the majority of the samples are moderately to strongly fractionated, is made (Furnes et al., 2012). However, the Zr-Cr covariations presented in Fig. 9.8, also suggest a mixing of an evolved magma as the general process (Furnes et al., 2006).

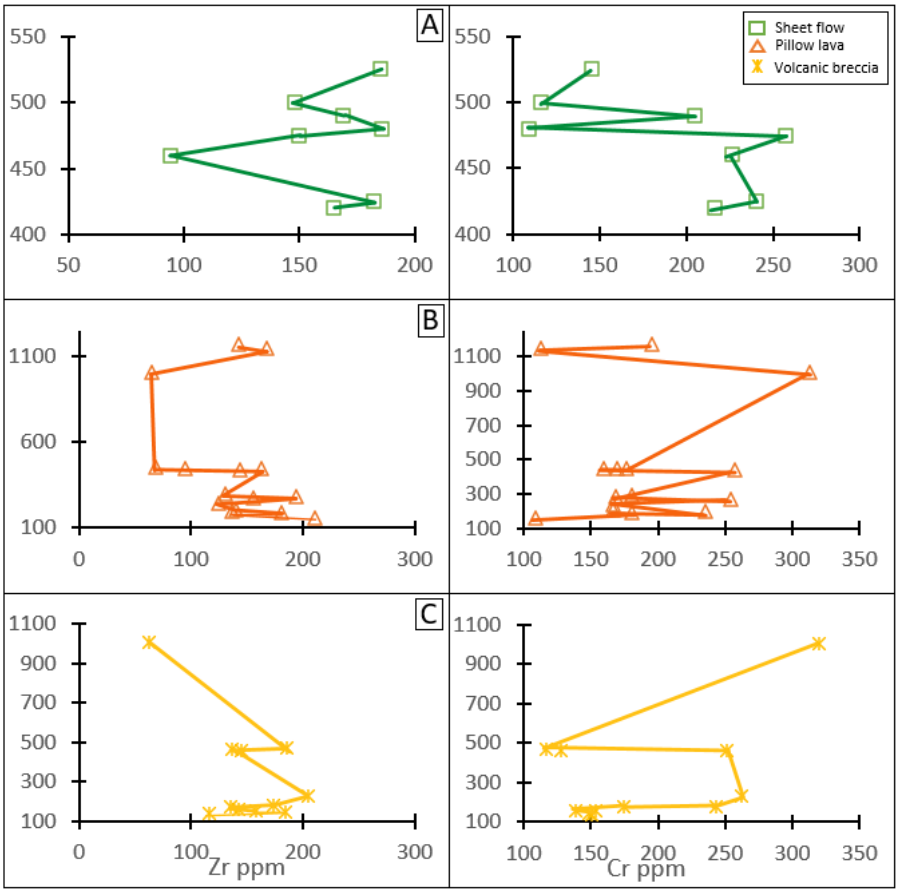

Fig.9.8: Zr and Cr plotted against stratigraphic heights for all the 34 different samples, divided in sheet flows, pillow lavas and volcanic breccias.

9.2.7 Discrimination diagrams

Classification of ophiolites can be predicted based on their lithological, geochemical, and structural features (Dilek and Furnes, 2011; 2014; Kusky et al., 2011; 2013; Pearce, 2014; Furnes and Dilek, 2017), and used to identify whether the metabasaltic samples of the SSOC in Grimelia is subduction-related or subduction-unrelated. In order to provide evidence for this, multiple diagrams are presented based on a combination of specific elements, such as Th, Yb, Nb, TiO2, and MORB-normalizes values for Th and Nb.

Fig. 9.9 displays two different types of discrimination diagrams, based on the study of Pearce (2008; 2014), where the elements Th, Yb, Nb, TiO_2, used in various combinations. The diagram that refers to template A (Nb/Yb - Th/Yb) is intended to distinguish between subduction-related and subduction-unrelated ophiolite, whereas template B (Nb/Yb - TiO_2/Yb) is used to separate the origin of the basalt by distinguishing between shallow depth melting (MORB array) and deep melting origin (OIB array). All samples from the different components plots within a narrow zone in the mantle array, close to the subduction-related boundary (Fig. 9.9 A). However, one sample from the pillow lavas is located on the x-axis, and one sample from the volcanic breccias crosses the mantle array and plots slightly within the suprasubduction zone (SSZ) (20GRI10;11 respectively, Fig. 9.5 for location). These two samples are located nearby the biggest ore-deposits in Grimelia and has slightly lower (pillow lava) and higher (volcanic breccia) Nb/Yb - Th/Yb values than the rest. All samples are slightly more depleted than the average N-MORB.

Furthermore, the samples are plotted in the TiO_2/Yb - Nb/Yb diagram, as the ratios functions as a good depth-indicator of the mantle melting (Pearce, 2014; Furnes et al., 2020). All samples plotted in the Nb/Yb - TiO_2/Yb diagram (Fig. 9.9 B), clearly define a N-MORB character with shallow-depth melting. The majority of the samples straddle the boundary of the dotted line, whereas two samples of both pillow lavas and volcanic breccias crosses the line.

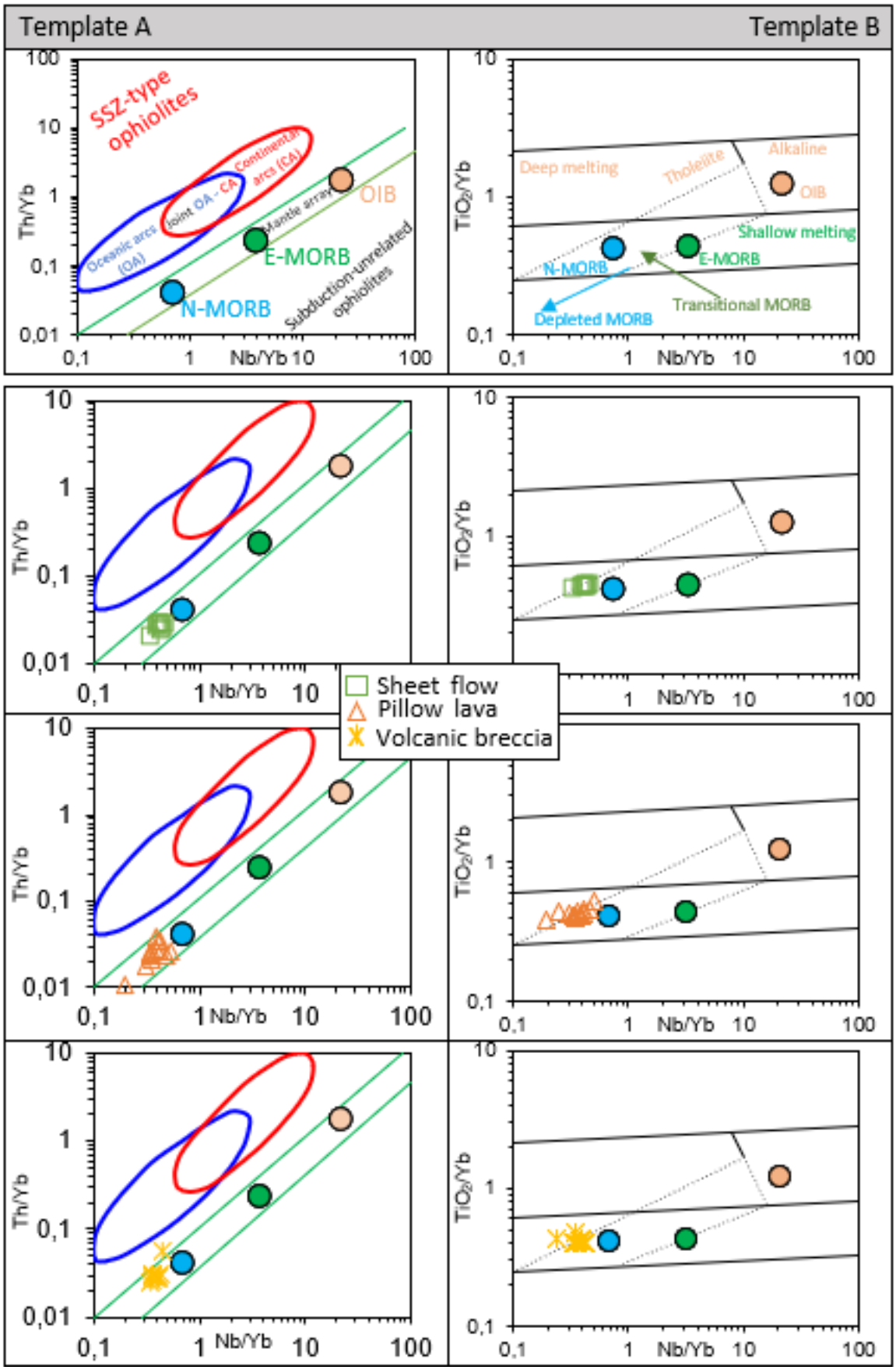

Fig.9.9: Discrimination diagrams from Pearce (2008;2014) with Nb/Yb vs. Th/Yb in template A (Pearce, 2008), and Nb/Yb vs. TiO_2/Yb in template B (Pearce, 2014). Template A distinguishes between subduction-related and subduction-unrelated ophiolites, whereas template B separates the origins of the basalt.

In a simplified discrimination diagram from Saccani (2015) (Fig. 9.10), MORB-normalized values for Th and Nb from Sun and McDonough (1989) are used. The diagram distinguishes basalts generated in oceanics, subduction-unrelated settings, rifted margins, and ocean-continent transition zones from subduction-related basalts, with a misclassification rate of <1% (Saccani, 2015). The metabasaltic samples of the SSOC in Grimelia plots within the boundaries of MORB and a backarc basin, that demonstrates the dominance of a subduction-unrelated character. However, previously presented diagrams indicate minor subduction influence of the metabasalts in Grimelia. Furthermore, two of the pillow lava samples, and one sheet flow sample, reflects more depletion than the rest.

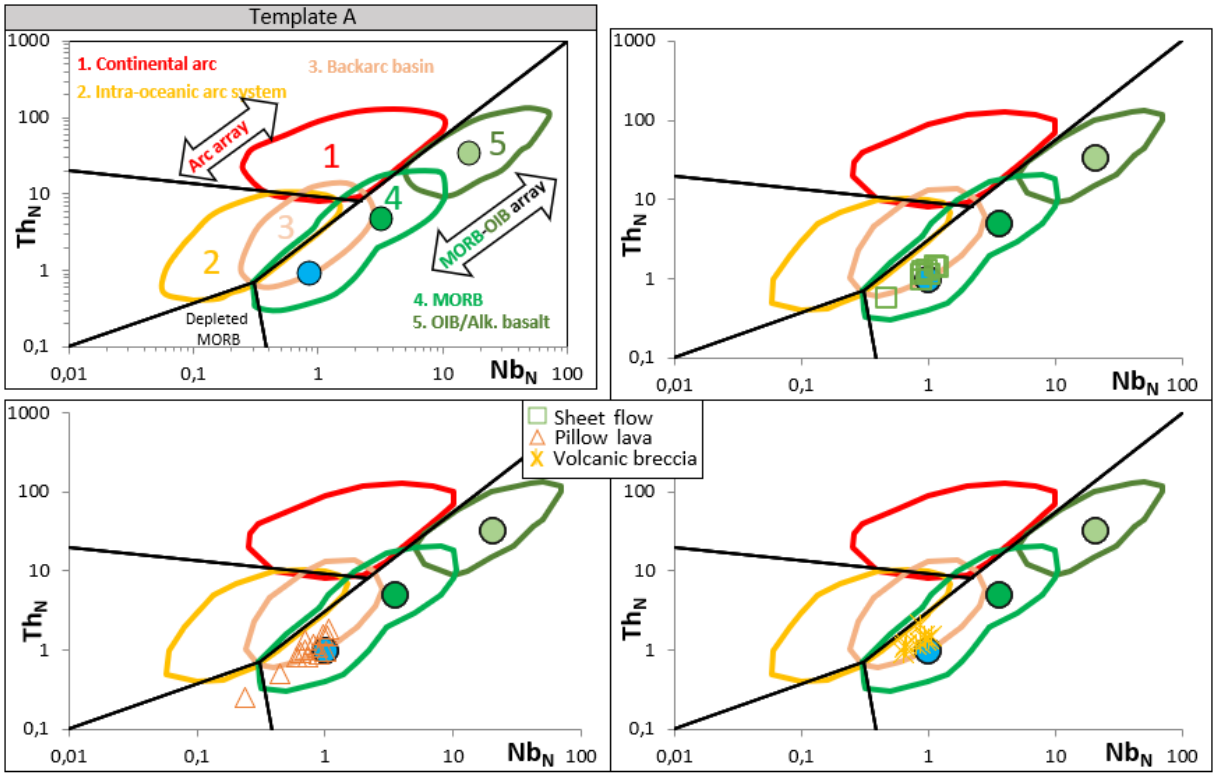

Fig.9.10: Simplified discrimination diagram from Saccani (2015), with normalized N-MORB values from Sun and McDonough (1989).

Subducted material returns to the Earth's surface through arc volcanisms, where magmatism is induced by the addition of fluids to the mantle wedge from devolatilization or melting of the subducted slab (Spandler and Pirard, 2013; Pi et al., 2016). During mantle melting, Th and Nb are highly incompatible elements with an almost-constant ratio. In most arc systems, Th will behave subduction-mobile and enriched during partial melting, whereas Nb will be subduction-immobile and depleted during partial melting (Pearce and Stern, 2006; Pearce, 2014). Due to this, the above-mentioned elements are used as a proxy for subduction/crustal

input. Ta behaves in similar ways as Nb, which leads to the fact that Th/Ta and Th/Nb are equivalent for this purpose (Pearce, 2014). However, Nb is used for this study due significantly lower concentrations than Nb, which hence gives a greater analytical uncertainty.

9.3 Tectonic evolution

Several studies of the tectonic evolution of the Solund-Stavfjord Ophiolite Complex have been conducted and discussed throughout time (e.g., Pedersen et al., 1992; Furnes et al., 2000;2003;2006;2012), where the most recent study proposes a weak subduction influence of the SSOC and an evolution adjacent to the Laurentian continental margin (Furnes et al., 2012) (Fig. 9.11). Due to several studies displaying interfingering of continentally derived sedimentary rocks (phyllite and graywacke) in the uppermost volcanic rocks of the SSOC, it has been proposed that the SSOC basin evolved adjacent to a continental margin (Furnes et al., 2003; 2006; 2012), which also is the case for the volcanic sequence in Grimelia. A study from Furnes et al. (1990) shows incompatible trace element compositions that are enriched due to smaller degree of partial melting of a less-depleted source, giving a weak subduction signal in the multi-element diagram (Pb, Th, and Cs enrichments, Nb depletion). It is therefore proposed that the metabasalts of the SSOC was formed from magmas that were produced in a trench-distal suprasubduction-zone (SSZ) setting. However, the setting was sufficiently far from the subducting slab and therefor only minor influence of slab-derived fluids in their melt evolution is registered (Furnes er al., 2012) (Fig. 9.11). Multi-element diagrams of the metabasalts in the Grimelia area (this study), including the results from the Våganes-area (Erga, 2021), also reflects a minor subduction influence, supporting the suggestion of an evolvement sufficiently far from the subducting slab.

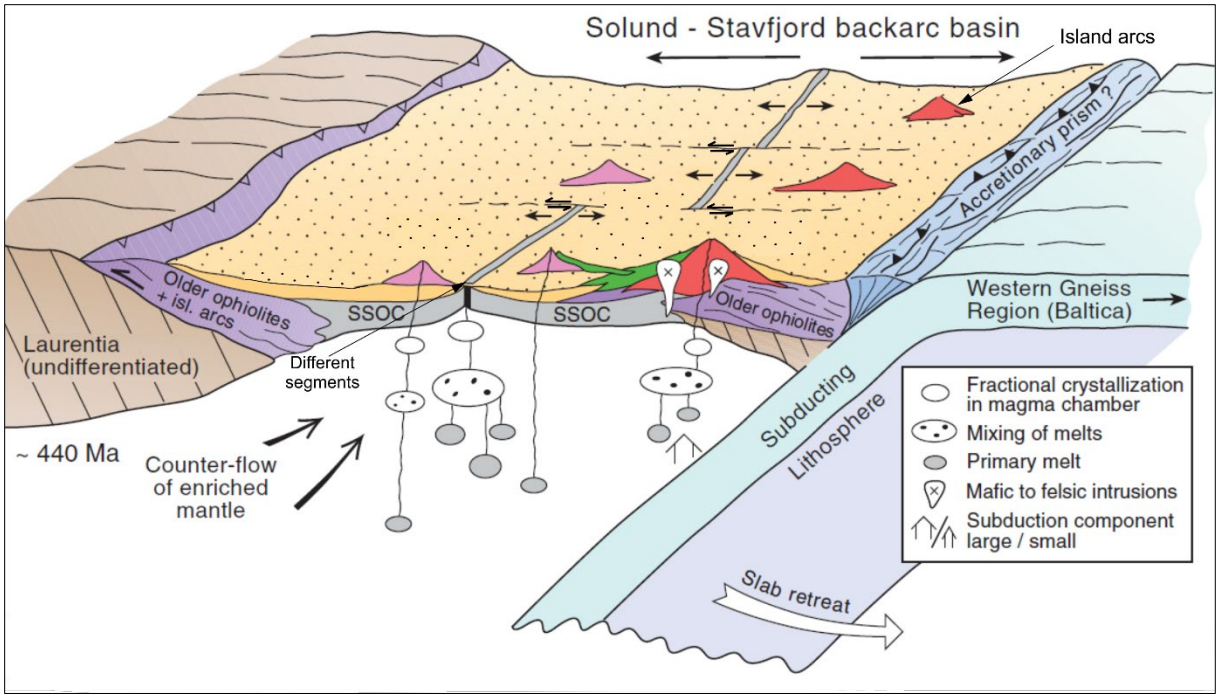

Fig.9.11: A model of the tectonic evolution of the Solund-Stavfjord Ophiolite Complex. The model reflects associated magmatic and sedimentary units in the backarc basin, that evolved adjacent to the Laurentian continental-margin. A slightly modified model from Furnes et al., 2012.

More recent and contemporary studies by e.g., Furnes and Dilek (2017); Furnes et al. (2020), illustrate the major tectonic settings in which subduction-related and subduction-unrelated oceanic crust undergoes its magmatic construction before emplacement onto continental margins as ophiolites (Fig. 9.12). Fig. 9.12 displays a backarc spreading system in which SSZ ophiolites form as part of a subduction zone, suggesting formation of the tectonic environment as a trench-proximal versus trench-distal setting (Dilek and Furnes, 2011; Furnes and Dilek, 2017). In their interpretation of the tectonic diagram, four main tectonic settings are presented (Backarc, Backarc to Forearc, Forearc, and Volcanic arc). The tectonic evolution in Grimelia is related to the backarc oceanic crust, which are lithological and structural comparable to the subduction-unrelated mid-ocean ridge (MOR) crust. The magmatic construction of such a type is also related to decompression melting of the upwelling asthenosphere beneath the spreading center (Furnes et al., 2020), further displayed in Fig.9.13.

The lower panel of Fig. 9.13 depicts the magma generation responsible for the subduction-related ophiolites, where the backarc ophiolites are related to decompression melting of the upwelling asthenosphere beneath the backarc spreading center. The upper panel of the figure indicates where the different settings take place. The illustration proposes that the evolution

of ophiolites (both subduction related/unrelated) is time dependent, giving large geochemical variations. The large geochemical variations can be a result of several parameters, such as 1) variation in slab dip-angles, 2) ridge jumps, 3) subduction rates, 4) spreading rates, 5) thermal structure, and 6) orientation of spreading axis (Furnes et al., 2020).

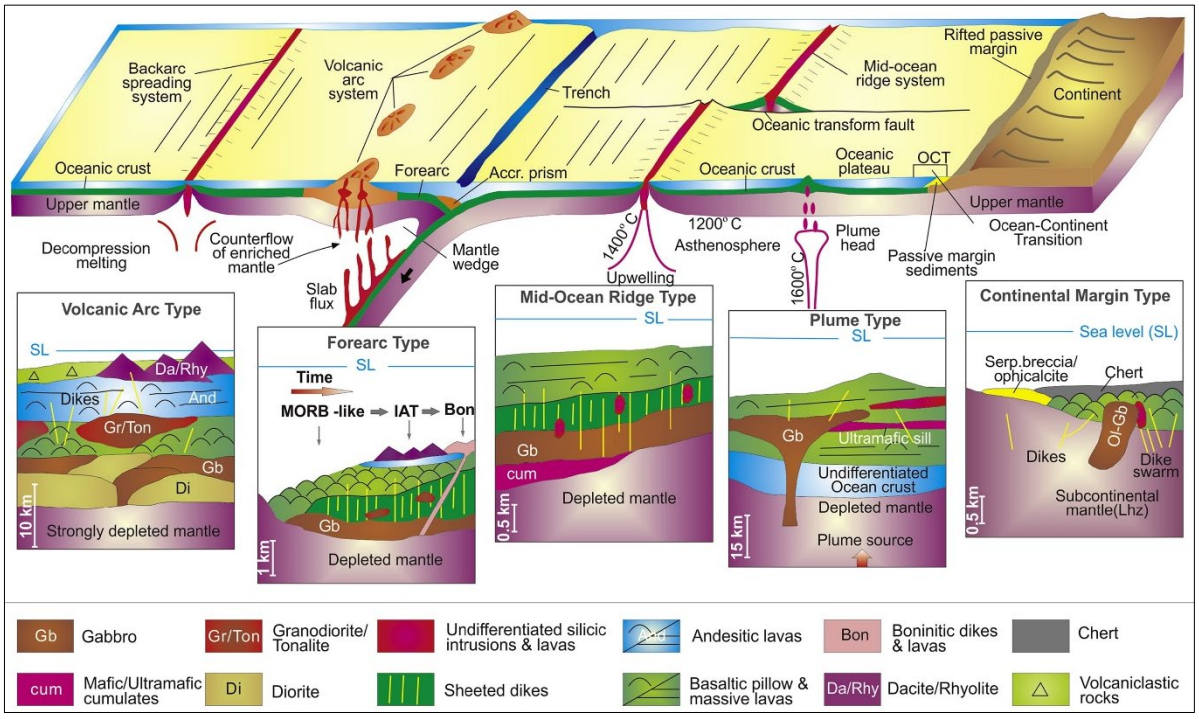

Fig.9.12: Plate tectonic diagram illustrating the major settings of magmatic constructions of the oceanic lithosphere (upper panel). The schematic diagram is not to scale. The lower panel depicts the structural architecture of the main types of oceanic lithosphere, evolved in different settings (Fig.9.13). From Furnes and Dilek, 2017 (modified from Dilek and Furnes, 2011;2014).

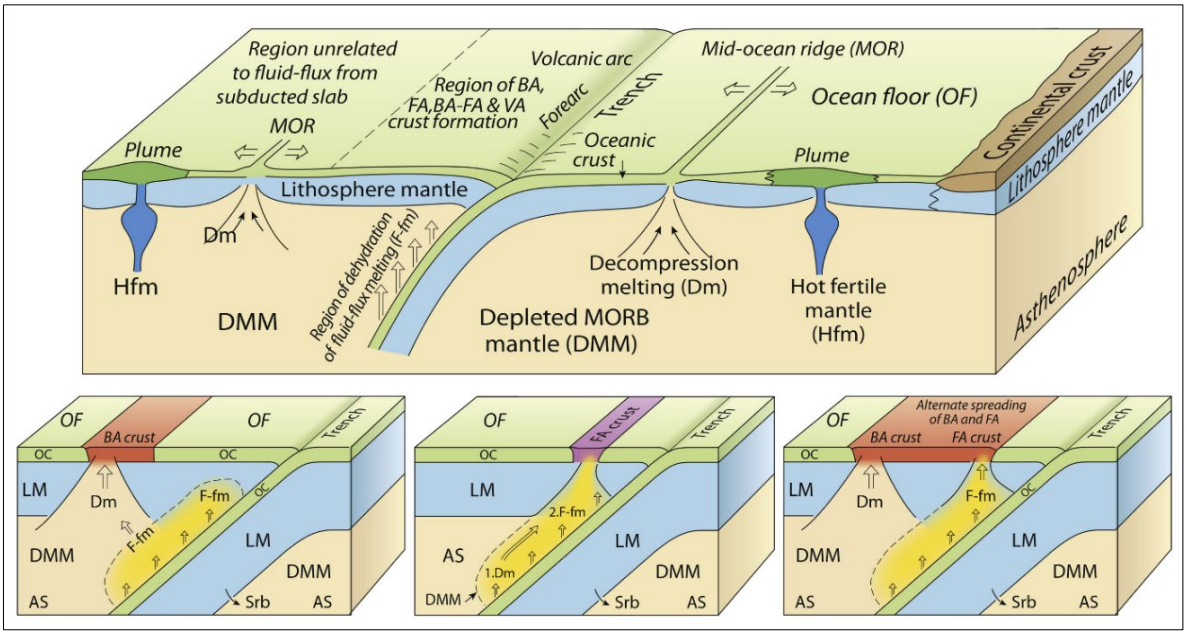

Fig.9.13: Detailed illustration of the magma production in the different settings during the evolution of plate tectonics (lower panel). The upper panel indicates where the different settings occur. Slightly modified from Furnes et al., 2020 (modified from Dilek and Furnes, 2009; Furnes and Dilek, 2017; Furnes and Safonova, 2019).

The first parameter indicates large variations in slab dip-angles as well as laterally differences in the slab geometry of the subducting environment (Guillaume et al., 2013). Laterally variations will affect the extent of subduction influence on its mantle under its spreading center, and further explain the geochemical heterogeneities in the backarc mantle. The second parameter is characterized by changes in geometry and kinematics of spreading centers within backarc basins, as a result of ridge jumping and ridge propagation. At fast-spreading mid-ocean ridges in major oceans, these processes are well documented (e.g., Mittelstaedt et al., 2008), as well as in modern backarc basins (e.g., Deschamps et al., 2008; Maldonado et al., 2014; Stern and Dickinson, 2010), and ophiolites (Dilek et al., 1997). According to Dilek et al. (1997) the SSOC contains three structural domains, which generated during two episodes of seafloor spreading, where each unit has its own geological characterization and different types of crustal architecture (Chapter 2.4.2). Their interpretation indicates that it is likely that the SSOC is influenced by the second parameter, causing geochemical differences within short distances.

The third parameter, controlled by subduction rates contributes to lateral differences in slab contributions to melt regimes beneath the SSZ spreading center. This is ruled by the amount of segments that is carried down within a subduction zone (e.g., Von Huene and Scholl, 1991; Clift and Vannucchi, 2004; Safonova et al., 2015), as well as the concentration of important slab derived elements (e.g., Th and Nb) in sediments (Plank and Langmuir, 1998). The fourth parameter characterized by different spreading rates along individual segments within backarc basins, produces significantly different morphological features and internal structures of the SSZ oceanic lithosphere (Furnes et al., 2020). The metamorphic dehydration P-T-t paths, as well as spatial distribution of slab-derived components in the SSZ environment, is affected by the thermal structure of a subducting slab (Van Keken, 2003) (fifth parameter).

The last controlling factor (sixth parameter), which may play a fundamental role in the geochemical signature of the ophiolite, is characterized by the orientation of the spreading axis within a backarc basin. The parameter is controlled by varying distances between the sites of magma production along spreading centers and the subduction zone. An example of this can be demonstrated by the North Fiji Basin (Price et al., 1990), as well as the South Sandwich Trench in the East Pacific (Leat et al., 2000) (Furnes et al., 2020). This parameter, as well as the fourth parameter, will result in various segments with different distances to the subduction

zone, meaning that the closes segment will reflect higher subduction influence than the segments furthest away (Erga, 2021). This is therefore a relevant parameter to the tectonic evolution of the SSOC, where the geochemical signatures of the volcanic sequence in Grimelia, Våganes-area (Erga, 2021) and from the 29 profiles of the Stavenes peninsula (Furnes et al., 2003), represents different degrees of subduction influence.

It is proposed from Furnes et al. (2020) that the above-mentioned parameters may be responsible for the geochemical variations in the SSOC, each process alone or as a combination of two more. The presented discrimination diagrams from Grimelia suggest minor subduction influence for volcanic breccias (Fig. 9.9), yet a dominance of subduction-unrelated character. This compliments the study of Furnes et al. (2012), suggesting that the metabasalt of the SSOC formed from magmas that were produced in a trench-distal suprasubduction-zone setting, sufficiently far from the subducting slab with only minor influence of slab-derived fluids. It is, however, important to highlight that the volcanic sequence of Grimelia is yet the thickest registered sequence in the area, further interpreted to be a result of the location at the magmatic spreading center during the evolution of the sequence (Chapter 8.5).

Chapter 10 – Conclusion

- The investigated area for this master thesis is located in Grimelia, between Solund and Bremanger, and represents part of the thoroughly investigated Solund-Stavfjord Ophiolite Complex (SSOC). The SSOC (443 $\pm$ 3 Ma) represents a remnant of the Iapetus oceanic lithosphere evolved in a Caledonian marginal basin
- As a result of detailed fieldwork and field-mapping, a Master profile is constructed through the area of interest, showing the pseudostratigraphy from bottom to top, including a sedimentary cover. The Master profile is further divided into two main parts and is predominantly composed of: 1) massive sheet flow, 2) pillow lava, and 3) volcanic breccia.
- Several discussed factors are used to calculate the degree of deformation in the area. The main factors are 1) vertical and horizontal axis for measured pillow lavas, 2) longest and shortest axis of observed epidote nodules and hyaloclastite fragments in the volcanic breccias, 3) as well as the texture of thin sections suggesting none to minor deformation of the massive sheet flows. These factors are compared with those of undeformed lava. In addition, adjustments regarding dip of strata are also used to predict the final result.
- A reconstruction of the volcanic sequence of Grimelia (Master profile) is presented, suggesting that the sequence goes from being 1205 m to 1430 m (new estimated thickness), which makes this, yet the longest registered volcanic sequence of the SSOC. The range of the sequence is, hence, interpreted to be located at the magmatic spreading center during the evolution of the sequence.
- Ore deposits observed within the defined field area is treated as part of the thesis and is considered with general knowledge about mineralization at spreading ridges. A proposed model for the Grimelia deposits is presented, suggesting that the deposits is bounded by a large fault, resulting in extremely localized physical and chemical conditions. Further, this controls the focused flow of hydrothermal fluids and resulting in focused discharge zones where the VMS deposits are located.
- A geochemical investigation is conducted based on 34 representative samples of metabasalt and is intended to reflect the geochemical signature for parts of the SSOC,

which in turn will be correlated with earlier proposed tectonic evolutionary models of the SSOC.

- Presented Zr-Y, Zr-TiO_2, Cr-Zr and Ni-Zr diagram, indicate that factional crystallization is the dominant magma-modifying process throughout the volcanic evolution, as in previously proposed studies. However, presented Zr-Cr covariations, also suggest a mixing of an evolved magma as the general process.
- The majority of the multi-element diagrams, with chondrite normalized REE plots and N-MORB normalized elements, indicate moderately to strongly fractionated rocks (negative Eu anomaly), as well as characteristic features for backarc basins ophiolitic crust with subduction influence (Pb and Cs enrichments, Ta and Nb depletion).
- Presented discrimination diagrams suggest minor subduction influence of the metabasaltic samples in Grimelia, yet a dominance of subduction-unrelated character.
- Several above-mentioned parameter may be responsible for the geochemical variations in the SSOC, each process alone or as a combination.
- In total, all observations compliment the study of Furnes et al. (2012), suggesting that the metabasalt of the SSOC formed from magmas that were produced in a trench-distal suprasubduction-zone setting, sufficiently far from the subducting slab with only minor influence of slab-derived fluids.

References

Alsaker, E., and Furnes, H., **1994.** *Geochemistry of the Sunnfjord Melange: sediment mixing from different sources during obduction of the Solund- Stavfjord Ophiolite Complex, Norwegian Caledonides.* Geological Magazine, v. 131, p. 105-121.

Alt, J. C., **1995**. *Subseafloor processes in mid-ocean ridge hydrothermal systems.* Seafloor Hydrothermal Systems: Physical, Chemical, Biological, and Geological Interactions. Geophysical Monograph, v.91, p. 85-105.

Alt, J. C., Teagle, D. A. H., Laverne, C., Vanko, D. A., Bach, W., Honnorez, J., Becker, K., Ayadi, M., and Pezard, P. A., **1996**. *Ridge-flank alteration of upper ocean crust in the eastern Pacific: Synthesis of results for volcanic rocks of Holes 504B and 896A.* Proceedings of the Ocean Drilling Program Scientific Results, v. 148, p. 435–450.

Andersen, T. B., **1998.** *Extensional tectonics in the Caledonides of southern Norway, an overview*. Tectonophysics, v. 285, p. 333-351.

Andersen, T.B., Skjerlie, K.P., Furnes, H., **1990.** *The Sunnfjord Melange, evidence of Silurian ophiolite accretion in the West Norwegian Caledonides*. Journal of the Geological Society, London, v. 147, p. 59–68.

Andersen, T. B., and Andresen, A., **1994.** *Stratigraphy, tectonostratigraphy and the accretion of outboard terranes in the Caledonides of Sunnhordland, W. Norway*. Elsevier, v. 231, p. 71-84.

Andersen, T.B., Osmundsen, P.T., Jolivet, L., **1994.** *Deep crustal fabrics and a model for the extensional collapse of the southwest Norwegian Caledonides*. Journal of Strucural Geology, v. 16, p. 1191–1203.

Ayadi, M., Pezard, P. A., Laverne, C., and Bronner, G., **1998**. *Multi-scalar structure at DSDP/ODP site 504, Costa Rica Rift, I. Stratigraphy of eruptive products and accretion processes.* Harvey PK, Lowell MA (eds) Core-log integration. Geological Society, London, Special Publications, v. 136, p. 297-310

Ballard R. D., and Moore J. G., **1977**. *Photographic atlas of the Mid-Atlantic Ridge rift valley*. Springer Verlag, New York

Barrie, C. T., and Hannington, M. D., **1997**. *Classification of Volcanic-Associated Massive Sulfide Deposits Based on Host-Rock Compositions*. Society of Economic Geologists, in book: Volcanic-associated massive sulfide deposits: Processes and examples in modern and ancient settings, chapter 8, p. 1-11

Bergh, S. G., and Sigvaldason, G. E., **1991**. *Pleistocene mass-flow deposits of basaltic hyaloclastite on a shallow submarine shelf, South Iceland*. Bulletin of Volcanology, v.53, p. 597–611.

Bergvesenet., **1980.** *Utskrift fra befaringsprotokoll TB ang. Grimeliens Verk*. Bergvesenet rapportnr: BV 1140. Rapportarkivet.

Bickle, M. J., and Teagle, D. A. H., **1992**. *Strontium alteration in the Troodos ophiolite: Implications for fluid fluxes and geochemical transport in mid-ocean ridge hydrothermal systems.* Earth and Planetary Science Letters, v. 113, p. 219–237

Bonatti, E., and C. G. A. Harrison., **1988.** *Eruption styles of basalt in oceanic spreading ridges and seamounts: Effects of magma temperature and viscosity*. Journal of Geophysical Research, v. 93, p. 2967–2980.

Brekke, H., and Solberg P.O., **1987.** *The geology of Atløy, Sunnfjord, western Norway*. Norges Geologiske Undersøkelse, Bulletin, v. 410, p. 73–94.

Carlisle, D., **1963**. *Pillow breccias and their aquagene tuffs, Quadra Island, British Columbia*. Journal of Geology, v. 71, p. 48–71.

Carracedo Sánchez, M., Sarrionandia, F., Juteau, T., and Gil Ibarguchi, J. I., **2012.** *Structure and organization of submarine basaltic flows: Sheet flow transformation into pillow lavas in shallow submarine environments*. International Journal of Earth Sciences, v. 101, p. 2201–2214.

Clift, R., and Vannucchi, P., **2004**. Controls on tectonic accretion versus erosion in subduction zones: Implications for the origin and recycling of the continental crust. Review of Geophysics, v. 42, p. 1-31

Corfu, F., and Andersen, T.B., **2002.** *U-Pb ages of the Dalsfjord Complex, SW Norway, and their bearing on the correlation of the allochthonous crystalline segments of the Scandinavian Caledonides.* International Journal of Earth Science, v. 91, p. 955-963.

Corfu, F., Roberts, R. J., Torsvik, T. H., Ashwal, L. D., and Ramsay, D. M., **2007**. *Peri-Gondwanan elements in the Caledonian Nappes of Finnmark, Northern Norway: Implications for the paleogeographic framework of the Scandinavian Caledonides*: American Journal of Science, v. 307, p. 434-458.

Dallmeyer, R.D. and Gee, D.G., **1986**. *$^{40}Ar/^{39}Ar$ mineral dates from retrogressed eclogites within the Baltoscandian miogeocline; Implications for a polyphase Caledonian orogenie evolution.* GSA Bulletin, v. 97, p. 26-34.

Deschamps, A., Shinjo, R., Matsumoto, T., Lee, C. -S., Lallemand, S. E., Wu, S., Scientific party of KR03 and KR04 cruises, **2008**. *Propagators and ridge jumps in a back-arc basin, the west Philippine Basin*. Terra Nova, v. 20, p. 327–332.

de Wit, M. J., Linol, B., Furnes, H., Muedi, T., and Valashiya, K., **2020**. *Pillow Talk*: *Volcanic rocks of the Karoo that formed many leagues under the Gondwanan Sea*. South African Journal of Geology, v. 123, p. 297–330.

Dilek, Y., **1998**. *Structure and tectonics of intermediate-spread oceanic crust drilled at DSDP/ODP Holes 504B and 896A, Costa Rica Rift*. In: Cramp, A., Macleod, C. J., Lee, S. V. and Jones, E. J. W. (eds). Geological Evolution of Ocean Basins: Results from the Ocean Drilling Program. Geological Society, London, Special Publication, v. 131, p. 179-197

Dilek, Y., and Furnes, H., **2009**. *Structure and geochemistry of Tethyan ophiolites and their petrogenesis in subduction rollback systems.* Lithos, v. 113, p. 1–20.

Dilek, Y., and Furnes, H., **2011.** *Ophiolite genesis and global tectonics: Geochemical and tectonic fingerprinting of ancient oceanic lithosphere*. Geological Society of America Bulletin, 123(3–4), p.387–411

Dilek, Y., and Furnes, H., **2014.** *Ophiolites and their origins*. Elements 10, p. 93-100.

Dilek, Y., Furnes, H., Skjerlie, K.P., **1997**. *Propagating rift tectonics of a Caledonian marginal basin: Multi-stage seafloor spreading history of the Solund- Stavfjorden ophiolite in western Norway.* Tectonophysics 280, p.213-238.

Dunning, G.R., and Pedersen, R.B., **1988.** *U/Pb ages of ophiolites and arc-related plutons of the Norwegian Caledonides: implications for the development of Iapetus.* Contributions to Mineralogy and Petrology, v. 98, p. 13-23.

Erga, A. S., **2021.** *A detailed field and geochemical investigation of the volcanic sequence in the Våganes-area: The Solund-Stavfjord Ophiolite Complex.* Unpublished master thesis, department of Earth Science, University of Bergen.

Fonneland-Jørgensen, H., Furnes, H., Muehlenbachs, K., and Dilek, Y., **2005**. *Hydrothermal alteration and tectonic evolution of an intermediate- to fast-spreading back-arc oceanic crust: Late Ordovician Solund-Stavfjord ophiolite, western Norway*. The Island Arc, v. 14, p. 517–541

Fossen, H., **1992**. *The role of extensional tectonics in the Caledonides of south Norway*: Journal of structural geology, v. 14, p. 1033-1046.

Fossen, H., and Hurich, C. A., **2005.** *The Hardangerfjord Shear Zone in SW Norway and the North Sea: a large-scale low-angle shear zone in the Caledonian crust*. Journal of the Geological Society, v. 162, p. 675-687.

Fossen, H., Pedersen, R.B., Bergh, S., and Andersen, A. **2013**. *En Fjellkjede blir til- Oppbygging av kaledonidene; ca. 500-405 millioner år.* I: Ramberg, I.B., Bryhni, I., Nøttvedt, A., og Rangnes, K. (red). *Landet blir til – Norges Geologi*. 2. utg. Trondheim. Norsk Geologisk Foreining, p. 183-232.

Fouquet, Y., Eissen, J. P., Ondreas, H., Barriga, F., Batiza, R., and Danyushevsky, L., **1998**. *Extensive volcaniclastic deposits at the Mid-Atlandic Ridge axis: Results of deep-water basaltic explosive volcanic activity?,* Terra Nova, v.10, p. 280–286.

Fox, C. G., Murphy, K. M., and Embley, R. W., **1987**. *Automated display and statistical analysis of interpreted deep-sea bottom photographs*. Marine Geology, v. 78, p. 199–216.

Francheteau, J., Juteau, T., and Rangan, C. **1979**. *Basaltic pillars in collapsed lava-pools on the deep ocean-floor*. Nature, v. 281, p. 209–211.

Franzson, H., Gudfinnsson, G. H., Frolova, J., Helgadóttir, H. M., Pauly, B., Mortensen, A. K., and Jakobsson, S. P., **2011**. *Icelandic Hyaloclastite Tuffs, Petrophysical Properties,*

Alteration and Geochemical Mobility. Report prepared for National Energy Authority and Reykjavík Energy. Iceland: ISOR, Reykjavik. ÍSOR-2011/064.

Furnes, H., **1972.** *Meta-Hyaloclastite breccias associated with Ordovician pillow lavas in the Solund area, West Norway.* Norsk Geologisk Tidsskrift, p.385-406.

Furnes, H., **1973.** *Variolitic structure in Ordovician Pillow Lava and its possible significance as an environmental indicator.* The Geological Society Of America, v. 1, p.27-30

Furnes, H., **1974.** *Structural and metamorphic history of the Lower Palaeozoic metavolcanics and associated sediments in the Solund area, Sogn*. Norges Geologiske Undersokelse, Bulletin 302, p. 33-74.

Furnes, H., and Fridleifsson, I. B., **1978**. *Relationship between the chemistry and axial dimensions of some shallow water pillow lavas of alkaline olivine basalt-and olivine tholeiitic composition*. Bulletin Volcanologique, v. 41, p. 136–146

Furnes, H., and Fridleifsson, I. B., **1979.** *Pillow block breccia – occurrences and mode of formation.* N.Jb. Geol. Paläont. Mh. Heft 3, p. 147-154.

Furnes, H., and Dilek, Y., **2017**. *Geochemical characterization and petrogenesis of intermediate to silicic rocks in ophiolites: A global synthesis.* Earth-Science Reviews, v. 166, p. 1-37.

Furnes, H., and Safonova, I., **2019**. *Ophiolites of the Central Asian Orogenic Belt: geochemical and petrological characterization and tectonic settings*. Geoscience Frontiers, v. 10, p. 1255–1284.

Furnes, H., Skjerlie, F.J., and Tysseland, M., **1976.** *Plate tectonic model based on greenstone geochemistry in the late Precambrian-Lower Palaeozoic sequence in the Solund-Stavfjorden areas, West Norway.* Norsk Geologisk Tidsskrift, p. 161-183.

Furnes, H., Roberts, D., Sturt, B., Thon, A., and Gale, G., **1979.** *Ophiolite fragments in the Scandinavian Caledonides*. Ophiolites—Proceedings International Ophiolite Symposium, Cyprus, p. 582-599.

Furnes, H., Ryan, P.D., Grenne, T., Roberts, D., Sturt, B. A., and Prestvik, T. **1985.** *Geological and geochemical classification of the ophiolite fragments in the Scandinavian Caledonides*. The Caledonide Orogen – Scandinavian and Related areas. Edited by D. G. Gee and B. A. Sturt. John Wiley & Sons, Chichester, p. 657-669.

Furnes, H., Skjerlie, K.P., Pedersen, R.B., Anderson, T.B., Stillman, C.J., Suthren, R., Tysseland, M., Garmann, L.B., **1990.** *The Solund-Stavfjorden Ophiolite Complex and associated rocks, west Norwegin Caledonides: Geology, geochemistry, and tectonic environment.* Geological Magazine, v. 127, p. 209-289.

Furnes, H., Skjerlie, K. P., and Dilek, Y., **2000**. *Petrology, tectonics, and hydrothermal alteration of a fossil backarc oceanic crust: Solund-Stavfjord ophiolite complex of the western Norwegian Caledonides-a review*. Special Papers, Geological Society of America, v. 349, p. 443–460.

Furnes, H., Hellevang, B., and Dilek, Y., **2001**. *Cyclic volcanic stratigraphy in a Late Ordovician marginal basin, west Norwegian Caledonides.* Bulletin of Volcanology, v.63, p.164–178

Furnes, H., Hellevang, H., Hellevang, B., Skjerlie, K.P., Robins, B., Dilek, Y., **2003**. *Volcanic evolution of oceanic crust in a Late Ordovician Back-arc basin: The Solund- Stavfjord Ophiolite Complex, West Norway.* AGU and the Geochemical Society (Geochemistry, Geophysics, Geosystems), v. 4, p. 1-26.

Furnes, H., Hellevang, B., Hellevang, H., & Robins, B., **2006.** *Evolution of lavas in the Late Ordovician/Early Silurian Solund-Stavfjord Ophiolite Complex, West Norway*. AGU and the Geochemical Society (Geochemistry, Geophysics, Geosystems), v. 7, p. 1-32.

Furnes, H., Dilek, Y., Pedersen, R.B., **2012**. *Structure, geochemistry, and tectonic evolution of trench-distal backarc oceanic crust in western Norwegian Caledonides, Solund-Stavfjord Ophiolite (Norway).* Geological Society of America Bulletin, v.124, p. 1027-1044

Furnes, H., De Wit, M., Dilek, Y., **2014.** *Four billion years of ophiolites reveal secular trends in oceanic crust formation.* Geoscience Frontiers, v. 5, p. 571-603.

Furnes, H., Dilek, Y., Zhao, G., Safonova, I., and Santosh, M., **2020**. *Geochemical characterization of ophiolites in the Alpine-Himalayan Orogenic Belt: Magmatically and tectonically diverse evolution of the Mesozoic Neotethyan oceanic crust.* Earth-Science Reviews, v. 208, 103258.

Gale, G. H., **1975.** *Ocean floor-type basalts from the Grimeli Formation, Stavenes Group, Sunnfjord*. Norges Geologiske Undersokelse. v. 319, p. 47-58.

Galley, A. G., Hannington, M. D., and Jonasson, I. R., **2007**. *Volcanogenic massive sulphide deposits*. Goodfellow, W.D., ed., Mineral Deposits of Canada: A Synthesis of Major Deposit-Types, District Metallogeny, the Evolution of Geological Provinces, and Exploration Methods: Geological Association of Canada, Mineral Deposits Division, Special Publication No. 5, p. 141-161.

Glancy, S., **2011**. *Submarine Lava Morphology*. GG711, Lect. 10.

Gregg, T.K.P., and Fink, J.H., **1995.** *Quantification of submarine lava-flow morphology through analog experiments.* Geology, v. 23, p. 73-76.

Griffith, R. W., and J.H. Fink. **1992**. *Solidification and morphology of submarine lavas: A dependence on extrusion rate.* Journal of Geophysical Research Atmospheres, v. 97, p. 729-737.

Guillaume, B., Husson, L., Funiciello, F., and Faccenna, C., **2013**. *The dynamics of laterally variable subductions: laboratory models applied to the Hellenides*. Solid Earth, v. 4, p.179–200.

Hannington, M.D., Jonasson, I.R., Herzig, P.M., and Petersen, S., **1995.** *Physical and Chemical Processes of Seafloor Mineralization at Mid-Ocean Ridges.* Seafloor Hydrothermal

Systems: Physical, Chemical, Biological, and Geological Interactions. Geophysical Monograph v. 91, p. 115-157.

Hannington, M.D., Galley, A.G., Herzig, P.M., and Petersen, S., **1998**. Chapter 28 - *Comparison of the TAG mound and stockwork complex with Cyprus type massive sulfide deposits*. Proceedings of the Ocean Drilling Program, Scientific Results v. 158, p. 389- 415.

Harris, A. J. L., and Rowland, S. K., **2015**. *Chapter 17 - Lava flow and Rheology*. From Encyclopedia of Volcanoes, Second Edition. Edited by Sigurdsson, H. Academic press, p. 321-342.

Hofmann, A., and Wilson, A. H., **2007**. *Chapter 5.5 - Silicified basalts, bedded cherts and other sea floor alteration phenomena of the 3.4 Ga Nondweni greenstone belt, South Africa.* In Van Kranendonk, M. J., Smithies, R. H., Bennett, V. C. (Eds.), Earth's Oldest Rocks. Developments in Precambrian Geology, v. 15, p. 571–605.

Honnorez, J., and Kirst, P., **1975**. *Submarine basaltic volcanism: Morphometric parameters for discriminating hyaloclastites from hyalotuffs*. Bulletin Volcanologique, v.39, p. 441, 465.

Humphris, S. E., and Thompson, G., **1978**. *Trace element mobility during hydrothermal alteration of oceanic basalts*. Geochimica et Cosmochimica Acta, v. 42, p. 127–136

Irvine, T. N., and Baragar, W. R. A., **1971.** *A guide to the chemical classification of the common volcanic rocks.* Canadian Journal of Earth Sciences, v. 8, p. 523–548.

Jones, J. G., **1969.** *Pillow lavas as depth indicators*. American Journal of Science, v. 267, p. 181–195.

Jones, J.G., **1970**. *Intraglacial volcanoes of the Laugarnvatn region, Southwest Iceland*. Journal of Geology, v. 78, p. 127-140.

Kappel, E. S., and Ryan, W. B. F., **1986**. *Volcanic episodicity and a non-steady state rift vally along Northeast Pacific spreading centers: evidence from Sea MARK I*. Journal of Geophysical Research, v. 91, p. 13925- 13940

Karson, J. A., **1998**. *Internal structure of oceanic lithosphere: a perspective from tectonic windows*. Buck R, Karson J, Delaney P, Sempere JC (eds). Faulting and magmatism at midocean ridges. American Geophysical Union, v. 106, p. 177-218.

Karson, J. A., and Rona, P. A., **1990**. *Block-tilting, transfer faults, and structural control of magmatic and hydrothermal processes in the TAG area, Mid-Atlantic Ridge 26° N*. Geological Society of America Bulletin, v. 102, p. 1635–1645.

Kelley, D. S., and Delaney, J. R., **1987**. *Two-phase separation and fracturing in mid-ocean ridge gabbros at temperatures greater than 700 °C*. Earth and Planetary Science Letters, v. 83, p. 53–66.

Kolderup, N. H., **1921.** *Der Mangeritsyenit und umgebende Gesteine zwischen Dalsfjord und Stavfjord in Sondfjord im westlichen Norwegen*. Bergen Museum Arbok 1920-21, (5).

Kolderup, N.-H., **1928**. *Fjellbygningen i kyststraket mellom Nordfjord og Sognefjord*. Bergen Museum Arbok 1928, Naturvitenskapelige rekke Nr. 1.

Korneliussen, A. and Often, M., **1980**: *Pyrite deposits in the Stavfjord area with particular reference to the Grimeli and Vågedalen deposits in Askvoll, Sogn and Fjordane County.* NGU report no. 1650/53A, Survey of the Norwegian States's Mining Rights

Kusky, T. M., Wang, L., Dilek, Y., Robinson, P., Peng, S., and Huang, X., **2011**. *Application of the modern ophiolite concept with special reference to Precambrian ophiolites*. Science China Earth Sciences, v. 54, p. 315–341.

Kusky, T. M., Windley, B. F., Safonova, I., Wakita, K., Wakabayashi, J., Polat, A., and Santosh, M., **2013**. *Recognition of ocean plate stratigraphy in accretionary orogens through Earth history: A record of 3.8 billion years of sea floor spreading, subduction, and accretion.* Gondwana Research, v. 24, p. 501–547.

Le Maitre, R. W., **1989**. *Igneous rocks*. *A classification of Igneous Rocks and Glossary of Terms.* Recommendations of the International Union of Geological Science Subcommission on the systems of Igneous rocks.

Leat, P. T., Livermore, R. A., Millar, I. L., & Pearce, J. A., **2000**. *Magma supply in back-arc spreading centre segment E2*. *East Scotia Ridge.* Journal of Petrology, v. 41, p. 845–866.

Macdonald, K. C., **1982**. *Mid-ocean ridges: fine scale tectonic, volcanic and hydrothermal processes within the plate boundary zone*. Annual Reviews, Earth Planet Science Letter, v. 10, p. 155-190

Maldonado, A., Bohoyo, F., Galindo-Zaldívar, J., Hernández-Molina, F. J., Lobo, F. J., Lodolo, E., Martos, Y. M., Pérez, L. F., Schreider, A. A., and Somoza, L., **2014**. *A model of oceanic development by ridge jumping: opening of the Scotia Sea.* Global and Planetary Change, v. 123, p. 152–173.

Mittelstaedt, E., Ito, G., and Behn, M. D., **2008**. *Mid-ocean ridge jumps associated with hotspot magmatism*. Earth and Planetary Science Letter, v. 266, p. 256–270.

Moore, J.G., **1965**. *Petrology of deep-sea basalt near Hawaii.* American Journal of Science. v.263, p. 40-52.

Natland, J. M., Dick, H. J. B., and the Leg 176 Shipboard Scientific Party., **1998.** *A long gabbro section in the ocean crust: results of Leg 176 drilling, Southwestern Indian Ridge*. JOIDES Journal 24, p. 11-14

Norton, M., **1987**. *The Nordfjord–Sogn Detachment, W. Norway*. Norsk Geologisk Tidsskrift, 67, p. 93–106.

Osmundsen, P.T., **1996**. *Late-orogenic structural geology and Devonian Basin formation in Western Norway: a study from the hanging-wall of the Nordfjord-Sogn Detachment in the Sunnfjord region*. Dr Scient Thesis, University of Oslo, Norway

Osmundsen, P.T., Andersen, T., Markussen, S., and Svendby A.K. **1998**. *Tectonics and sedimentation in the hangingwall of a major extensional detachment: the Devonian Kvamshesten Basin, western Norway*. Basin Research, v. 10, p. 213-234.

Osmundsen, P.T., Bakke, B., Svendby, A.K., Andersen, T.B., **2000**. *Architecture of the Middle Devonian Kvamshesten Group, Western Norway: Sedimentary response to deformation above a ramp-flat extensional faulting*. Special Publication Geological Society, London, v. 180, p. 503–535

Pearce, J. A., **2008**. *Geochemical fingerprinting of oceanic basalts with applications to ophiolite classification and the search for Archean oceanic crust*. Lithos, v. 100, p. 14-48.

Pearce, J.A., **2014.** *Immobile element fingerprinting of ophiolites.* Elements, v. 10, p. 101–

108.

Pearce, J. A., and Stern, R. J., **2006**. *Origin of back-arc basin magmas: Trace element and isotope perspectives.* Geophysical Monograph series, v. 166, p. 63-86

Pechishcheva, N. V., Shunyaev, K. Y., and Melchakova, O. V., **2018**. *Zirconium in modern analytical chemistry*. Reviews in Analytical Chemistry, v. 37, p. 1-20.

Pedersen, R. B., and Hertogen, J., **1990**. *Magmatic evolution of the Karmøy Ophiolite Complex, SW Norway: relationships between MORB-IAT-boninitic-calc-alkaline and alkaline magmatism*. Contributions to Mineralogy and Petrology, v. 104, p. 277-293

Pedersen, R. B., and Dunning, G. R., **1997**. *Evolution of arc crust and relations between contrasting sources: U-Pb (age), Nd and Sr isotope systematics of the ophiolitic terrain of SW Norway*. Contributions to Mineralogy and Petrology, v. 128, p. 1-15.

Pedersen, R.B., Furnes, H., and Dunning, G., **1991.** A U/Pb age for the Sulitjelma Gabbro, North Norway: further evidence for the development of a Caledonian marginal basin in Ashgill-Llandovery time. Geological Magazine 128, 141-153.

Pedersen, R. B., Bruton, D., and Furnes, H., **1992**. *Ordovician faunas, island arcs and ophiolites in the Scandinavian Caledonides*. Terra Nova, v. 4, p. 217-222.

Pedersen, R. B., Furnes, H., and Dunning, G.R., **1988**. *Some Norwegian ophiolite complexes reconsidered*. Norges Geologiske Undersøkelse Special Publication, v. 3, p. 80-85.

Phipps Morgan, J., Harding, A., Orcutt, J., Kent, G., and Chen, Y. J., **I994**. *Chapter 7 - An observational and theoretical synthesis of magma chamber geometry and crustal genesis along a mid-ocean ridge spreading center*. Ryan MP (ed) Magmatic Systems. International Geophysics, v. 57, p. 139-178

Pi, J.-L., You, C.-F., and Wang, K.-L., **2016**. *The influence of Ryukyu subduction on magma genesis in the Northern Taiwan Volcanic Zone and Middle Okinawa Trough - Evidence from boron isotopes*. Lithos, v. 260, p. 242–252.

Plank, T., and Langmuir, C. H., **1998**. *The chemical composition of subducting sediment and its consequences for the crust and mantle*. Chemical Geology, v. 145, p. 325–394.

Price, R. C., Johnson, E. L., Crawford, A. J., **1990**. *Basalts of the North Fiji Basin: the generation of back arc basin magmas by mixing of depleted and enriched mantle sources*. Contributions to Mineralogy and Petrology, v. 105, p. 106–121.

Ravnås, R., and Furnes, H., **1995**. *The use of geochemical data in determining the provenance and tectonic setting of ancient sedimentary successions: The Kalvåg mélange, western Norwegian Caledonides*. Sedimentary Facies Analysis: A Tribute to the Research and Teaching of Harold G. Reading: International Association of Sedimentologists Special Publication 22, p. 237–264.

Richardson, C. J., Cann, J. R., Richards, H. G., and Cowan, J. G., **1987**. *Metal-depleted root zones of the Troodos ore-forming hydrothermal systems, Cyprus*. Earth and Planetary Science Letters, v. 84, p. 243-253.

Roberts, D., **1988**. *The terrane consept and the Scandinavian Caledonides: a synthesis*. Norges Geologiske Undersokelse Bulletin, v. 413, p. 93-99.

Roberts, D., **2003**. *The Scandinavian Caledonides: event chronology, palaeogeographic settings and likely modern analogues.* Tectonophysics, v. 365, p. 283-299.

Roberts, D., and Gee, D. G., **1985**. *An introduction to the structure of the Scandinavian Caledonides: The Caledonian Orogen- Scandinavia and related areas.* v. 1, p. 55-68.

Rona, P. A., **1988**. *Hydrothermal mineralization at oceanic ridges*. Canadian Mineralogist., v. 26, p. 431-465.

Ross, P. -S., and Bedard, J. H., **2009**. *Magmatic affinity of modern and ancient subalkaline volcanic rocks determined from trace-element discriminant diagrams*. Canadian Journal of Earth Sciences., v. 46, p. 823–839.

Rønning, J.S., **1981**. *CP-målinger i Grimelidfeltet.* Bergvesenet rapport nr: BV 1598, NGU-rapport nr. 1800/53C.

Saccani, E., **2015**. *A new method of discriminating different types of post-Archean ophiolitic basalts and their tectonic significance using Th-Nb and Ce-Dy-Yb systematics.* Geoscience Frontiers, v. 6, p. 481–501.

Safonova, I., Kojima, S., Nakae, S., Romer, R. L, Seltmann, R., Sano, H., and Onoue, T., **2015**. *Oceanic island basalts in accretionary complexes of SW Japan: Tectonic and petrogenetic implications.* Journal of Asian Earth Sciences, v. 113, p. 508–523.

Scott, R. B., and Hajash, A., **1976**. *Initial submarine alteration of basaltic pillow lavas: A microprobe study.* American Journal of Science, v. 276, p. 480–501.

Seyfried, W. E., Mottl, M., and Bischoff, J. L., **1978**. *Seawater/basalt ratio effects on the chemistry and mineralogy of spilites from the ocean floor*. Nature, v. 275, p. 211–213.

Seyfried, W. E., Berndt, M. E., and Seewald, J. S., **1988**. *Hydrothermal alteration processes at mid-ocean ridges: Constraints from diabase alteration experiments, hot-spring fluids and composition of the oceanic crust*. Canadian Mineralogist, v. 26, p. 787–804.

Skjerlie, F. J., **1969**. *The pre-Devonian rocks in the Askvoll - Gaular area and adjacent districts, western Norway*. Norges Geologiske Undersokelse, V.258, p.325-59.

Skjerlie, F. J., **1974**. *The Lower Palaeozoic sequence of the Stavfjord district, Sunnfjord.* Norges Geologiske Undersokelse, V.302, p.1-32.

Skjerlie, K.P. and Furnes, H., **1990**. *Evidence for a fossil transform fault in the Solund-Stavfjord Ophiolite Complex: West Norwegian Caledonides.* Tectonics, v. 9, 1631-1648.

Smith, D. K., Cann, J. R., **1993**. *Building the crust at the Mid-Atlantic Ridge*. Nature, v. 365, p. 707-715

Spandler, C., and Pirard, C., **2013**. *Element recycling from subducting slabs to arc crust: a review*. Lithos, v. 170-171, p. 208–223

Staudigel, H., Plank, T., White, B., and Schmincke, H. U., **1996**. *Geochemical fluxes during seafloor alteration of the Basaltic upper oceanic crust: DSDP sites 417 and 418*. Geophysical Monograph series, v. 96, p. 19-36

Stensrud, A. **1976**: En malmgeologisk undersøkelse av Grimeli-forekomsten, Askvoll, Sogn og Fjordane [An ore geology survey of the Grimeli deposit, Askvoll, Sogn and Fjordane]. Dissertation in ore geology. Geol. Inst. NTH, 82 p.

Stephens, M.B. and Gee, D.G., **1989**. *Terranes and polyphase accretionary history in the Scandinavian Caledonides*. The Geological Society of America, Spec. Pap., v. 230, p. 17-30.

Stern, R. J., Dickinson, W. R., **2010**. *The Gulf of Mexico is a Jurassic backarc basin*. Geosphere, v. 6, p. 739–754.

Strekeisen, A., **2020**. *Greenschist. Retrieved* From: [http://www.alexstrekeisen.it/english/meta/greenschist.php], 17.09.2021.

Stubseid, H. H., **2017**. *Geological evolution and stratigraphic relationship of the ophiolitic terrane in the outer Hardangerfjord area: evidence from geochronology and geochemistry*. Master Thesis. University of Bergen, Norway.

Sturt, B.A., Furnes, H., and Roberts, D., **1984**. *A conspectus of Scandinavian Caledonian ophiolites*. Geological Society, London, Special Publications, v. 13, p. 381-391.

Sun, S.-s., and McDonough, W. F., **1989**. *Chemical and isotopic systematics of oceanic basalts: Implications for mantle composition and processes*. Geological Society, London, Special Publications, v. 42, p. 313–345.

Torsvik, T., Furnes, H., Muehlenbachs, K., Thorseth, I. H., and Tumyr, O., **1998**. *Evidence for microbial activity at the glass-alteration interface in oceanic basalts.* Earth and Planetary Science Letters, v. 162, p. 165–176.

Van Andel, T. H. and Ballard, R. D., **1979**. *The Galapagos Rift at 86° W. 2. Volcanism, structure and evolution of the rift valley*. Journal of Geophysical Research, Solid Earth, v. 84, p. 5390-5406

Van Keken, P. E., **2003**. *The structure and dynamics of the mantle wedge*. Earth and Planetary Science Letter, v. 215, p. 323–338.

Von Huene, R., and Scholl, D. W., **1991**. *Observations at convergent margins concerning sediment subduction, sediment erosion, and the growth of continental crust*. Reviews of Geophysics, v. 29, p. 279–316.

Walker, G. P. L., **1992**. *Morphometric study of pillow-size spectrum among pillow lavas*. Bulletin of Volcanology, v. 54, p. 459–474

White, J. D. L., McPhie, J., and Soule, A. S., **2015**. *Chapter 19 - Submarine Lavas and Hyaloclastite.* The encyclopedia of Volcanoes (second edition), p. 365-375.

White, S. M., R. M. Haymon., D. J. Fornari., M. R. Perfit., and K. C. Macdonald., **2002**. *Correlation between volcanic and tectonic segmentation of fast-spreading ridges: Evidence from volcanic structures and lava flow morphology on the East Pacific Rise at 9°-10°N.* Journal of Geophysical Research, Solid Earth, v. 107, p. EMP 7-1 to EMP 7-20.

Winchester, J.A., and Floyd, P.A., **1977**. *Geochemical discrimination of different magma series and their differentiation products using immobile elements*. Chemical Geology, v. 20, p. 323–343.

Wohletz, K. H., **1983**. *Mechanisms of hydrovolcanic pyroclast formation: Grain-size, scanning electron microscopy, and experimental studies*. Journal of Volcanology and Geothermal Research, v. 17, p. 31– 63.

Appendix

Appendix 1

Table 1.1.1: Measurements of pillow lavas, hyaloclastites/fragments, epidote-nodules, and foliation, presented in one table. The different measurements are connected to detail profiles 1-13.

Location (nearest profile)	Measured pillows (cm)	Measured hyaloclastites/Pillow fragments (cm)	Measured epidote-nodules (CM)	Foliation (average)
Detail profile 1	15x3, 22x5, 45x10	16x4, 5x2	-	240/70
Detail profile 2	30x6, 30x5, 22x6	12x0.7, 6x0.2, 26x1, 14x1cm	-	270/60
Detail profile 3	35x10, 80x20, 18x7, 100x25, 40x5, 30x3, 78x9, 20x1, 58x7, 54x5, 120x10, 40x6, 10x4, 35x4, 20x5, 270x70, 30x15, 100x40, 40x10, 120x50, 140x25, 80x20, 60x15, 50x25	35x0.5, 3x0.3, 5x1, 5x0.3, 4x0.2	-	270/50
Detail profile 4	70x25, 30x15, 55x15, 20x5, 20x10, 40x10, 65x17	-	-	280/60
Detail profile 5	30x20, 40x10, 50x15, 80x18, 70x25, 40x15, 50x15, 65x10, 40x10	-	-	230/70
Detail profile 6	70x10, 60x10, 40x20, 40x10, 40x10, 20x5, 40x20	10x3, 5x0.3, 5x0.3, 5x0.3	-	240/65
Detail profile 7	10x2, 12x1.5, 6x0.5, 20x4, 28x5, 12x3, 24x4, 33x5, 28x5, 12x3, 24x4	40x1, 9x3, 22x2, 10x2	15x7, 3x1.5	250/45
Detail profile 8	50x12, 72x18, 58x8, 40x7, 30x5, 34x8, 40x8, 84x24, 38x10, 38x11, 42x4, 55x10, 28x7, 17x6, 11x3, 18x9, 40x14, 46x7, 47x8, 38x3, 40x10	8x2, 14x4, 7x1, 10x2, 5x0.6, 5.5x0.4, 16x1.6	-	260/65
Detail profile 9	100x30, 66x10, 48x6, 66x10, 12x3, 38x9, 47x10, 75x8, 80x15, 55x5, 55x12, 48x13, 30x6, 50x15	-	-	285/65
Detail profile 10	68x15, 48x6, 60x6, 24x5, 60x10, 35x6, 30x10, 70x10, 65x10, 12x20, 60x10, 50x5, 70x8, 60x7, 100x20, 17x3, 45x7, 90x15, 80x16, 20x5, 36x10, 38x10, 40x10, 30x7, 50x10, 125x40, 95x20, 50x10, 53x20, 40x12, 45x13, 65x20, 45x15, 90x27, 38x12, 67x22, 33x10, 85x16, 100x15	6x0.1, 6x0.2, 13x0.4, 3x0.3, 3x0.1, 5x0.4, 3.5x0.1, 11x0.2, 3x0.3, 5x0.3, 2x0.2, 6x0.4, 10x0.5, 4x0.3, 5x0.1	30x5, 10x6, 20x16, 11x14, 14x9, 12x15 (right outside the profile)	265/50

Detail profile 11	30x5, 50x15, 30x10, 40x10, 50x15, 50x10, 50x8, 55x5, 30x8, 60x22, 70x20, 38x11, 40x3, 50x8, 40x10, 38x7, 30x6, 90x20	5.5x0.8, 17x0.3, 5x0.1	-	255/50
Detail profile 12	70x20, 30x20, 50x20, 70x15,	3x0.1	10x11, 40x70, 8x15, 85x20, 60x20, 90x20	270/40 Drain-out floors: 230/50, 297/60, 200/60, 310/65
Detail profile 13	60x70, 60x9, 65x18, 48x10, 66x7, 46x7, 44x5, 50x11, 30x4, 22x4, 85x15, 45x8, 77x24, 73x15, 60x15, 30x7, 90x16, 30x18, 120x30, 110x40, 180x60, 20x5, 38x12, 40x14, 35x10, 40x12, 20x6, 50x15, 66x13, 46x6, 55x9, 50x6, 130x25, 110x20, 70x16, 100x19, 70x20, 50x15, 47x15, 50x20, 60x15, 70x28, 40x7, 26x9, 40x8, 18x6, 70x17, 55x6, 47x13, 38x10, 40x20, 86x27, 100x25, 170x40, 46x13, 90x25, 60x25, 70x28, 80x26, 46x13, 40x15, 40x12, 55x12, 36x10, 50x16, 52x10, 60x8, 30x5, 65x11, 66x20, 47x17, 110x35, 80x17, 97x20, 60x20, 250x90, 130x70, 120x40, 110x40, 100x40, 90x30, 90x20, 10x4, 60x8, 30x6, 55x15, 37x11, 39x9, 70x16, 60x15, 50x7, 60x17, 65x24, 47x16, 70x10, 80x18, 38x9, 69x18	3x0.3, 2x0.3	55x25	250/35

Appendix 2

*Table 2.1.1: Explanations from the cyclic units within the volcanic sequence. From the Master profile (with part 1A), 8 cyclic units at a large scale is defined, where all three components are present towards the end of the profile (number 6 and 7) (*Figure 1*). From the detail profiles, cyclic units are registered at detail profile 6 and 11. PL: pillow lavas. VB: volcanic breccia. MSF: massive sheet flow. CS: cover sediments.*

Cyclic units (Masterprofile)	**Components (m above sheeted dike complex)**	**Cyclic units (Detail profiles)**	**Components (m above sheeted dike complex)**
1	PL:25-455m	Detail profile 6	MSF: 0.6m, VB: 0.4m, MSF: 4m, VB: 8m, MSF: 2m
2	MSF: 455-465m, VB: 465-475m, ending with MSF: 475m.	Detail profile 11	MSF: 0.4m, VB: 0.1m, PL: 0.5m
3	MSF:475-555. Ending with missing data from 555-765m. It is assumed that the cyclic unit continues into the next layer. VB:765-845m, ending with PL: 845m.		
4	PL: 845-880, ending with MSF: 880m.		
5	MSF: 880-890m, PL: 890-935m, ending with MSF: 935m.		
6	MSF: 953-950, PL: 950-975m, VB: 975-1040m, ending with MSF: 1040m.		
7	MSF: 1040-1080m, PL: 1080-1105m, VB: 1105-1140m. Ending with PL: 1140		
8	PL: 1140-1215 (excluding cover sediments).		

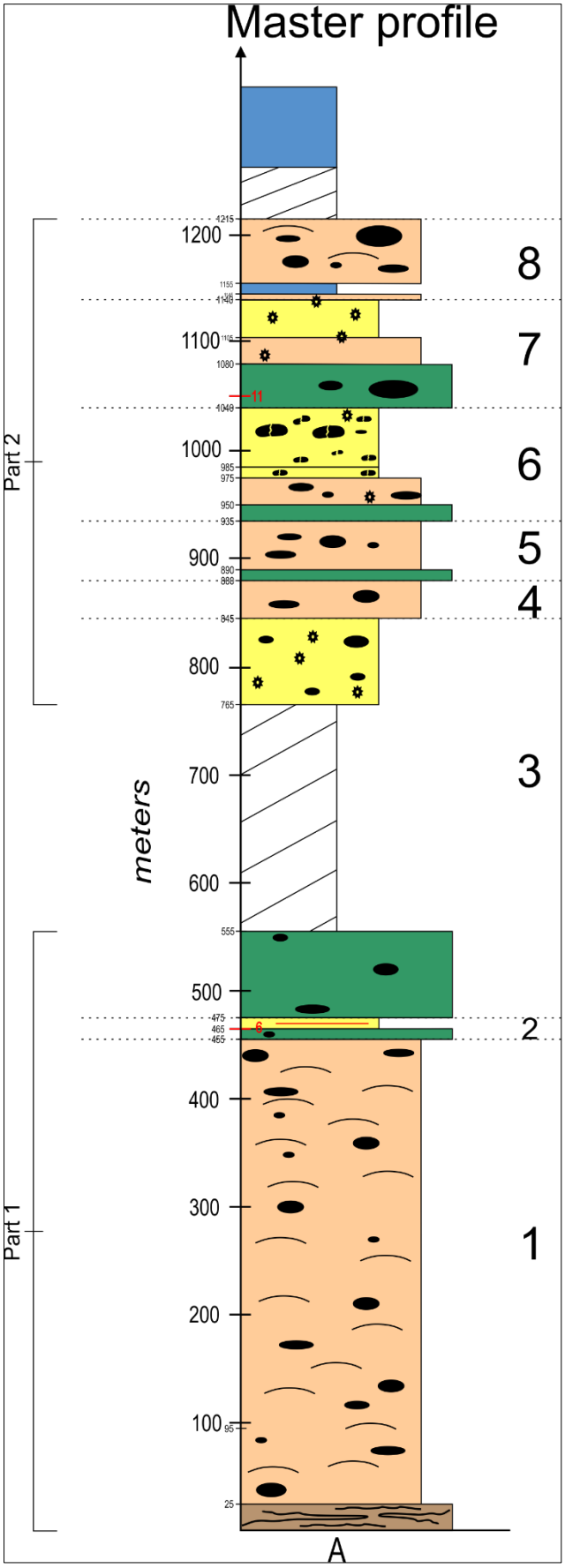

Figure 1: Slightly simplified Master profile depicting cyclic units at a large scale. In total, 8 cyclic units are registered.

Appendix 3

Step 1: Adjustments regarding dip of strata

Within the volcanic sequence of Grimelia, an average dip of the strata is measured to be 59° (α). However, the actual dip within each sequence gives a more accurate result and therefor used when calculating. By using trigonometric formulas, a calculation of the actual thickness of the strata can be made. Table 3.1.1 shows the calculations to adjust the thickness of the various components within the volcanic sequence of Grimelia, by using the formula: $\sin(\alpha) = \frac{a}{c}, where\ a = calculated\ thickness, and\ c = current\ length\ (m)$

$$a = \sin(\alpha) \cdot c$$

Table 3.1.1: calculations and adjustments regarding dip of strata.

Different components within the Master Profile (Figure 2)	Part	Current length (m), above the sheeted dike complex	length **(c)**	Foliation, from detail profile:	Calculated length (m) $\boldsymbol{a = \sin(\alpha) \cdot c}$	Current length (m), above the sheeted dike complex
100% sheeted dike complex	0	0-25	25	From measured dikes	$a = \sin(70) \cdot 23.5$	0-23.5
Pillow lava	1	25-455	430	3	$a = \sin(50) \cdot 430 = 329.5$	23.5-353
Sheet flow	2	455-465	10	5	$a = \sin(70) \cdot 10 = 9.5$	353-362.5
Volcanic breccia	3	465-475	10	6	$a = \sin(65) \cdot 10 = 9$	362.5-371.5
Sheet flow	4	475-555	80	6	$a = \sin(65) \cdot 80 = 72.5$	371.5-444
Missing data	5	555-765	210	Average	$a = \sin(59) \cdot 210 = 180$	444-624
Volcanic breccia	6	765-845	80	7	$a = \sin(45) \cdot 80 = 56.5$	624-680.5
Pillow lava	7	845-880	35	8	$a = \sin(65) \cdot 35 = 32$	680.5-712.5
Sheet flow	8	880-890	10	8	$a = \sin(65) \cdot 10 = 9$	712.5-721.5
Pillow lava	9	890-935	45	8	$a = \sin(65) \cdot 45 = 41$	721.5-762.5
Sheet fow	10	935-950	15	9	$a = \sin(65) \cdot 15 = 13.5$	762.5-776
Pillow lava	11	950-975	25	9	$a = \sin(65) \cdot 25 = 22.5$	776-798.5
Volcanic breccia	12	975-1040	65	10	$a = \sin(50) \cdot 65 = 50$	798.5-848.5
Sheet flow	13	1040-1080	40	11	$a = \sin(50) \cdot 40 = 30$	848.5-878.5
Pillow lava	14	1080-1105	25	11	$a = \sin(50) \cdot 25 = 19$	878.5-897.5

Volcanic breccia	15	1105-1140	35	12	$a = \sin(40) \cdot 35 = 22.5$	897.5-920
Pillow lava	16	1140-1205 (excluding CS)	65	13	$a = \sin(35) \cdot 65 = 37$	920-957

New total length after adjustments regarding dip of the strata: 957 m

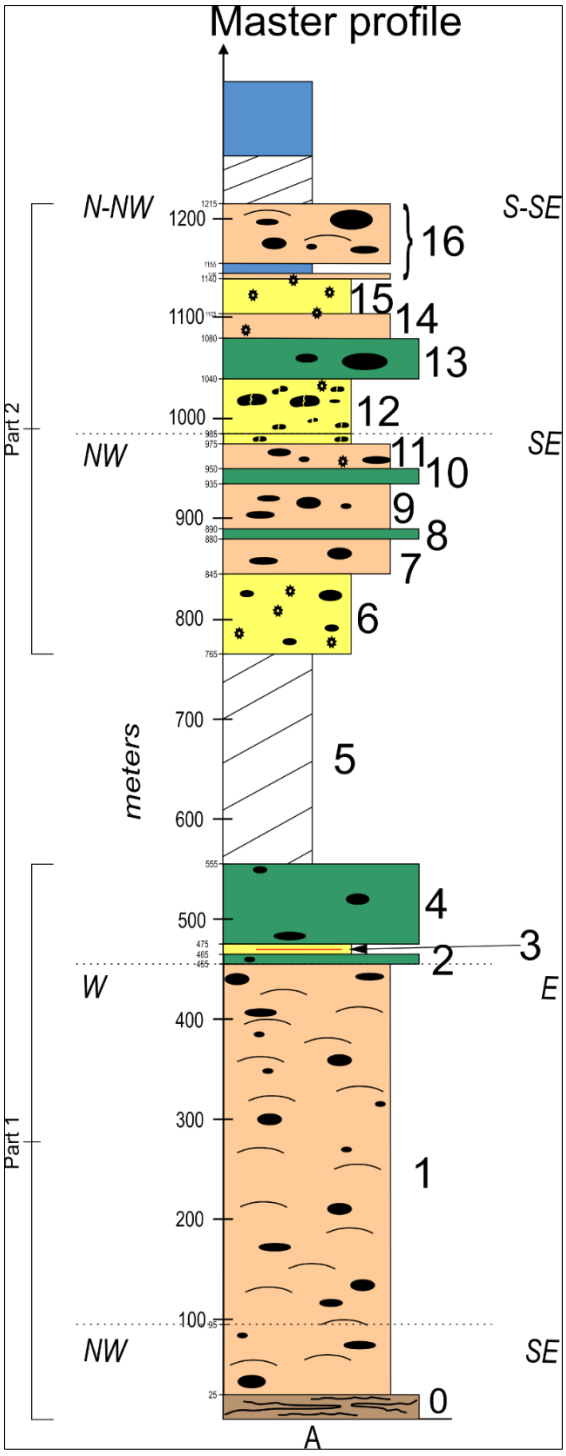

Figure 2: Master profile of the volcanic sequence in Grimelia, showing the different components and their locations regarding the adjustment (not adjusted).

Step 2: Adjustments regarding deformation

The deformation within the volcanic sequence of Grimelia is predicted based on V/H ratios on measured pillows in the area, compared to various undisturbed pillow lavas (Furnes and Fridleifsson, 1978) and hyaloclastite fragments (Franzson et al., 2011), from Iceland. The calculations are presented in Table 3.2.1.

Sheet flows:

Based on the interpretation of the volcanic sequence and the thin section from the massive sheet flow, it is concluded that the deformation of the massive sheet flows is minor. Hence, not necessary to do adjustments regarding deformation for this component.

Pillow Lava:

The deformation ratio of pillow lavas is calculated based on the V/H ratios on measured pillows within the volcanic sequence of Grimelia, compared to undisturbed pillows at Mosfell, Iceland (Furnes and Fridleifsson, 1978). The average pillow dimensions are used to get an average V/H ratio for the sequence, based on measured pillows from detail profile 13.

Total V/H ratio for pillow lavas: $\frac{29.36}{17.98} = \mathbf{1.6}$

However, part 1 of the Master profile (Fig. 3.2, A), comprises predominantly large lobate (tortoise) pillows, indicating that the pillow lava-sequence of this area is less deformed than the pillows within part 2. It can be assumed that these pillows are less deformed, due to large pillow-bodies and more massive pillows. The thin section of the pillow lava sequence also confirms the presumption of a less/partly deformed sequence (Fig. 7.1 B). Therefore, the deformation rate is slightly decreased.

Total V/H ratio for pillow lavas in part 1 of the Master Profile: $\mathbf{1.3}$

Volcanic breccia:

The deformation ratio of the hyaloclastite fragments is calculated based on the longest and shortest axis on measured hyaloclastite fragments from thin sections originating from the SSOC, compared to thin sections from supposedly similar type of deposits of Iceland, studied by Franzson et al. (2011). Total deformation ratio for volcanic breccias:

Total V/H ratio of fragments: $\frac{0.578}{0.212} = \mathbf{2.7}$

*Table 3.2.1: Calculations and adjustments regarding dip and deformation of strata. * The missing data section is multiplied by 1.15 as it is impossible to predict what this area consists of. It is likely to assume that it is composed of a mixture of sheet flow, pillow lava and volcanic breccia, hence estimated to be 1.15 (half of the difference between the pillow lava ratios (1.6-1.3)*

Different components within the Master Profile (Figure 2)	Part	Calculated length regarding deformation (m)	New profile length, after adjustments
Pillow lava	1	$329.5 \cdot 1.3 = 428.5$	23.5-452
Sheet flow	2	$9.5 \cdot 1 = 9.5$	452-461.5
Volcanic breccia	3	$9 \cdot 2.7 = 24.5$	461.5-486
Sheet flow	4	$72.5 \cdot 1.3 = 94$	486-580
Missing data	5	$180 \cdot 1.15^{*} = 207$	580-787
Volcanic breccia	6	$56.5 \cdot 2.7 = 152.5$	787-939.5
Pillow lava	7	$32 \cdot 1.6 = 51$	939.5-990.5
Sheet flow	8	$9 \cdot 1 = 9$	990.5-999.5
Pillow lava	9	$41 \cdot 1.6 = 65.5$	999.5-1065
Sheet fow	10	$13.5 \cdot 1 = 13.5$	1065-1078.5
Pillow lava	11	$22.5 \cdot 1.6 = 36$	1078.5-1114.5
Volcanic breccia	12	$50 \cdot 2.7 = 135$	1114.5-1249.5
Sheet flow	13	$30 \cdot 1 = 30$	1249.5-1279.5
Pillow lava	14	$19 \cdot 1.6 = 30.5$	1279.5-1310
Volcanic breccia	15	$22.5 \cdot 2.7 = 61$	1310-1371
Pillow lava	16	$37 \cdot 1.6 = 59$	1371-1430

Profile thickness before reconstruction: 1205 m (excluding sedimentary cover).

Estimated profile thickness after reconstruction regarding dip of strata and deformation: 1430 m.

Appendix 4

Samples of metabasalt from Grimelia, part of the SSOC

Table 4.1.1: Samples of metabasalt from the study area, together with GPS-coordinates and their stratigraphic heights in the Master profile (Fig.3.2; Fig.9.5). The indicated colors in the table represent the different lithologies of the samples. Green: sheet flow, orange/red: pillow lava, yellow: volcanic breccia.

Sample ID	Latitude	Longitude	Stratigraphic height
20GRI1	61,442258	5,074809	525 m
20GRI2	61,442219	5,0751	500 m
20GRI4	61,442239	5,075256	490 m
20GRI5	61,442227	5,075429	475 m
20GRI6	61,442247	5,077195	440 m
20GRI8	61,442397	5,077447	445 m
20GRI9	61,442397	5,077447	445 m
20GRI10	61,442494	5,077486	450 m
20GRI11	61,442586	5,077292	465 m
20GRI12	61,442528	5,077379	460 m
20GRI13	61,442528	5,077379	460 m
20GRI15	61,442623	5,077433	470 m
20GRI16	61,442644	5,077363	480 m
20GRI18	61,442967	5,07896	420 m
20GRI19	61,443116	5,079225	425 m
21GRI20	61,442551	5,081342	295 m
21GRI22	61,442523	5,081553	280 m
21GRI23	61,442521	5,081754	270 m
21GRI24	61,442486	5,082367	240 m
21GRI25	61,442434	5,082457	230 m
21GRI26	61,44226	5,082764	205 m
21GRI27	61,442276	5,082861	195 m
21GRI28	61,442364	5,083675	178 m
21GRI29	61,442427	5,08379	175 m
21GRI31	61,442344	5,084174	155 m
21GRI32	61,442322	5,084341	140 m
21GRI34	61,442267	5,084274	145 m
21GRI36	61,442237	5,083875	160 m
21GRI37	61,442237	5,083875	160 m
21GRI39	61,442564	5,083544	190 m
21STA1	61,448001	5,072548	1145 m
21STA2	61,448143	5,071597	1170 m
21STA3	61,446822	5,072515	1005 m
21STA4	61,446822	5,072515	1005 m

Geochemical analysis

*Table 4.1.2: Trace element composition in ppm of the samples of metabasalt in Grimelia. Green: sheet flow, orange/red: pillow lava, yellow: volcanic breccia. *Corrected Zr values (Chapter 9.1.2). See the next table for added values to the corrected Zr.*

Sample ID	Li	Sc	V	Cr	Co	Ni	Cu	Zn	Rb	Sr	Y	Zr*	Nb	Cs	Ba	La	Ce
20GRI1	3,28	47,97	538,9	145,2	41,48	65,15	37,20	131,4	0,340	134,2	58,60	185,31	2,73	0,020	3,73	5,32	17,57
20GRI2	5,11	41,69	413,5	116,2	41,07	51,55	113,7	169,2	0,970	110,0	47,11	147,80	2,03	0,070	8,39	3,96	13,35
20GRI4	6,24	48,19	472,8	204,7	41,61	67,07	20,54	117,1	0,850	127,9	53,18	168,9	2,34	0,030	5,27	4,65	15,42
20GRI5	3,55	47,74	427,1	257,4	41,43	56,35	36,34	99,09	0,740	140,3	46,51	150,0	2,06	0,020	4,74	4,08	13,61
20GRI6	3,11	48,49	430,0	256,8	43,29	64,34	57,00	99,85	0,290	123,2	46,48	143,44	1,71	0,030	3,86	3,40	11,83
20GRI8	2,33	45,08	351,5	159,3	51,25	69,70	99,88	87,53	0,170	131,2	33,90	94,41	1,03	0,020	2,11	2,27	7,71
20GRI9	1,72	47,37	455,9	169,0	41,27	52,91	23,71	121,8	0,330	115,2	49,44	163,04	2,04	0,020	3,10	4,23	14,08
20GRI10	3,11	47,29	312,0	176,5	45,50	54,46	59,11	90,18	0,810	95,10	26,71	68,74	0,550	0,080	4,75	1,40	4,91
20GRI11	4,40	36,91	473,9	128,0	31,33	46,87	26,31	93,57	0,300	261,9	44,52	136,5	1,99	0,080	5,83	4,43	13,69
20GRI12	2,61	47,03	402,0	250,8	34,39	53,65	30,08	84,94	0,480	188,8	47,47	145,1	2,00	0,020	5,83	3,83	12,94
20GRI13	2,34	37,42	322,3	226,2	36,86	65,47	29,45	75,40	0,330	215,3	31,46	94,18	1,08	0,020	4,30	2,53	8,35
20GRI15	4,46	42,80	460,1	117,1	28,31	42,29	14,01	173,0	0,420	139,8	55,47	185,00	2,45	0,020	5,08	5,22	17,31
20GRI16	4,97	44,29	474,6	108,6	36,06	47,79	48,74	153,7	0,640	130,4	56,37	185,5	2,60	0,070	5,48	5,12	17,34
20GRI18	4,50	39,45	385,2	216,0	29,69	53,27	18,54	97,23	0,430	124,4	45,90	164,97	2,09	0,040	3,66	4,71	15,44
20GRI19	4,67	43,30	417,2	240,0	35,86	55,33	25,35	107,2	0,730	129,5	50,98	182,3	2,25	0,030	5,49	5,12	16,86
21GRI20	2,62	34,73	326,8	180,6	29,08	49,84	11,22	115,5	0,410	96,37	36,95	130,7	1,63	0,020	2,20	3,48	11,42
21GRI22	3,04	44,08	446,9	168,2	35,74	47,29	46,15	122,9	0,710	121,2	56,42	193,4	2,48	0,020	8,33	5,54	17,89
21GRI23	5,86	39,95	372,0	253,8	35,76	81,29	28,48	159,7	0,410	142,2	44,80	155,14	1,90	0,040	5,87	4,31	14,27
21GRI24	2,69	41,08	378,5	166,0	27,09	32,06	16,47	198,9	0,440	156,2	37,68	124,22	1,41	0,040	4,87	3,54	11,44
21GRI25	4,53	48,74	440,7	262,1	28,84	20,28	42,38	-	0,150	154,1	56,94	204,3	2,18	0,030	1,29	8,34	23,82
21GRI26	4,72	42,48	374,4	166,0	32,28	43,64	23,31	170,2	0,290	132,7	42,19	140,1	1,61	0,060	2,38	3,76	12,41
21GRI27	2,75	42,99	368,8	235,6	31,19	63,21	39,03	257,6	0,160	103,0	41,35	136,15	1,52	0,040	2,73	3,46	11,69
21GRI28	2,55	42,65	419,3	174,1	32,13	32,12	8,94	102,9	0,390	148,4	49,50	173,74	2,22	0,020	4,47	5,28	16,77
21GRI29	1,66	39,64	350,3	242,6	31,98	46,54	43,16	258,3	0,150	105,2	40,28	135,75	1,50	0,010	1,80	3,73	12,38
21GRI31	2,42	41,59	387,6	153,7	41,73	50,87	58,57	298,2	0,320	75,83	46,60	158,5	1,88	0,030	3,11	4,43	14,41
21GRI32	1,93	38,05	402,2	150,5	17,76	5,38	192,9	-	0,100	17,02	34,76	116,0	1,53	0,010	0,740	2,69	9,61

21GRI34	2,03	39,83	416,8	148,8	36,58	48,67	39,77	232,7	0,240	98,26	51,98	184,57	2,31	0,060	3,41	5,49	17,94
21GRI36	1,53	29,20	298,3	139,0	25,75	39,15	16,47	123,9	0,320	75,38	37,27	142,33	1,57	0,020	2,68	4,11	13,52
21GRI37	1,08	40,50	433,9	109,1	38,25	41,78	41,22	143,4	0,170	99,83	56,80	211,0	2,41	0,020	4,05	5,67	19,10
21GRI39	2,64	40,16	360,6	180,6	26,41	49,30	33,56	215,2	0,240	99,98	46,58	181,1	2,25	0,030	3,13	5,23	16,57
21STA1	4,99	46,33	432,0	113,0	42,66	44,30	29,57	103,4	2,05	179,6	50,59	167,27	2,36	0,176	6,92	5,01	16,08
21STA2	8,05	49,81	377,6	195,4	35,54	51,67	57,01	104,4	2,06	105,5	42,03	142,19	2,11	0,165	8,92	3,95	12,96
21STA3	2,68	40,18	245,4	319,2	37,73	85,38	72,39	58,28	0,532	165,5	22,87	61,99	0,562	0,054	3,45	1,47	5,10
21STA4	10,40	40,50	250,9	312,8	46,19	97,07	49,94	77,42	2,77	106,5	23,17	65,21	0,574	0,058	4,09	1,40	5,13

Table 4.1.3: Conducted corrections for Zr- values. The calculated Zr is represented by the stated added value, where the result is presented in the previous diagram. Green: sheet flow, orange/red: pillow lava, yellow: volcanic breccia.

Sample ID	**20GRI 1**	**20GRI 2**	**20GRI 4**	**20GRI 5**	**20GRI 6**	**20GRI 8**	**20GRI 9**	**20GRI 10**	**20GRI 11**	**20GRI 12**	**20GRI 13**	**20GRI 15**	**20GRI 16**	**20GRI 18**	**20GRI 19**	**21GRI 20**	**21GRI 22**
Added value	10	75	60	20	55	30	70	30	30	25	46,5	100	80	70	0	30	65
Sample ID	**21GRI 23**	**21GRI 24**	**21GRI 25**	**21GRI 26**	**21GRI 27**	**21GRI 28**	**21GRI 29**	**21GRI 31**	**21GRI 32**	**21GRI 34**	**21GRI 36**	**21GRI 37**	**21GRI 39**	**21STA1**	**21STA2**	**21STA3**	**21STA4**
Added value	70	50	85	40	40	100	70	50	10	85	55	100	70	110	95	35	45

Table 4.1.4: Trace element composition in ppm of the samples of metabasalt in Grimelia. Green: sheet flow, orange/red: pillow lava, yellow: volcanic breccia.

Sample ID	**Pr**	**Nd**	**Sm**	**Eu**	**Gd**	**Tb**	**Dy**	**Ho**	**Er**	**Tm**	**Yb**	**Lu**	**Hf**	**Ta**	**Pb**	**Th**	**U**
20GRI1	3,29	18,75	6,64	2,17	8,94	1,65	10,62	2,34	6,62	0,970	6,01	0,870	2,56	0,180	3,81	0,170	0,070
20GRI2	2,53	14,59	5,22	1,79	6,97	1,30	8,55	1,87	5,34	0,780	4,85	0,710	2,02	0,140	0,860	0,120	0,050
20GRI4	2,90	16,66	5,90	2,00	7,90	1,46	9,55	2,08	5,98	0,870	5,49	0,800	2,79	0,150	0,490	0,140	0,060
20GRI5	2,51	14,70	5,18	1,80	6,94	1,27	8,49	1,82	5,27	0,760	4,89	0,730	3,37	0,140	0,620	0,140	0,060
20GRI6	2,33	13,83	5,03	1,74	6,95	1,29	8,50	1,86	5,24	0,780	4,82	0,720	2,52	0,120	0,530	0,100	0,130
20GRI8	1,52	8,91	3,40	1,39	4,77	0,910	5,89	1,32	3,70	0,560	3,42	0,520	1,84	0,070	0,890	0,060	0,030
20GRI9	2,67	15,23	5,42	1,68	7,39	1,36	8,99	1,95	5,51	0,810	5,01	0,740	2,72	0,140	1,00	0,130	0,080

20GRI10	1,01	6,12	2,48	1,01	3,74	0,710	4,80	1,08	3,05	0,460	2,86	0,440	1,31	0,040	1,57	0,030	0,020
20GRI11	2,47	13,76	4,76	1,69	6,47	1,17	7,88	1,72	4,98	0,740	4,65	0,700	2,77	0,130	1,46	0,250	0,090
20GRI12	2,49	14,17	5,09	1,63	6,95	1,27	8,47	1,86	5,25	0,780	4,82	0,730	3,21	0,140	1,49	0,150	0,090
20GRI13	1,59	9,21	3,33	1,65	4,72	0,870	5,76	1,28	3,60	0,530	3,26	0,480	1,56	0,080	1,50	0,070	0,060
20GRI15	3,26	18,43	6,42	2,12	8,89	1,62	10,78	2,38	6,78	0,980	6,14	0,870	2,58	0,190	10,86	0,180	0,080
20GRI16	3,25	18,55	6,57	1,97	9,13	1,65	11,05	2,43	6,92	1,02	6,32	0,920	3,23	0,190	5,59	0,180	0,070
20GRI18	2,89	16,37	5,71	1,90	7,70	1,41	9,36	2,05	5,77	0,840	5,29	0,780	2,96	0,170	1,29	0,150	0,070
20GRI19	3,16	17,99	6,26	2,12	8,54	1,54	10,28	2,25	6,35	0,930	5,83	0,860	3,21	0,180	1,12	0,160	0,080
21GRI20	2,17	12,32	4,41	1,43	5,98	1,11	7,36	1,64	4,66	0,700	4,34	0,660	3,03	0,130	1,57	0,160	0,060
21GRI22	3,42	19,22	6,75	2,31	9,12	1,68	11,08	2,48	6,84	1,02	6,37	0,960	3,74	0,190	1,99	0,220	0,100
21GRI23	2,64	15,22	5,39	1,85	7,48	1,33	9,00	1,93	5,55	0,800	5,06	0,730	2,61	0,150	2,09	0,140	0,060
21GRI24	2,09	11,99	4,27	2,21	5,93	1,06	7,23	1,58	4,56	0,660	4,18	0,630	2,32	0,110	6,84	0,100	0,080
21GRI25	4,08	21,77	7,02	3,73	9,36	1,67	11,16	2,43	6,97	1,02	6,35	0,950	3,43	0,170	4,32	0,180	0,100
21GRI26	2,38	13,47	4,88	1,74	6,72	1,26	8,34	1,86	5,22	0,780	4,79	0,740	3,04	0,130	5,87	0,120	0,050
21GRI27	2,27	12,94	4,68	1,44	6,60	1,22	8,03	1,80	5,04	0,750	4,66	0,710	2,89	0,120	7,62	0,110	0,050
21GRI28	3,13	17,43	6,08	2,14	8,28	1,52	10,02	2,22	6,22	0,920	5,70	0,830	2,50	0,170	0,780	0,160	0,070
21GRI29	2,33	13,37	4,77	2,69	6,55	1,20	7,98	1,76	4,96	0,730	4,54	0,660	1,88	0,120	11,89	0,110	0,080
21GRI31	2,71	15,66	5,55	1,84	7,67	1,39	9,31	2,06	5,81	0,860	5,40	0,800	3,18	0,150	3,69	0,140	0,060
21GRI32	1,80	11,12	4,23	0,650	6,03	1,07	7,50	1,62	4,79	0,690	4,48	0,650	2,81	0,120	1,75	0,130	0,060
21GRI34	3,35	18,92	6,62	2,21	8,89	1,66	10,82	2,37	6,73	0,990	6,16	0,910	3,15	0,190	5,32	0,170	0,070
21GRI36	2,44	14,10	4,88	1,72	6,44	1,18	7,80	1,70	4,87	0,710	4,53	0,660	2,71	0,130	2,40	0,140	0,070
21GRI37	3,56	20,88	7,36	2,38	9,94	1,84	12,10	2,65	7,61	1,11	6,98	1,02	3,76	0,200	14,55	0,180	0,070
21GRI39	3,12	17,33	6,02	2,51	8,00	1,52	9,74	2,18	6,06	0,910	5,54	0,840	3,44	0,190	18,50	0,190	0,350
21STA1	2,99	16,83	5,79	1,93	7,84	1,41	9,26	1,99	5,71	0,819	5,03	0,689	1,81	0,190	6,41	0,115	0,203
21STA2	2,43	13,95	5,02	1,21	6,72	1,21	8,02	1,72	4,80	0,692	4,18	0,566	1,73	0,171	1,77	0,106	0,224
21STA3	1,01	6,13	2,34	0,93	3,42	0,622	4,18	0,906	2,59	0,375	2,33	0,334	1,03	0,055	5,37	<0.0013	0,028
21STA4	1,04	6,37	2,47	0,99	3,54	0,644	4,34	0,938	2,64	0,380	2,35	0,327	0,892	0,055	1,23	<0.0013	0,028

Table 4.1.5: Major element composition in w% of the samples of metabasalt in Grimelia. Green: sheet flow, orange/red: pillow lava, yellow: volcanic breccia.

Sample ID	SiO2	TiO_2	Al_2O_3	Fe_2O_3	MnO	MgO	CaO	Na_2O	K_2O	P_2O_5	LOI (%)	Total
20GRI1	49,21	2,69	12,66	15,21	0,25	6,08	10,31	2,19	0,00	0,45	0,98	100
20GRI2	55,41	2,15	11,97	11,93	0,20	5,88	8,30	2,85	0,00	0,32	1,26	100
20GRI4	49,83	2,34	12,59	14,15	0,22	6,64	10,09	2,38	0,00	0,39	1,37	100
20GRI5	50,13	2,07	12,95	13,13	0,19	6,37	11,66	2,26	0,00	0,35	0,89	100
20GRI6	49,32	2,11	13,81	12,59	0,19	7,47	10,19	2,94	0,00	0,34	1,04	100
20GRI8	49,52	1,46	14,02	11,89	0,18	6,97	12,13	2,35	0,00	0,21	1,27	100
20GRI9	48.98	2,26	11,45	14,67	0,23	7,40	11,35	2,47	0,00	0,36	0,83	100
20GRI10	50,18	1,10	13,81	11,48	0,19	7,75	12,17	2,05	0,00	0,13	1,14	100
20GRI11	54,51	1,87	12,18	12,35	0,18	5,13	10,98	0,93	0,00	0,43	1,44	100
20GRI12	52	1,94	13,30	11,51	0,17	6,19	9,98	3,54	0,00	0,33	1,04	100
20GRI13	50,65	1,35	13,94	11,17	0,18	6,20	13,13	1,91	0,00	0,24	1,24	100
20GRI15	49,72	2,60	12,35	14,44	0,24	6,62	9,53	2,70	0,00	0,43	1,37	100
20GRI16	49,17	2,66	12,50	14,79	0,28	6,68	9,32	2,92	0,00	0,46	1,22	100
20GRI18	50,08	2,25	13,24	12,79	0,21	6,52	10,78	2,62	0,00	0,39	1,12	100
20GRI19	48,11	2,47	13,55	13,96	0,21	6,80	10,58	2,88	0,00	0,44	1,00	100
21GRI20	47,67	1,77	14,14	12,98	0,20	6,14	15,06	0,58	0,00	0,28	1,18	100
21GRI22	48,25	2,66	12,82	14,60	0,23	6,65	10,75	2,86	0,00	0,44	0,74	100
21GRI23	47,57	2,11	13,95	14,40	0,23	7,21	9,92	2,16	0,00	0,40	2,05	100
21GRI24	48,18	1,72	13,31	13,76	0,22	7,12	11,83	2,32	0,00	0,23	1,31	100
21GRI25	45,58	2,57	14,52	16,60	0,31	6,79	9,66	0,42	0,00	0,39	3,16	100
21GRI26	50,37	1,95	12,96	13,15	0,23	6,66	10,89	2,12	0,00	0,30	1,37	100
21GRI27	49,54	1,90	13,82	13,35	0,19	6,25	11,17	2,63	0,00	0,33	0,82	100
21GRI28	49,18	2,38	12,95	14,44	0,21	5,77	11,81	2,02	0,00	0,42	0,82	100
21GRI29	54,02	1,84	12,47	12,22	0,28	6,48	9,78	1,48	0,00	0,33	1,10	100
21GRI31	51,14	2,19	12,75	13,93	0,32	6,92	8,91	2,10	0,00	0,40	1,34	100
21GRI32	47,23	2,11	11,68	21,59	0,30	8,23	3,41	0,34	0,00	0,31	4,80	100
21GRI34	49,56	2,54	12,98	14,92	0,25	6,44	9,84	1,84	0,00	0,49	1,14	100

21GRI36	62,58	1,81	9,56	11,63	0,17	5,05	6,58	1,70	0,00	0,34	0,58	100
21GRI37	49,44	2,79	12,48	15,25	0,23	6,42	9,86	2,55	0,00	0,53	0,45	100
21GRI39	49,86	2,32	12,98	15,15	0,32	5,83	7,90	3,86	0,00	0,46	1,32	100
21STA1	49,53	2,33	12,61	13,88	0,22	6,22	10,34	2,72	0,00	0,41	1,74	100
21STA2	50,24	2,15	13,13	13,32	0,20	6,73	8,80	3,27	0,00	0,38	1,78	100
21STA3	51,11	1,01	14,44	9,74	0,15	6,80	12,42	2,48	0,00	0,14	1,71	100
21STA4	48,35	1,05	14,80	10,95	0,17	9,65	10,67	1,94	0,00	0,15	2,27	100

Quality control of the samples

As stated in chapter 9.1.2, a quality control is done by USGS CRM BCR2 (Basalt, Columbia River). During the analytical run, the synthetic water CRM SPS-SW-2 (Spectrapure Standards AS) is analyzed repeatedly. This provides a direct control of the calibration curves and the monitoring of the performance. The quality control states that the samples range from $\pm$ 6 % (averagely) of the recommended values.

Table 4.1.6: The table is representing a quality control of 15 elements, analyzed six times by USGS CRM BCR2. The result from the upper panel is divided on the BCR2 recommended values (from the second panel), to get the recovery%. #: USGS certificate original, #i: USGS certificate information original, &: GeoRem complied.

mg/kg	Y	La	Ce	Pr	Nd	Sm	Eu	Gd	Tb	Dy	Ho	Er	Tm	Yb	Lu
BCR2-1	35,42	25,37	51,61	6,81	29,33	6,74	2,06	6,96	1,10	6,70	1,35	3,84	0,54	3,52	0,53
BCR2-2	36,50	25,66	52,11	6,87	29,68	6,83	2,07	6,89	1,12	6,78	1,39	3,95	0,56	3,55	0,54
BCR2-3	34,04	26,20	52,58	7,03	30,62	6,98	2,17	7,17	1,15	7,04	1,44	4,11	0,58	3,74	0,56
BCR2-4	34,31	24,80	49,08	6,62	28,80	6,55	2,04	6,78	1,07	6,46	1,33	3,75	0,53	3,37	0,51
BCR2-5	35,29	25,15	50,93	6,76	29,12	6,72	2,05	6,86	1,09	6,62	1,36	3,83	0,55	3,46	0,53
BCR2-6	35,60	25,24	50,66	6,81	29,22	6,82	2,10	6,92	1,10	6,74	1,37	3,84	0,55	3,49	0,53
Isotope (ppm)	**$Y^{\#}$**	**$La^{\#}$**	**$Ce^{\#}$**	**$Pr^{\#i}$**	**$Nd^{\#}$**	**$Sm^{\#i}$**	**$Eu^{\#}$**	**$Gd^{\#}$**	**$Tb^{\#}$**	**$Dy^{\&}$**	**$Ho^{\#i}$**	**$Er^{\&}$**	**$Tm^{\#i}$**	**$Yb^{\#}$**	**$Lu^{\#i}$**
BCR2 (recom values)	37,00	25	53	6,8	28	6,7	2	6,8	1,07	6,41	1,33	3,66	0,54	3,5	0,51
Variation +/-	2,00	1	2	0,3	2	0,3	0,1	0,3	0,04	inf.	0,06	inf.	inf.	0,2	0,02

GeoRem range	28.1-40.1	20.0-31	44.8-66	5.8-7.5	23.3-31.7	5.55-7.3	1.2-2.43	2.02-7.9	0.86-2	5.43-7.35	0.62-2	1.84-4.4	0.43-1	2.85-4.08	0.26-1
Recovery%	**Y**	**La**	**Ce**	**Pr**	**Nd**	**Sm**	**Eu**	**Gd**	**Tb**	**Dy**	**Ho**	**Er**	**Tm**	**Yb**	**Lu**
BCR2-1	95,74	101,50	97,38	100,11	104,77	100,54	103,06	102,36	102,48	104,51	101,35	105,04	100,13	100,58	103,07
BCR2-2	98,66	102,63	98,32	100,97	106,00	102,01	103,65	101,37	104,65	105,77	104,79	107,98	102,89	101,35	106,01
BCR2-3	92,00	104,82	99,20	103,45	109,34	104,23	108,47	105,51	107,79	109,83	108,46	112,22	107,98	106,74	110,68
BCR2-4	92,74	99,20	92,60	97,32	102,87	97,76	101,86	99,78	99,54	100,78	100,20	102,40	99,04	96,39	100,52
BCR2-5	95,37	100,61	96,09	99,37	103,99	100,27	102,47	100,92	101,92	103,22	101,94	104,73	102,00	98,89	104,73
BCR2-6	96,22	100,95	95,59	100,22	104,37	101,75	104,94	101,79	103,11	105,08	102,66	104,94	102,05	99,59	104,37
Average Recovery%	95,12	101,62	96,53	100,24	105,22	101,09	104,07	101,95	103,25	104,86	103,23	106,22	102,35	100,59	104,90
Precision (RSD%)	**Y**	**La**	**Ce**	**Pr**	**Nd**	**Sm**	**Eu**	**Gd**	**Tb**	**Dy**	**Ho**	**Er**	**Tm**	**Yb**	**Lu**
BCR2-1	0,96	0,53	0,36	1,11	0,56	0,5	0,41	0,4	0,6	1,01	0,58	1,27	1,17	0,77	2,46
BCR2-2	0,93	1,07	0,48	0,95	1,12	1	1,02	0,08	1,5	1,22	1,13	0,69	0,5	0,71	0,91
BCR2-3	0,86	1,15	0,83	0,14	0,82	0,57	0,68	0,97	0,58	1,06	0,43	0,96	1,09	0,54	0,71
BCR2-4	1,27	1	0,84	0,9	1,01	0,55	1,51	0,55	0,9	0,52	1,18	0,85	0,24	1,7	0,91
BCR2-5	1,18	1,57	1,26	1,26	2,05	1,12	1,5	0,77	1,65	0,64	0,98	1,05	0,87	1,29	1,35
BCR2-6	1,76	1,74	1,32	1,82	2,32	2,19	1,59	3,24	2,03	2,84	1,51	1,65	1,2	1,63	1,39